AD-A051 795 ARMY ENGINEER WATERWAYS EXPERIMENT STATION VICKSBURG MISS F/G 13/2
STRENGTH AND DEFORMATION PROPERTIES OF ROCK FILL.(U)
JAN 78 R T DONAGHE, M W COHEN
UNCLASSIFIED WES-TR-S-78-1 NL

1 OF 2
AD
A051 795

TECHNICAL REPORT S-78-1

STRENGTH AND DEFORMATION PROPERTIES OF ROCK FILL

by

Robert T. Donaghe and Melvin W. Cohen

Soils and Pavements Laboratory
U. S. Army Engineer Waterways Experiment Station
P. O. Box 631, Vicksburg, Miss. 39180

AD A051795

January 1978

Final Report

Approved For Public Release; Distribution Unlimited

Prepared for Office, Chief of Engineers, U. S. Army
Washington, D. C. 20314

AD No.
DDC FILE COPY

DDC
RECEIVED
MAR 27 1978
B

Unclassified

SECURITY CLASSIFICATION OF THIS PAGE (When Data Entered)

REPORT DOCUMENTATION PAGE		READ INSTRUCTIONS BEFORE COMPLETING FORM
1. REPORT NUMBER Technical Report S-78-1	2. GOVT ACCESSION NO.	3. RECIPIENT'S CATALOG NUMBER 9
4. TITLE (and Subtitle) 6 STRENGTH AND DEFORMATION PROPERTIES OF ROCK FILL,		5. TYPE OF REPORT & PERIOD COVERED Final report,
		6. PERFORMING ORG. REPORT NUMBER
7. AUTHOR(s) 10 Robert T. Donaghe Melvin W. Cohen		8. CONTRACT OR GRANT NUMBER(s)
9. PERFORMING ORGANIZATION NAME AND ADDRESS U. S. Army Engineer Waterways Experiment Station Soils and Pavements Laboratory P. O. Box 631, Vicksburg, Miss. 39180		10. PROGRAM ELEMENT, PROJECT, TASK AREA & WORK UNIT NUMBERS
11. CONTROLLING OFFICE NAME AND ADDRESS Office, Chief of Engineers, U. S. Army Washington, D. C. 20314		12. REPORT DATE 11 January 1978
		13. NUMBER OF PAGES 98
14. MONITORING AGENCY NAME & ADDRESS(if different from Controlling Office) 12 111p.		15. SECURITY CLASS. (of this report) Unclassified
		15a. DECLASSIFICATION/DOWNGRADING SCHEDULE

16. DISTRIBUTION STATEMENT (of this Report)

Approved for public release; distribution unlimited.

14 WES-TR-S-78-1

DDC
RECEIVED
MAR 27 1978
B

17. DISTRIBUTION STATEMENT (of the abstract entered in Block 20, if different from Report)

18. SUPPLEMENTARY NOTES

19. KEY WORDS (Continue on reverse side if necessary and identify by block number)

Aggregates
Consolidation
Deformation
Gravels
Rock fills

20. ABSTRACT (Continue on reverse side if necessary and identify by block number)

During the past 25 years there ~~has been~~ was a large increase in the use of rock fill materials for the construction of high dams and embankments. The South Pacific (SPD) Laboratory of the U. S. Army Corps of Engineers (CE) ~~has been~~ was engaged in developing equipment and methods to determine the strength and deformation properties of such materials since 1953. This report presents summaries of previously published but not generally available reports prepared by the SPD Laboratory dealing with the influence of gradation, → (Continued) → next page

DD FORM 1 JAN 73 1473 EDITION OF 1 NOV 65 IS OBSOLETE

Unclassified

SECURITY CLASSIFICATION OF THIS PAGE (When Data Entered)

038100 LB

20. ABSTRACT (Continued).

cont.

confining pressure, relative density, and engineering properties of individual aggregate particles on the consolidated-drained strength and deformation properties of gravelly materials. Also presented in the report are results of additional unpublished laboratory investigations performed on rock fill materials by the SPD Laboratory dealing with the influence of end restraint and particle shape on consolidated-drained characteristics and with the influence of particle size on one-dimensional consolidation characteristics.

PREFACE

The investigations reported herein were performed for the Office, Chief of Engineers (OCE), under Item ES 526 of the Soil Mechanics Engineering Studies Program and Items CWIS 31202 and 31171 of the Civil Works Investigation Studies Program. Authorization for the work was by multiple letter ENGCW-EC, 1 November 1962, subject: "Civil Works Investigation - FY 1963." Since July 1973, funding of the studies has been from the U. S. Army Engineer Waterways Experiment Station (WES).

The studies were performed under the general direction of Mr. A. L. O'Neill, Chief, Geology, Soils and Materials Branch, South Pacific Division (SPD); and Mr. D. D. Leslie, former Chief.

The testing and preparation of this report were performed under the direction of Mr. M. W. Cohen, Chief, Soils Section, under the supervision of Mr. E. A. Hein, former Chief, Soils Section, and direction of Messrs. J. E. Ott and R. A. Chisolm, former Directors, and Mr. C. V. McNicol, Director, all of the South Pacific Division Laboratory. This report was written by Mr. R. T. Donaghe of the Soils Research Facility, Soil Mechanics Division, Soils and Pavements Laboratory (S&PL), WES, and Mr. Cohen. It was reviewed by Mr. S. J. Johnson, Special Assistant to the Chief, S&PL, WES.

Directors of WES during the preparation and publication of this report were COL G. H. Hilt, CE, and COL J. L. Cannon, CE. Technical Director was Mr. F. R. Brown.

ACCESSION for
NTIS White Section ☑
DDC Buff Section ☐
UNANNOUNCED ☐
JUSTIFICATION

BY
DISTRIBUTION/AVAILABILITY CODES
Dist. AVAIL. and/or SPECIAL
A

CONTENTS

CONVERSION FACTORS, U. S. CUSTOMARY TO METRIC (SI) UNITS OF MEASUREMENT

U. S. customary units of measurement used in this report can be converted to metric (SI) units as follows:

Multiply	By	To Obtain
inches	2.54	centimeters
pounds (mass)	0.45359237	kilograms
pounds (mass) per cubic foot	16.0185	kilograms per cubic meter
pounds per square inch	6894.757	pascals

STRENGTH AND DEFORMATION PROPERTIES OF ROCK FILL

PART I: INTRODUCTION

1. The increasing use of rock-fill materials in the construction of dams created a need to obtain more knowledge of the strength and deformation properties of such materials. The South Pacific Division (SPD) Laboratory of the U. S. Army Corps of Engineers (CE) has been engaged in developing equipment and methods to provide such information since 1963.

2. Table 1 lists titles and publication dates of reports previously published by the SPD Laboratory dealing with the following: the influence of gradation, confining pressure, and relative density on the consolidated-drained strength and deformation characteristics of gravelly materials; the influence of engineering properties of individual aggregate particles on consolidated-drained strength and deformation properties investigated; and a preliminary study of the behavior of a rock-fill material under consolidated-undrained conditions. These reports were published in limited quantities and are not generally available. Summaries of several of the more fundamental investigations contained in these reports are given in Part II of this report.

3. Since March 1972, several additional unpublished laboratory investigations have been completed by the SPD Laboratory on rock-fill materials. These investigations were meant to supplement the previously published investigations and deal with the influence of end restraint and particle shape on consolidated-drained characteristics, and with the influence of particle size on one-dimensional consolidation characteristics. Results of these investigations are given in Part III of this report.

PART II: SUMMARY OF PREVIOUS INVESTIGATIONS PRIOR TO 1972

Investigation of Effects of Gradation

4. The purpose of this investigation described in the report entitled "Shear Strength of Rockfill, Alluvial Gravel, Engineering Study No. 526," was to determine the influence of gradation on the strength and deformation properties of rock fill. Two types of straight-line gradations were tested: (a) modeled gradations having a constant coefficient, C_u , with maximum particle sizes from 2 in.* to 1/4 in. and minimum particle sizes from No. 4 to No. 30 (Figure 1), and (b) variable coefficients of uniformity, C_u , with maximum sizes from 2 in. to 1/4 in. and a minimum size of No. 30 (Figure 2). The material tested was an alluvial gravel having subangular but fairly well rounded edges obtained from the site of Black Butte Dam located on Stony Creek, a tributary of the Sacramento River in California. Six-in.-diam specimens were tested for the 1/4-, 1/2-, and 1-in. maximum particle size gradations and 12-in.-diam specimens were tested for the 2-in. minimum particle size gradation. Specimens were tested at high relative density (D_r = approximately 100 percent) at 60-psi confining pressure.

Angle of internal friction

5. The values of the angle of internal friction, ϕ' , plotted as a function of maximum particle size are shown in Figure 3.** From this figure (Figure 3) it may be seen that in the case of the constant C_u tests, strengths were approximately the same for all gradations. There was, however, a tendency toward a decrease in ϕ' with increasing maximum particle size. The difference in ϕ' in the case of the constant Cu between the 1/4- and 2-in. gradations was 1.4 deg. For the variable

---

* A table of factors for converting metric (SI) units of measurement to U. S. customary units is presented on page 3.

** In all of the investigations, the angle of internal friction was defined as the angle formed by a line through the origin and tangent to the Mohr circle taken at the maximum deviator stress.

C_u tests, Figure 3 shows that ϕ' increased 2.4 deg between these same gradations. The curve for the variable C_u tests indicates little change in strength (ϕ') for maximum particle sizes above 1 in.

Axial strain at failure

6. Figure 4 shows curves for the relationship between axial strain at failure and maximum particle size. This figure shows that axial strains at failure decreased with maximum particle size for the variable C_u tests and increased with maximum particle size for the constant C_u tests. Between the 1/4- and 2-in. gradations, the increase in strain for the variable C_u tests was 3.8 percent and the decrease in strain for the constant C_u tests was 3.4 percent.

Volumetric strain at failure

7. Plots of volumetric strain at failure versus maximum particle size are shown in Figure 5 for $\sigma_3 = 60$ psi. This figure shows that volumetric strains at failure increases with increasing maximum particle size for the constant C_u tests and remained almost unchanged with increasing maximum particle sizes for the variable C_u tests, with a tendency toward smaller volumetric compression with increasing particle size. The difference in volumetric strain at failure between the 1/4- and 2-in. gradations was 1.9 percent for the constant C_u tests and 0.4 percent for the variable C_u tests.

Conclusions

8. The following conclusions were made from the investigation of effects of modeled gradations with a constant C_u :

a. Strength does not change significantly with increasing maximum particle size. Consequently, modeled gradations may be used for strength determinations for materials having larger maximum particle sizes.

b. Axial strain at failure increases with increasing maximum particle size.

c. Volumetric compression during shear increases with increasing maximum particle sizes.

d. Since axial and volumetric strains during shear change significantly with increasing maximum particle sizes, modeled gradations may not be used to determine deformation properties for materials having larger maximum particle sizes.

9. The following conclusions were made from the investigation of modeled gradations with a variable C_u :

a. Strength increases with increasing maximum particle size up to about 1 in. and increasing C_u . Little increase in strength was found above 1 in. maximum particle size.

b. Axial strain at failure decreases with increasing maximum particle size and increasing C_u .

c. Volumetric compression during shear decreases slightly with increasing maximum particle size and increasing C_u .

Investigation of Effects of Confining Pressure

10. This investigation, contained in the report entitled "Shear Strength of Rockfill, Alluvial Gravel, Engineering Study No. 526," had the objective of determining the influence of confining pressure on the strength and deformation properties of rock fill. Gradations having variable coefficients of uniformity, C_u , with maximum particle sizes from 3- to 1/4-in. and a minimum particle size of No. 30 (Figure 6) were tested. The material tested was the same Black Butte alluvial gravel used in the gradation study. Specimens were tested at both high and medium relative densities using confining pressures ranging from 60 to 500 psi. Six-in.-diam specimens were tested for the 1/4-, 1/2-, and 1-in. maximum particle size gradations, and 12-in.-diam specimens were tested for the 2- and 3-in. maximum particle size gradation.

Angle of internal friction

11. Values of the angle of internal friction, ϕ' , adjusted to 100 percent relative density* and plotted as a function of confining pressure are given in Figure 7. As shown in this figure, ϕ' decreased with increasing confining pressure for all gradations. The average reduction of ϕ' with confining pressure for the gradations tested was 9 deg. The rate of change in ϕ' with confining pressure decreased

---

* Since the strength of specimens varied with density, angles of internal friction were normalized by interpolation at 100 percent relative density using relative density values taken after consolidation for high and medium density specimens.

with increasing confining pressure and suggests there may be little effect on strength due to confining pressure at higher confining pressures (> 500 psi). Plots of ϕ' versus the logarithim of confining pressure given in Figure 8 show that the decrease in ϕ' is linear with log increase in confining pressure.

Axial strain at failure

12. Figure 9 shows the curves of axial strain at failure plotted as a function of confining pressure. As may be seen, the curves indicate an increase in axial strain at failure with increasing confining pressure for each gradation tested. The total change in axial strain at failure with increasing confining pressure increased with decreasing maximum particle size. The total change for the 3-in. maximum gradation was approximately half that for the 1/4-in. maximum gradation.

Volumetric strain at failure

13. Plots of volumetric strain at failure versus confining pressure are shown in Figure 10. The curves for these relationships indicate that volumes of specimens increased at failure for the lowest confining pressure (60 psi) and decreased at failure for each of the higher confining pressures. The finest gradations, i.e., specimens with the lowest C_u values, exhibited the greatest volume change at each confining pressure.

Conclusions

14. The following conclusions were made from the investigation of effects of confining pressure:

a. The angle of internal friction, ϕ', decreases with increasing confining pressure.

b. Axial strain at failure increases with increasing confining pressure.

c. The change in volume of specimens at failure is positive (volume increase) at low confining pressures and negative (volume decrease) at high confining pressures. Finer gradations exhibit the greatest change in volume at each confining pressure.

Investigation of Effects of Physical Properties

15. The purpose of this study, which is contained in the report

entitled "Shear Strength of Rock Fill, Physical Properties, Engineering Study No. 526," was to correlate physical properties of rock-fill materials with strength and deformation properties. Seven varieties of crushed rock of varying hardness and mineralogy were tested. In order to eliminate the variable of gradation, all tests on all varieties of rock were prepared using the gradation shown in Figure 11. Table 2 summarizes results of the physical tests performed on each rock type. Twelve-in.-diam specimens were tested under consolidated-drained conditions at both high and low densities using confining pressures of 60, 125, 300, and 400 psi. Test results were normalized by interpolation at 100 percent relative density so that effects of physical properties could be isolated.

Angle of internal friction

16. Relationships between the angle of internal friction, ϕ' , and confining pressure are given in Figure 12. This figure shows that for all materials ϕ' decreased with increasing confining pressure and that the rate of change of ϕ' was lowest at the higher confining pressures. Figure 12 also shows that as confining pressure increased, the difference in ϕ' between materials diminished; at a confining pressure of 60 psi, the maximum difference in ϕ' was 10 deg, whereas at a confining pressure of 400 psi, the maximum difference in ϕ' was only 3 deg. If results for the Napa basalt material are neglected, the difference in ϕ' for the remaining six materials at a confining pressure of 400 psi is only 1.5 deg. The shape and relative positions of the curves for the softer materials (Laurel sandstone and Buchanan granite) indicate that they were less affected by confining pressure than the harder materials.

17. Graphs showing plots of ϕ' versus results of the physical tests are shown in Figures 13 and 14. As may be seen, ϕ' increased with decreasing abrasion loss and with increasing compressive strength (Figures 13a and 13b). Except for the two softest materials, ϕ' was not affected by soundness (Figure 13c). The angle of internal friction, ϕ' , also increased with hardness (Figure 14a), and there was a trend of increasing ϕ' with increasing shape factor (Figure 14b).

Axial strain at failure

18. Plots of axial strain at failure for tests at 60-psi confining pressure versus results of the physical tests are given in Figure 15. Plots of axial strain at failure at confining pressures greater than 60 psi are not shown since many low-density specimens did not reach peak strength before the strain limit of the testing apparatus was reached. From Figures 15a and 15c, it may be seen that axial strain at failure generally decreased with increasing shape factor and compressive strength. There was, however, no conclusive trend in axial strain at failure with abrasion loss or hardness as indicated by the scatter of points in Figures 15b and 15d.

Volumetric strain at failure

19. Figure 16 shows plots of volumetric strain at failure versus physical test results. These plots (Figures 16a and 16c) show that compression of both high and low density specimens during shear generally increased with increasing shape factor and compressive strength. As may be seen by the scatter of points in Figures 16b and 16d, however, there was not a definite relationship between volume change at failure and abrasion loss or hardness.

Conclusions

20. The following conclusions were made from the investigation of effects of physical properties:

a. The decrease in the angle of internal friction, ϕ' , with increasing confining pressures was greater for hard materials than for softer materials.

b. Compressive strength, resistance to abrasion, and hardness were found to best define strength.

c. Physical properties of soft rocks did not correlate as well as hard rocks. Low values of compressive strength and hardness, and the inability to resist abrasion were the overriding characteristics of Laurel sandstone and Buchanan granite. For these materials, the effect of shape factor on axial and volumetric strain was greatly reduced by their inability to resist applied axial and confining stresses.

d. The best indicator of volumetric and axial strain at failure was shape factor; however, shape factor was not a good indicator of strength.

PART III: TESTS OF ROCK-FILL MATERIALS SINCE 1972

Objectives

21. The objectives of the tests described in this Part were to supplement previous investigations by determining the effects of several additional variables on strength and deformation properties of rock fill. The additional tests described herein have not been previously published. Specifically, the effects investigated were:

- a. Influence of end restraint and particle shape on strength and deformation characteristics of rock-fill materials as ascertained by consolidated-drained triaxial compression tests.
- b. Influence of particle size on one-dimensional consolidation characteristics of rock-fill materials.

Scope of Testing

22. These effects were investigated by comparing the results of tests performed on specimens of a single rock-fill material using standard and low-friction end platens with results of tests of three rock-fill materials in which the angularity of particles was varied by crushing or abrasion. Effects of particle size in one-dimensional consolidation tests were determined by comparing results of a series of tests performed on a single rock-fill material in which the maximum particle size was varied.

Materials

23. Rock-fill materials tested in the investigations are referred to by names related to their location and rock type. A brief description of the materials tested is given in the following paragraphs. The gradations of all samples were made up and controlled to provide desired characteristics.

Napa basalt

24. This material was obtained from Blue Rock Quarry of Basalt Rock Company near Napa, California, and was produced primarily for

aggregate. It is a grayish-black, dense basalt in fresh and hard condition with cubical, pyramidal, and tabular particle shapes. X-ray diffraction of this material indicates that it is composed principally of plagioclase feldspar with interstitial glass and lesser quantities of labradorite and andesine with traces of montmorillonite clay. Photographs of pit run and abraided (less angular) samples are given in Figure 17.

Carters Dam quartzite

25. This material was used in the construction of a dam located on the Cossawattee River, 80 miles northwest of Atlanta, Georgia. It is a fresh, bluish-gray, medium grained, hard, impure quartzite composed primarily of interlocking, irregular quartz grains. Particle shapes are predominantly cubical, pyramidal, and tabular with a tendency toward flattness in the smaller sizes. X-ray diffraction of this material indicates that the predominant mineral is quartz; however muscovite, biotite, calcite, and pyrite are also present. Figure 18 shows photographs of crushed and abraided samples of this material.

Bear River gravel

26. This material was obtained from a source located on the Bear River in northern California. It is a white to dark gray river gravel in hard condition composed principally of quartz. Particle shapes are generally cubical, tabular, and pyramidal. Photographs of crushed and uncrushed samples are given in Figure 19.

Testing Program

Consolidated-drained triaxial tests

27. Effects of end restraint. Tests to determine effects of end restraint were performed on 6-in.-diam specimens of pit run Napa basalt having the straight-line gradation given in Figure 20. Two series of tests were performed using low-friction and standard end platens. One series was performed on specimens compacted to approximately 100 percent relative density and the other to approximately 70 percent relative density (maximum and minimum densities were 124.1 and 98.5 pcf,

respectively). Confining pressures in each series were 60, 125, 300, and 500 psi.

28. Effects of particle shape. Effects due to particle shape were determined in tests of Napa basalt, Carters Dam quartzite, and Bear River gravel having the gradations given in Figure 21. Specimen diameters were 6-in. for the Bear River material and 12-in. for the Carters Dam and Napa basalt materials. Two series of tests were performed on specimens of each material compacted to approximately the same relative density. One series was performed on specimens having more angular particles and the other on specimens having less angular particles. Particles of each material were either crushed or abraided to increase or decrease their angularity. Confining pressures for each series were 60, 125, 300, and 400 psi except for tests performed on specimens of the Bear River gravel material where the maximum confining pressure was 450 psi. The Bear River gravel was tested at both high and medium relative densities (approximately 100 and 70 percent, respectively), whereas the Napa basalt and Carters Dam quartzite materials were tested at only a high relative density.

One-dimensional consolidation tests

29. Effects of particle size on one-dimensional consolidation characteristics were determined in both dry and inundated tests performed on 12-in.-diam specimens of pit run Napa basalt at high and medium relative densities for each of the gradations shown in Figure 22. Maximum particle sizes varied from 1/4 to 3 in. The maximum vertical consolidation stress was 800 psi in each case.

Equipment

Consolidated-drained triaxial compression tests

30. Triaxial compression tests were performed on 12-in.-diam specimens of the Napa basalt and Carters Dam quartzite materials using the SPD Laboratory apparatus shown in Figure 23. This equipment

accommodates a specimen 12-in. in diameter by 27.7-in. high and is designed for a maximum chamber pressure of 500 psi and an axial load of 200,000 lb. The apparatus shown in Figure 24 was used to test 6-in.-diam specimens of the Bear River gravel and Napa basalt materials. The chamber shown in Figure 24 accommodates specimens 5.87-in. in diameter by 13.80-in. in length and is placed in the loading device shown in Figure 23 for the shear phase of the test. Low-friction caps and bases used in tests to determine effects of end restraint were slightly larger in diameter than the specimen and had plane bearing surfaces. Low-friction characteristics were obtained by applying a layer of silicone grease between two rubber disks separating the specimen from the cap and base. Specimen drainage was provided through holes located in the center of the disks and a small porous insert located in the center of the end platens. Standard caps and bases used in the investigation were those normally used for routine testing. They have the same diameter as the specimen and have bearing surfaces made of phenolic (layers of canvas impregnated with epoxy).

One-dimensional
consolidation tests

31. Consolidation tests were performed only on specimens of the Napa basalt material using the apparatus shown in Figure 25. The apparatus contains a 12-in.-diam fixed-ring, steel consolidometer that accommodates a 10-in.-high specimen.

Material Processing

32. Crushed samples of the rock-fill materials were obtained using an 8- by 10-in. jaw crusher for production of sizes larger than 1 in. and a gyratory crusher for smaller sizes. After crushing, the material was separated into six gravel sizes and four sand sizes using a trammel and sieve shaker, then washed and dried. Rounded samples were abraided in a concrete mixer until sharp edges were worn away. Pit run samples of the Napa basalt material were washed and sieved from material as received.

Specimen Preparation and Testing Procedures

Consolidated-drained triaxial compression tests

33. Triaxial specimens were prepared by vibrating each of four equal weight batches of air-dry material to the required density in the appropriate mold (6- or 12-in. diameter). After removal of the mold, the height and circumference of each specimen was measured and a second membrane was placed over the specimen. Membrane thickness varied from 0.048- to 0.063-in. In order to prevent puncturing of the membranes by sharp particles at the higher lateral pressures, specimens tested at lateral pressures of 300 psi and above had strips of 0.020-in.-thick low-density polyethlene between the membranes. These strips were 2-1/8-in. wide and extended the full height of the specimen. The specimens were saturated by allowing water to flow from the bottom to the top of the specimen under a differential vacuum head controlled by applying a vacuum of -14.5 psi to the top of the specimen and a regulated lower vacuum to the water reservoir connected to the bottom of the specimen. Consolidation of the specimens was accomplished by applying the desired chamber pressure and recording volume changes in a burette connected to both the top and bottom of the specimen. Generally, 30 to 60 min were required to complete consolidation. Specimens were sheared by applying axial load at a strain rate of 0.25 percent per min. Loading continued for at least 8 min after the peak deviator stress was developed or until the limit of the pinton travel was reached. After completion of shear, the entire specimen was oven-dried at least 16 hr. Density, moisture content, and gradation were then determined.

One-dimensional consolidation tests

34. Consolidation specimens were prepared by placing the required air-dry weight of material into the ring in two layers, vibrating each layer to the desired density. The specimens were loaded incrementally with each load increment remaining on the specimen for at least 24 hr. After completion of consolidation under the final load (800 psi),

specimens were unloaded incrementally and removed from the apparatus. Specimens were oven-dried at least 16 hr. Density, moisture content, and gradation were then determined.

Test Results and Discussion

35. Results for the consolidated-drained triaxial compression tests are summarized in Tables 3 through 8 and presented graphically in Figures 26 through 49. One-dimensional consolidation test results are summarized in Table 9 and presented graphically in Figures 50 through 75. The tests are grouped in the tables and figures according to the effect investigated.

Effects of end restraint, consolidated-drained triaxial tests

36. Angle of internal friction. Curves showing the relationship between confining pressure and angle of internal friction, ϕ', for tests performed on specimens of Napa basalt having the gradation given in Figure 20 using standard and low-friction caps and bases are given in Figure 39. Values of ϕ' were normalized by interpolation to a void ratio value of 0.398 so that effects due to variations in density could be neglected. This figure shows that ϕ' varied similarly with increasing confining pressure for both boundary conditions. In both cases angles of internal friction were reduced by 12.2 deg when confining pressures were increased from 60 to 500 psi. As may be seen, ϕ' values for specimens tested using standard caps and bases were approximately 1 deg higher than those for specimens tested using low-friction caps and bases.

37. Axial strain and volumetric strain at failure. Plots of axial and volumetric strain at failure versus confining pressure are given in Figure 40. The axial strain at failure plots show that strain values at failure increased with increasing confining pressure for both boundary conditions. The rate of increase, however, was lower at the higher confining pressures. With the exception of tests performed at a confining pressure of 500 psi, specimens tested using standard caps and bases

failed at slightly lower strain values than those tested using low-friction caps and bases. Axial strain values at failure ranged from 7.9 to 17.8 percent for specimens tested using standard caps and bases and from 9.0 to 15.1 percent for specimens tested using low-friction caps and bases. The volumetric strain at failure plots show that volumetric strains at failure decreased with increasing confining pressure for both boundary conditions. The boundary conditions, however, did not have a significant effect on the magnitude of the strain values. Values of volumetric strain at failure ranged from +0.6 (expansion) to -7.6 percent (contraction) for specimens tested using standard caps and bases, and from zero to -7.0 percent for specimens tested using low-friction caps and bases.

Effects of particle shape, consolidated-drained triaxial compression tests

38. Angle of internal friction. Relationships between confining pressure and the angle of internal friction, ϕ', for tests performed on crushed and abraided specimens of each material are given in Figures 41 through 43. Values of ϕ' were normalized by interpolation to 100 percent relative density so that variations in density could be neglected. The interpolation was accomplished using ϕ' values from high and medium or low relative density tests and the corresponding specimen relative densities after consolidation. Where necessary, data from previous investigations were used to accomplish the interpolation. As may be seen (Figures 41, 42, and 43), although both more and less angular specimens of each soil had the same gradation, there is a separate relationship for each condition. This should have been expected, of course, since the maximum density of the materials (and therefore the strength) varied with the change in angularity of the particles resulting from crushing or abraiding. Maximum densities obtained for less angular and more angular specimens of each material are as follows:

Material	Less Angular $\gamma_{d\ max}$ pcf	More Angular $\gamma_{d\ max}$ pcf	More Angular $\gamma_{d\ max}$ Minus Less Angular $\gamma_{d\ max}$ pcf
Napa basalt	130.7	131.4	+0.7
Carters Dam quartzite	132.2	117.0	-15.2
Bear River gravel	122.7	116.2	-6.5

It is interesting to note that this tabulation shows that less angular specimens of the Carters Dam quartzite and Bear River gravel materials had significantly higher maximum densities than more angular specimens whereas maximum densities for both crushed and abraided Napa basalt specimens were approximately the same. Figure 44, which is a plot of the change in ϕ' due to the increase in particle angularity (more angular ϕ' minus less angular ϕ') versus confining pressure for all three materials, shows that increasing particle angularity may result in either a positive or negative change in ϕ' and that although the change in ϕ' varies with confining pressure, the relationship between them is such that no conclusions may be made.

39. The effect of the differences in maximum densities on ϕ' values may be seen in Figure 45. For the Napa basalt material where the change in maximum density due to increased particle angularity was only +0.7 pcf, Figure 45 shows that the average change in ϕ' for confining pressures ranging from 60 to 400 psi was +2.0 deg. Since there was little difference in maximum density, most of the change in ϕ' was probably due to the change in particle angularity. In the case of the Carters Dam quartzite specimens (Figure 45) where there was the greatest difference in maximum density (15.2 pcf), the average change in ϕ' due to increased particle angularity was -3.8 deg. The major portion of this change in ϕ' was probably due to the large difference in maximum density rather than the change in particle angularity. According to this figure, ϕ' may be increased by approximately 1 deg in tests on specimens where particle angularity is altered without changing the maximum density. It is interesting to note that in the case of the Bear River gravel material which had naturally rounded particles, crushing

particles (increasing their angularity) actually decreased the average ϕ' value taken at 100 percent relative density.

40. <u>Axial strain and volumetric strain at failure.</u> Plots of axial and volumetric strain at failure, $(\sigma_1 - \sigma_3)_{max}$, versus confining pressure are given in Figures 46 through 48. The plots show that in the case of both angular and less angular specimens, axial strains at failure increased and volumetric strains at failure decreased with increasing confining pressure. In both cases the rate of change in strain values was less at the higher confining pressures. Curves showing the relationship between the change in axial strain at failure due to increased particle angularity versus confining pressure are given in Figure 49. These curves indicate that the change in axial strain at failure due to increased particle angularity generally increased with confining pressure for the Carters Dam quartzite and Bear River gravel materials, and remained relatively unchanged for the Napa basalt material. The relationship between the change in volumetric strain at failure due to increased particle angularity, also given in Figure 49, shows that increased particle angularity resulted in only slight differences in the changes in volumetric strain at failure with increasing confining pressures. Figure 45 shows the average change in axial and volumetric strains at failure plotted as a function of the change in maximum density due to increased particle angularity. As may be seen, the greatest change in axial and volumetric strains at failure due to increased particle angularity occurred for the Carters Dam quartzite material for which the greatest change in maximum density occurred. Napa basalt, which had the smallest change in maximum density due to increased particle angularity, showed the least change in strains at failure. Average changes in axial strain at failure due to increased particle angularity ranged from -1.0 percent for the Napa basalt material to +7.8 percent for the Carters Dam quartzite material. Average changes in volumetric strain at failure due to increased particle angularity ranged from +0.7 percent for the Napa material to -3.8 percent for the Carters Dam material. It is interesting to note that for specimens where particle angularity is altered without changing the maximum density

(Figure 45), the average change in volumetric strain at failure due to increased particle angularity is +0.4 percent and the average change in axial strain at failure is -0.5 percent.

Effects of particle size, one-dimensional consolidation tests

41. Percent consolidation. Values of percent consolidation plotted as a function of maximum particle size are shown in Figure 70. Percent consolidation is defined as the vertical deformation from the initial no-load condition to that under the maximum pressure times 100 divided by the initial specimen height. In the case of these tests, the maximum consolidation pressure was 800 psi. From this figure, it may be seen that percent consolidation decreased with increasing maximum particle size; i.e., with increasing C_u values, for both high and medium density specimens tested both dry and inundated. In all cases the greatest reduction in percent consolidation occurred between maximum particle sizes of 1/4 in. to 1 in., with only slight reductions occurring for particle sizes greater than 1 in. By comparing curves, it may be seen that percent consolidation for medium density specimens was greater than that for high density specimens, and that inundating specimens resulted in higher values of percent consolidation for both high and medium density specimens. Values of percent consolidation ranged from 4.9 to 9.7 percent for inundated, medium density specimens, and from 1.9 to 3.9 percent for dry, high density specimens. The difference in percent consolidation values between dry and inundated conditions for both high and medium density specimens was approximately 2 percent and did not vary significantly with maximum particle size.

42. Relationships between percent consolidation and the coefficient of uniformity, C_u, shown in Figure 71 indicate that, as would be expected, values of percent consolidation for all tests also decreased with increasing C_u values. The greatest reduction in percent consolidation occurred between coefficients of uniformity of 2.9 and 7.0. There was little change in values of percent consolidation for coefficients of uniformity above 7.

43. Curves 1 and 2 in Figure 72 show differences between values

of percent consolidation for dry and inundated specimens plotted against coefficient of uniformity. These curves indicate that effects of inundation were greatest for medium density specimens having coefficients of uniformity, C_u , less than about 9 (specimens having maximum particle sizes less than 2 in.). Effects of inundation were approximately the same for both medium and high density specimens at a C_u value of 10 and were slightly greater for high density specimens at C_u values greater than 10. The greatest difference between the change in values of percent consolidation due to inundation was approximately 3 percent. Curves 3 and 4 in this figure (Figure 72) show differences in percent consolidation between saturated and unsaturated specimens computed using changes in height based on a consolidation pressure of 120 psi. These curves were included to indicate effects due to inundation at a lower consolidation pressure. As may be seen (from curves 3 and 4), effects due to inundation were slightly greater for medium density specimens over the entire range of coefficients of uniformity tested (from 2.9 to 12.3). In this case, however, the greatest difference between the change in values of percent consolidation due to inundation was approximately 0.4 percent as compared to a difference of approximately 1 percent based on the 800 psi consolidation pressure, thus indicating that effects due to inundation may not be as great at lower stress levels.

44. <u>Compression index.</u> Compression index, C_c , was calculated from the void ratio-pressure curves using the following equation:

$$C_c = \frac{e_1 - e_2}{\log_{10}p_2 - \log_{10}p_1}$$

where p_1 and p_2 are selected pressures from the straight-line portion of the curve, and e_1 and e_2 are the corresponding void ratios. Since the void ratio-pressure curves did not develop a straight-line at higher pressures, the 250- and 800-psi pressures were used to calculate compression index.

45. Curves showing the relationship between compression index and

maximum particle size are given in Figure 73. These curves show that compression index values for inundated specimens are reduced by approximately 50 percent and those for dry specimens are reduced by approximately 30 percent when the maximum particle size is increased from 1/4 in. to 2 in. In both cases the values are relatively unchanged when maximum particle sizes are increased above 2 in. Compression index values for the dry specimens varied from 0.15 to 0.06 for the medium density specimens and from 0.08 to 0.05 for the high density specimens. In the case of inundated specimens, compression index values ranged from 0.20 to 0.09 for the medium density specimens and from 0.13 to 0.07 for the high density specimens.

46. Plots of compression index versus coefficient of uniformity for all tests are given in Figure 74. As may be seen, in each case the compression index values decreased with increasing values of coefficient of uniformity. The greatest reduction in compression index values occurred between coefficients of uniformity of 2.9 and 9.5. There was no significant change in compression index values for coefficients of uniformity above 9.5.

47. Figure 75 shows differences between dry and inundated C_c values plotted against maximum particle size. These plots (Figure 75) show that effects on C_c values due to inundation were greatest for maximum particle sizes lower than 1 in. Differences between C_c values for dry and inundated specimens ranged from 0.055 to 0.082 for medium density specimens and from 0.048 to 0.015 for high density specimens.

Conclusions

48. Based on the results of the tests performed in these investigations, the following conclusions have been drawn.

49. Consolidated-drained triaxial compression tests.

a. End restraint.

(1) There was a slight reduction (approximately 1 percent) in the valve obtained for the angle of internal friction, ϕ', due to the use of low friction end restraints as compared with standard caps and bases and specimen height to diameter ratios of 2.

(2) Generally increased end restraint imposed by standard caps and bases results in slightly lower axial strains at failure.

(3) Increased end restraint imposed by standard caps and bases does not significantly affect volumetric strain at failure.

b. Particle shape.

(1) Where specimens of a given material and gradation are prepared at 100 percent relative density, the change in angle of internal friction, ϕ' , due to increased particle angularity may be positive or negative, depending on the change in maximum density resulting from crushing or abraiding particles. The magnitude of the change in ϕ' due to increased particle angularity may be as high as ± 3 deg.

(2) In tests where the angularity of particles is altered without changing the maximum density, there may be an increase in the angle of internal friction of approximately 1 deg due to increased particle angularity.

(3) In the case of a material having well rounded particles, crushing particles (increasing their angularity) may actually decrease the angle of internal friction taken at 100 percent relative density since the maximum density of the crushed material may be much lower than that of the uncrushed material.

(4) Where specimens of a given material and gradation are prepared to 100 percent relative density, the change in axial and volumetric strain at failure due to increased particle angularity may be positive or negative, depending on the extent to which maximum density is changed by the increased particle angularity.

50. One-dimensional consolidation tests.

a. Compression index and percent consolidation values decrease with increasing maximum particle size, i.e., increasing C_u values, for both dry and inundated specimens tested at both high and medium relative densities. The greatest reduction in these values occurs between maximum particle sizes of 1/4 and 1 in.

b. Compression index and percent consolidation values are not significantly changed when maximum particle sizes are increased in the range from 2 to 3 in., thus suggesting that compression index and percent consolidation values determined from tests performed on specimens having 2-in. maximum particle sizes may be used to represent those having greater particle sizes.

c. Compression index and percent consolidation values based on a maximum consolidation pressure of 800 psi are increased approximately 30 percent when specimens are inundated. At lower consolidation pressures, effects of inundation may not be as great.

Table 1

Previous Reports by the South Pacific Division Laboratory on Rock-Fill Materials

Title	Publication Date
Shear Strength of Rock Fill, Physical Properties, Engineering Study No. 526	October 1975
Shear Strength of Rock Fill, Alluvial Gravel, Engineering Study 526	March 1972
Shear Strength of Rock Fill, Engineering Study 526. Crushed Basalt and Metavolcanic Straight-Line Gradations	December 1967
"R" Type Triaxial Compression Tests on Gravel, Civil Works Investigation No. 521-C	November 1963
Triaxial Shear Tests on Sands and Gravels. Civil Works Investigation No. 521-B, Combined Report	September 1961
Effect of Rock Sizes on Shear Strength, Civil Works Investigation No. 488, Interim Report	February 1956
Shear Strength of Gravelly Soils, Civil Works Investigation No. 512	March 1953

Table 2

Physical Properties

Rock	Los Angeles Abrasion Loss, % Grading A	Grading B	Soundness by Mg SO_4. Loss, % Coarse	Fine	Average	Unconfined Compressive Strength* psi	Scratch Hardness Moh's Scale	Shape Factor r_v
Napa basalt	15	13	2	11	3	30,000	6	0.73
New Hogan Dam metavolcanic	13	12	1	10	2	20,000	5-1/2 to 6	0.62
Carters Dam quartzite	26	25	1	10	2	30,000	5-1/2 to 6	0.65
Cougar Dam basalt	21	21	6	42	10	17,000	6	0.54
Sonora dolomite	42	47	2	43	7	24,000	5	0.66
Buchanan Dam granite	69	93	25	40	27	10,000**	4	0.64
Laurel Dam sandstone	86	99	95	54	91	--†	4-1/2	0.59

* Tests performed on 2-in.-diam cores drilled from boulders.

** Core was less weathered than average material used for all other tests.

† Particles sufficiently large to drill 2-in.-diam core were not available.

Table 3

Triaxial Compression Test Data, ES 526, Napa Basalt, End-Restraint Study,

1 in. to No. 30 Gradation (See Figure 20)

	High Density															
	Compaction Test		Specimen Test Conditions									Shear Data				
			Before Consolidation				After Consolidation									
Test No.	Maximum Density pcf	Minimum Density pcf	Density pcf*	Density pcf**	Void Ratio**	D_r %†	Density pcf	Void Ratio	D_r %	Water Content %	Saturation %	σ_3 psi	Maximum Deviator Stress psi	Strain at Maximum $\sigma_1 - \sigma_3$	Void Ratio at Failure	ϕ Degrees
							Low Friction Specimen Ends									
268	124.1	98.5	126.6	127.8	0.397	100	128.6	0.388	102	13.4	99	60	363.5	8.8	0.348	48.8
269			126.3	127.6	0.398	100	129.8	0.375	105	13.1	100	125	594.7	10.9	0.344	44.7
270			126.7	127.6	0.399	100	131.1	0.361	109	12.6	100	300	1161	17.1	0.291	41.2
271			126.7	127.6	0.399	100	133.2	0.340	114	11.8	99	500	1563	15.1	0.252	37.5
							Regular Specimen Ends									
272	124.1	98.5	126.6	126.9	0.407	98	128.1	0.393	101	13.6	99	60	388.5	8.0	0.458	49.8
273			126.5	126.9	0.406	98	129.1	0.383	103	13.4	100	125	618.0	9.7	0.380	45.4
274			126.5	126.9	0.406	98	130.0	0.372	106	13.0	100	300	1174	16.3	0.296	41.4
275			126.5	127.4	0.401	99	132.5	0.343	113	12.1	100	500	1737	17.7	0.238	39.4

Note: Coefficient of uniformity, 6.7; coefficient of curvature, 0.7; specimen diameter, 5.9 in.; and specimen height, 13.8 in.

* By vibration.

** After evacuation at 14 psi.

† Computed from maximum value in 5th column of table.

Table 4

Triaxial Compression Test Data, ES 526, Napa Basalt, End-Restraint Study, 1 in. to No. 30 Gradation (See Figure 20)

Test No.	Compaction Test: Maximum Density pcf	Compaction Test: Minimum Density pcf	Before Consolidation: Density pcf*	Before Consolidation: Density pcf**	Before Consolidation: Void Ratio**	Before Consolidation: D_r %†	After Consolidation: Density pcf	After Consolidation: Void Ratio	After Consolidation: D_r %	After Consolidation: Water Content %	After Consolidation: Saturation %	σ_3 psi	Maximum Deviator Stress psi	Strain at Maximum $\sigma_1 - \sigma_3$	Void Ratio at Failure	ϕ Degrees
							Low Friction Specimen Ends									
276	124.1	98.5	116.6	117.6	0.518	71	120.2	0.484	79	16.9	100	60	297.9	12.6	0.461	45.5
277			116.8	117.8	0.515	72	121.6	0.468	83	16.2	99	125	479.9	16.2	0.403	41.1
278			117.0	117.8	0.515	72	124.6	0.432	92	15.0	99	300	1015	26.3	0.304	38.9
279			116.8	117.4	0.520	70	127.1	0.404	98	14.1	100	500	1403	24.4	0.273	35.7
							Regular Specimen Ends									
280	124.1	98.5	117.2	118.7	0.503	74	121.1	0.474	81	16.4	99	60	287.6	9.7	0.448	44.9
281			117.1	117.8	0.515	72	121.8	0.465	84	16.3	100	125	508.6	16.1	0.403	42.1
282			116.9	117.9	0.514	72	125.8	0.419	95	14.6	99	300	1079	21.1	0.300	40.0
283			116.9	117.3	0.521	70	128.1	0.393	101	13.8	100	500	1562	22.1	0.268	37.5

Medium Density; Specimen Test Conditions; Shear Data (σ_3 through ϕ).

Note: Coefficient of uniformity, 6.7; coefficient of curvature, 0.7; specimen diameter, 5.9 in.; and specimen height, 13.8 in.
* By vibration.
** After evacuation at 14 psi.
† Computed from maximum value in 5th column of table.

Table 5

Triaxial Compression Test Data, ES 526, Particle Shape Study, Napa Basalt (For Gradation, See Figure 21)

	Specimen Test Conditions											Shear Data				
	Compaction Test		Before Consolidation				After Consolidation									
Test No.	Maximum Density pcf	Minimum Density pcf	Density pcf*	Density pcf**	Void Ratio**	D_r %†	Density pcf	Void Ratio	D_r %	Water Content %	Saturation %	σ_3 psi	Maximum Deviator Stress psi	Strain at Maximum $\sigma_1 - \sigma_3$	Void Ratio at Failure	ϕ Degrees
							Subangular Rock									
196	130.7	108.7	128.8	130.7	0.365	100	131.8	0.354	104	11.7	95	60	350.5	13.4	0.335	48.2
197			128.6	128.8	0.385	93	131.2	0.360	102	11.9	94	125	603.4	14.1	0.302	45.0
198			128.4	130.2	0.371	98	134.5	0.327	114	11.0	96	300	992	17.8	0.243	38.5
199			128.3	130.0	0.373	97	135.1	0.321	116	10.6	94	400	1300	18.8	0.231	37.5
							Pit Run									
206	131.4	103.5	129.1	130.9	0.363	99	132.3	0.349	102	11.7	96	60	428.8	12.0	0.334	51.3
207			129.3	131.4	0.358	100	133.9	0.332	107	11.4	98	125	621.0	16.7	0.295	45.5
208			129.3	131.2	0.361	100	135.5	0.317	111	11.1	100	300	1131	13.4	0.247	40.8
209			129.0	130.0	0.373	96	135.8	0.314	112	10.8	98	400	1439	18.4	0.230	40.0

Note: Coefficient of uniformity, 9.0; coefficient of curvature, 1.5; specimen diameter, 12.0 in.; and specimen height, 27.6 in.
* By vibration.
** After evacuation at 14 psi.
† Computed from maximum value in 5th column of table.

Table 6

Triaxial Compression Test Data, ES 526, Particle Shape Study,

Carters Dam Quartzite (For Gradation, See Figure 21)

	Specimen Test Conditions											Shear Data				
	Compaction Test		Before Consolidation				After Consolidation									
Test No.	Maximum Density pcf	Minimum Density pcf	Density pcf*	Density pcf**	Void Ratio**	D_r %†	Density pcf	Void Ratio	D_r %	Water Content %	Saturation %	σ_3 psi	Maximum Deviator Stress psi	Strain at Maximum $\sigma_1 - \sigma_3$	Void Ratio at Failure	ϕ Degrees
								Angular								
180	117.0	95.1	119.3	120.6	0.413	96	123.0	0.385	104	12.4	88	60	328	14.6	0.288	47.1
181			119.5	120.7	0.412	97	124.1	0.372	107	12.3	90	125	563	16.6	0.277	43.8
182			119.5	121.7	0.399	100	129.2	0.319	120	11.4	98	300	1147	21.9	0.205	41.0
183			118.7	121.4	0.403	99	130.8	0.303	124	10.7	96	400	1352	21.7	0.193	38.9
184	117.0	95.1	95.9	98.3	0.733	15	101.9	0.672	31	22.5	91	60	206	30.0	0.436	39.1
185			96.0	99.4	0.714	20	106.9	0.594	50	21.1	97	125	419	31.9	0.304	38.8
186			96.4	101.2	0.684	27	117.3	0.452	86	14.0	85	300	915	28.9	0.244	37.1
187			96.4	100.9	0.688	26	118.3	0.440	90	16.0	99	400	1122	28.3	0.246	35.7
								Subangular								
228	132.2	108.7	131.4	131.8	0.293	98	133.4	0.277	104	10.1	99	60	340.5	7.7	0.286	47.7
229			131.9	132.2	0.289	100	133.8	0.273	105	8.9	88	125	663.3	10.3	0.261	46.5
230			131.2	131.7	0.293	98	133.6	0.275	105	9.4	94	125	639.3	10.5	0.267	46.0
231			132.1	132.2	0.287	100	135.5	0.255	112	8.8	94	300	1268	13.1	0.198	42.8
232			131.4	132.0	0.290	99	136.6	0.247	115	8.7	96	400	1514	12.3	0.181	40.9

Note: Coefficient of uniformity, 9.0; coefficient of curvature, 1.5; specimen diameter, 12.0 in.; and specimen height, 27.6 in.
* By vibration.
** After evacuation at 14 psi.
† Computed from maximum value in 5th column of table.

Table 7

Triaxial Compression Test Data, ES 526, Particle Shape Study,

Bear River Gravel (For Gradation, See Figure 21)

Crushed

Test No.	Compaction Test: Maximum Density pcf	Compaction Test: Minimum Density pcf	Before Consolidation: Density pcf*	Before Consolidation: Density pcf**	Before Consolidation: Void Ratio**	Before Consolidation: D_r %†	After Consolidation: Density pcf	After Consolidation: Void Ratio	After Consolidation: D_r %	After Consolidation: Water Content %	After Consolidation: Saturation %	Shear Data: σ_3 psi	Shear Data: Maximum Deviator Stress psi	Shear Data: Strain at Maximum $\sigma_1 - \sigma_3$	Shear Data: Void Ratio at Failure	Shear Data: ϕ Degrees
258	116.2	96.0	120.1	120.7	0.380	100	122.6	0.359	108	13.4	100	60	273.3	5.2	0.367	44.0
259			120.1	120.4	0.385	99	122.3	0.362	107	13.5	99	125	483.6	6.1	0.355	41.2
260			119.9	120.4	0.384	99	124.0	0.343	113	12.7	99	300	991.2	13.3	0.299	38.5
261			119.8	120.0	0.388	98	124.9	0.334	115	12.3	99	450	1401	16.3	0.270	37.5
262			111.4	112.8	0.477	73	114.5	0.455	80	16.8	99	60	203.7	10.1	0.437	39.0
263			111.4	112.2	0.484	71	114.6	0.454	81	16.6	98	125	386.8	17.2	0.406	37.4
264			111.3	112.8	0.477	73	117.1	0.423	90	15.6	99	300	864.8	19.8	0.319	36.2
265			111.4	112.7	0.479	72	119.4	0.396	98	14.7	99	450	1299	22.7	0.276	36.2

Note: Coefficient of uniformity, 6.67; coefficient of curvature, 0.68; specimen diameter, 5.9 in.; specimen height, 13.8 in.; and specific gravity, 2.67.

* By vibration.

** After evacuation at 14 psi.

† Computed from maximum value in 5th column of table.

Table 8

Triaxial Compression Test Data, ES 526, Particle Shape Study, Bear River Gravel (For Gradation, See Figure 21)

Uncrushed

	Specimen Test Conditions											Shear Data					
	Compaction Test		Before Consolidation				After Consolidation										
Test No.	Maximum Density pcf	Minimum Density pcf	Density pcf*	Density pcf**	Void Ratio**	D_r %+	Density pcf	Void Ratio	D_r %	Water Content %	Saturation %	σ_3 psi	Maximum Deviator Stress psi	Strain at Maximum $\sigma_1 - \sigma_3$	Void Ratio at Failure	ϕ Degrees
250	122.7	103.3	126.2	126.8	0.314	97	127.8	0.303	101	11.2	99	60	282.9	3.7	0.319	44.6
251			125.8	127.6	0.306	100	128.6	0.296	103	10.9	98	125	514.8	3.9	0.300	42.3
252			125.8	126.7	0.315	97	129.4	0.288	106	10.8	100	300	963.9	7.6	0.270	38.1
253			125.1	125.8	0.324	94	130.4	0.278	109	10.5	100	450	1386	11.8	0.246	37.4
254			117.8	119.0	0.400	69	121.0	0.377	77	14.0	99	60	218.5	6.0	0.385	40.2
255			117.9	118.6	0.405	68	121.2	0.375	77	14.0	100	125	401.5	6.7	0.366	38.0
256			117.6	118.9	0.401	69	122.0	0.366	80	13.5	99	300	899.7	16.1	0.317	36.9
257			117.8	118.7	0.404	68	122.6	0.359	83	13.2	98	450	1299	20.8	0.277	36.2

Note: Coefficient of uniformity, 6.67; coefficient of curvature, 0.68; specimen diameter, 5.9 in.; specimen height, 13.8 in.; and specific gravity, 2.67.

* By vibration.

** After evacuation at 14 psi.

† Computed from maximum value in 5th column of table.

Table 9

Summary of One-Dimensional Consolidation Test Results

Napa Basalt

				Specimen Conditions						Consolidation Data		
				Before Test			After Test					
Test No.	Maximum Particle Size in.	Coefficient of Uniformity C_u	Type of Test	Water Content %	Void Ratio e	Dry Unit Weight pcf	Water Content %	Void Ratio e	Saturation %	Compression Index* C_c	Percent Consolidation**	Percent Rebound†
						High Density Tests						
1	3	12.3	Saturated††	0	0.347	132.5	10.6	0.312	97	0.065	3.6	1.1
2			Unsaturated	0	0.342	133.0	0	0.313	0	0.050	1.7	0.9
3	2	9.5	Saturated††	0	0.373	130.0	10.2	0.334	88	0.071	4.1	1.3
4			Unsaturated	0	0.364	130.8	0	0.339	0	0.051	3.0	1.2
5	1	6.6	Saturated††	0	0.415	126.2	10.6	0.364	84	0.085	4.7	1.2
6			Unsaturated	0	0.420	125.7	0	0.382	0	0.073	4.2	1.5
7	1/2	4.8	Saturated††	0	0.472	121.2	12.2	0.417	84	0.099	4.9	1.2
8			Unsaturated	0	0.466	121.9	0	0.435	0	0.061	3.3	1.2
9	1/4	2.9	Saturated††	0	0.556	114.7	16.5	0.482	97	0.125	5.9	1.2
10			Unsaturated	0	0.555	114.8	0	0.514	0	0.077	3.9	1.3
						Medium Density Tests						
11	3	12.3	Saturated††	0	0.388	128.6	10.9	0.329	92	0.087	4.9	0.7
12			Unsaturated	0	0.388	128.6	0	0.355	0	0.053	3.5	1.1
13	2	9.5	Saturated††	0	0.428	124.5	11.8	0.388	92	0.101	5.4	2.7
14			Unsaturated	0	0.429	124.5	0	0.388	0	0.071	4.1	1.2
15	1	6.6	Saturated††	0	0.467	121.2	12.0	0.406	85	0.101	5.5	1.4
16			Unsaturated	0	0.469	121.0	0	0.419	0	0.077	4.2	0.9
17	1/2	4.8	Saturated††	0	0.567	113.9	14.0	0.457	88	0.162	8.4	1.5
18			Unsaturated	0	0.564	114.1	0	0.490	0	0.117	6.1	1.4
19	1/4	2.9	Saturated††	0	0.654	107.9	14.9	0.516	83	0.202	9.7	1.5
20			Unsaturated	0	0.653	108.0	0	0.564	0	0.147	6.8	1.6

Note: All gradations were straight lines with the smallest particle size in each case being that retained on the No. 30 sieve.

* The 250 and 800 psi pressures and the corresponding void ratios were used to compute the compression index since the void ratio - pressure curves did not develop a straight line at higher pressures.

** Percent consolidation is defined as the vertical deformation from the initial no load condition to the maximum pressure multiplied by 100 divided by the initial specimen height.

† Percent rebound is defined as the vertical deformation from the maximum pressure to the final no load condition divided by the height of the specimen under the maximum pressure multiplied by 100.

†† Saturated specimens were inundated under a consolidation pressure of 15 psi.

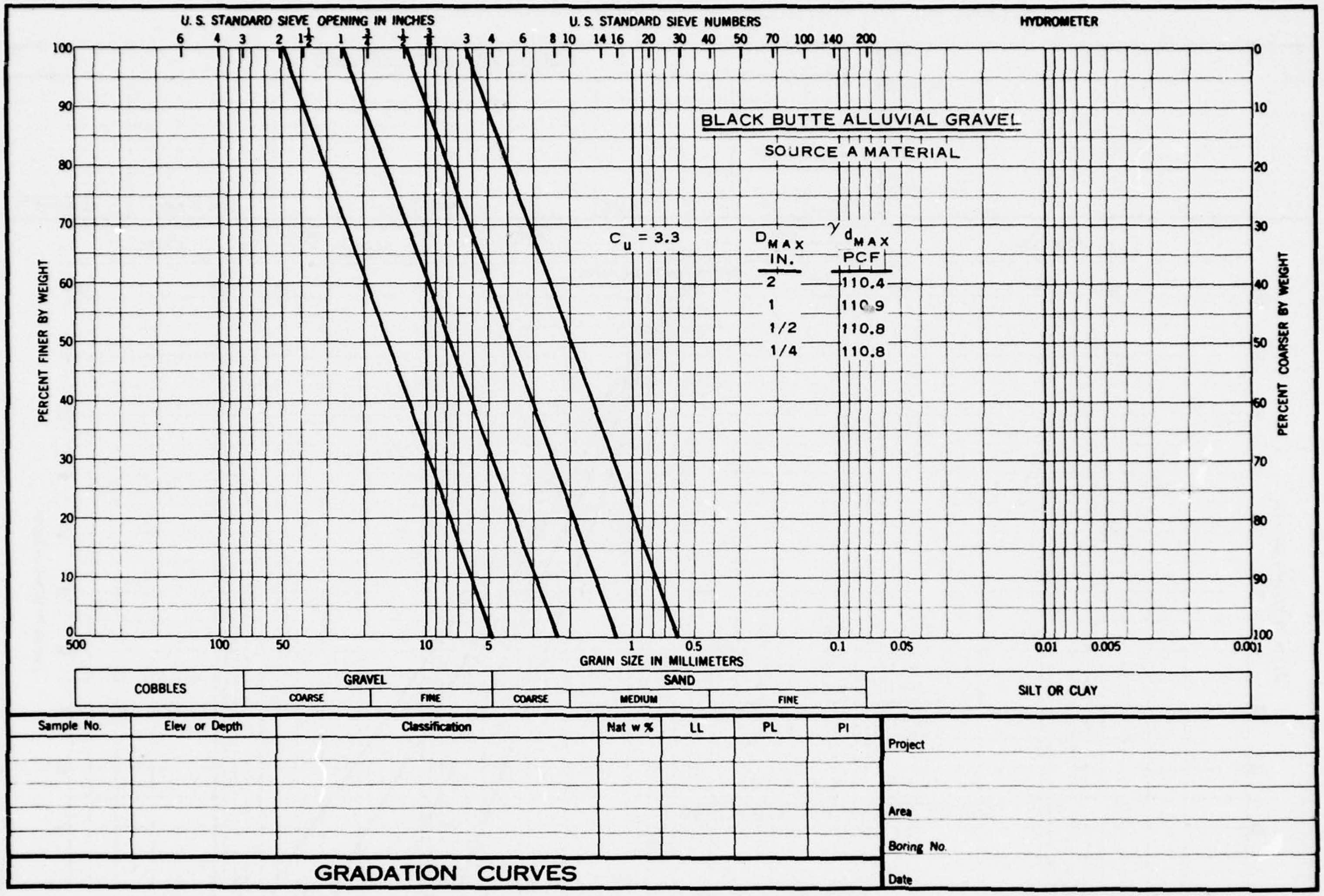

Figure 1. Modeled gradations having constant coefficient of uniformity, C_u

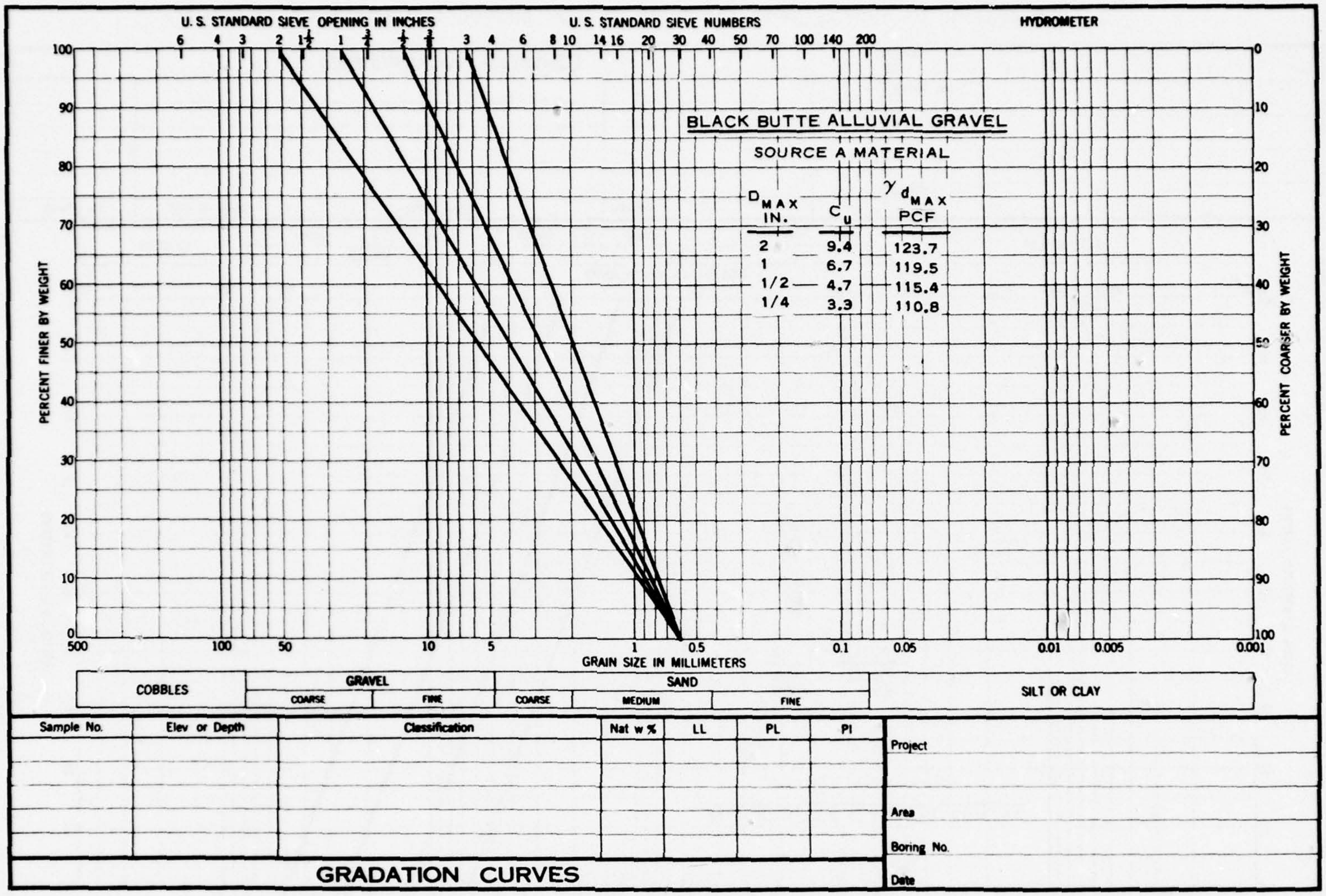

Figure 2. Gradations having variable coefficients of uniformity, C_u

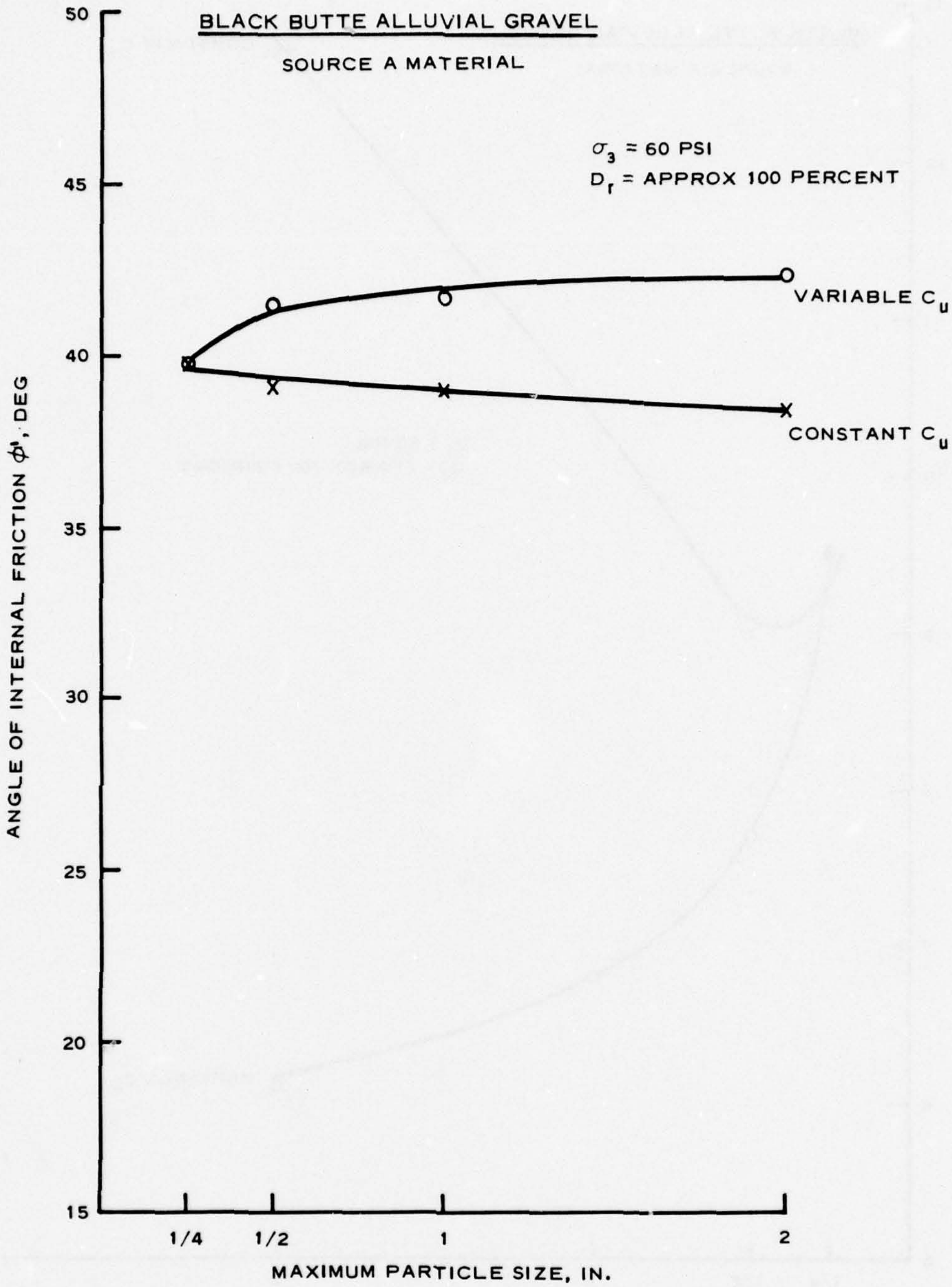

Figure 3. Angle of internal friction, ϕ' , versus maximum particle size, effects of gradation study

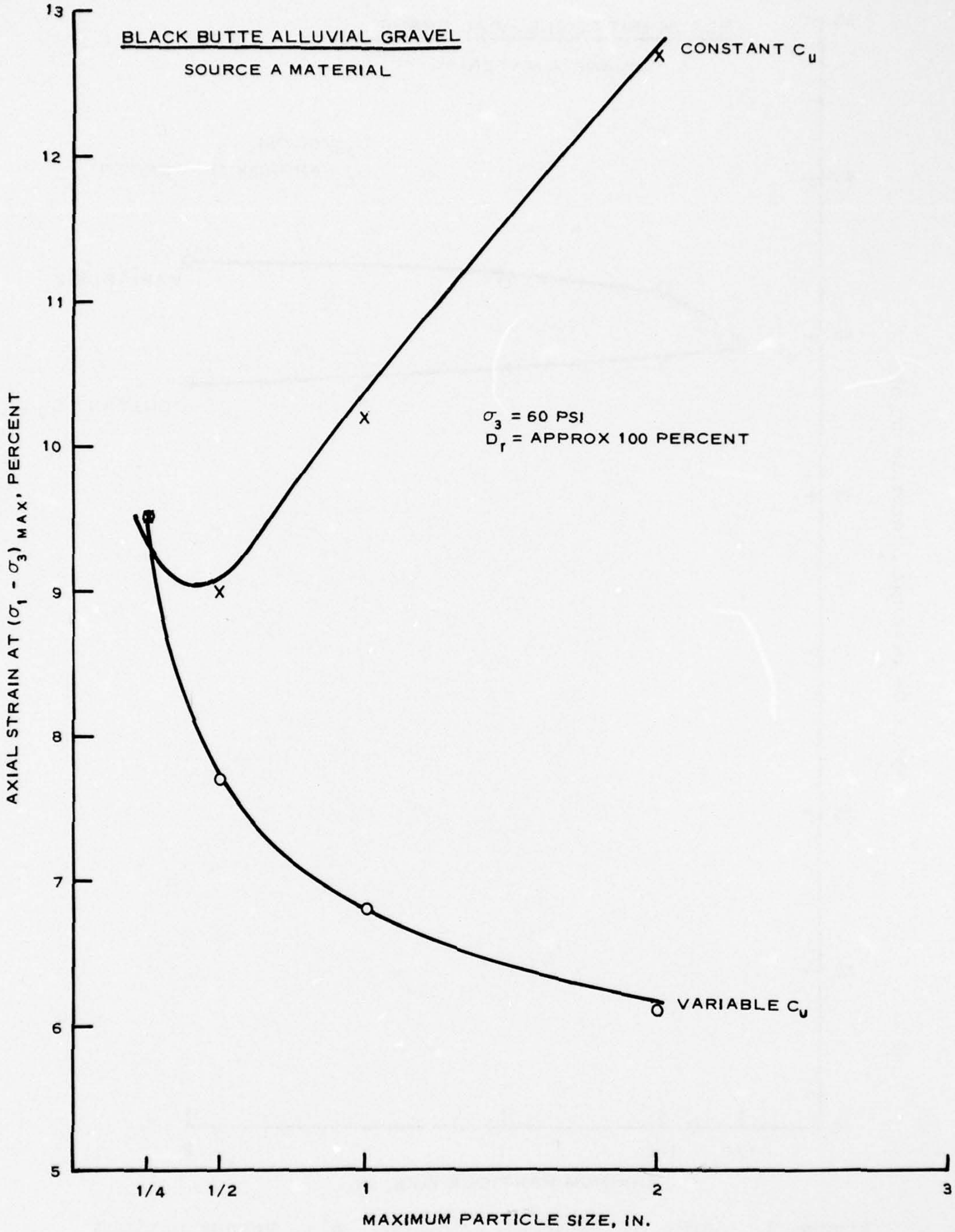

Figure 4. Axial strain at maximum deviator stress $(r_1 - r_3)_{max}$, versus maximum particle size, effects of gradation study

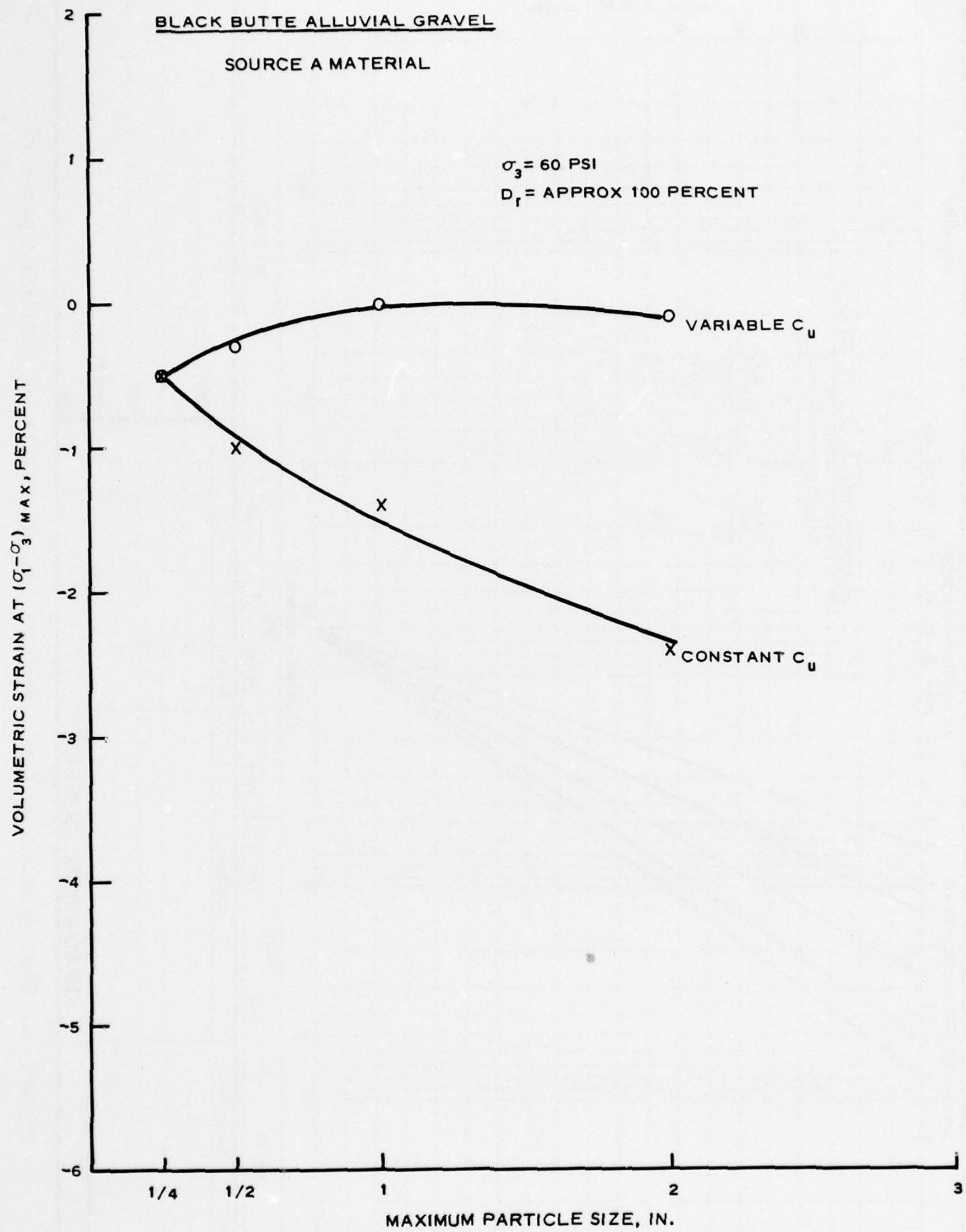

Figure 5. Volumetric strain at maximum deviator stress $(r_1 - r_3)_{max}$, versus maximum particle size, effects of gradation study

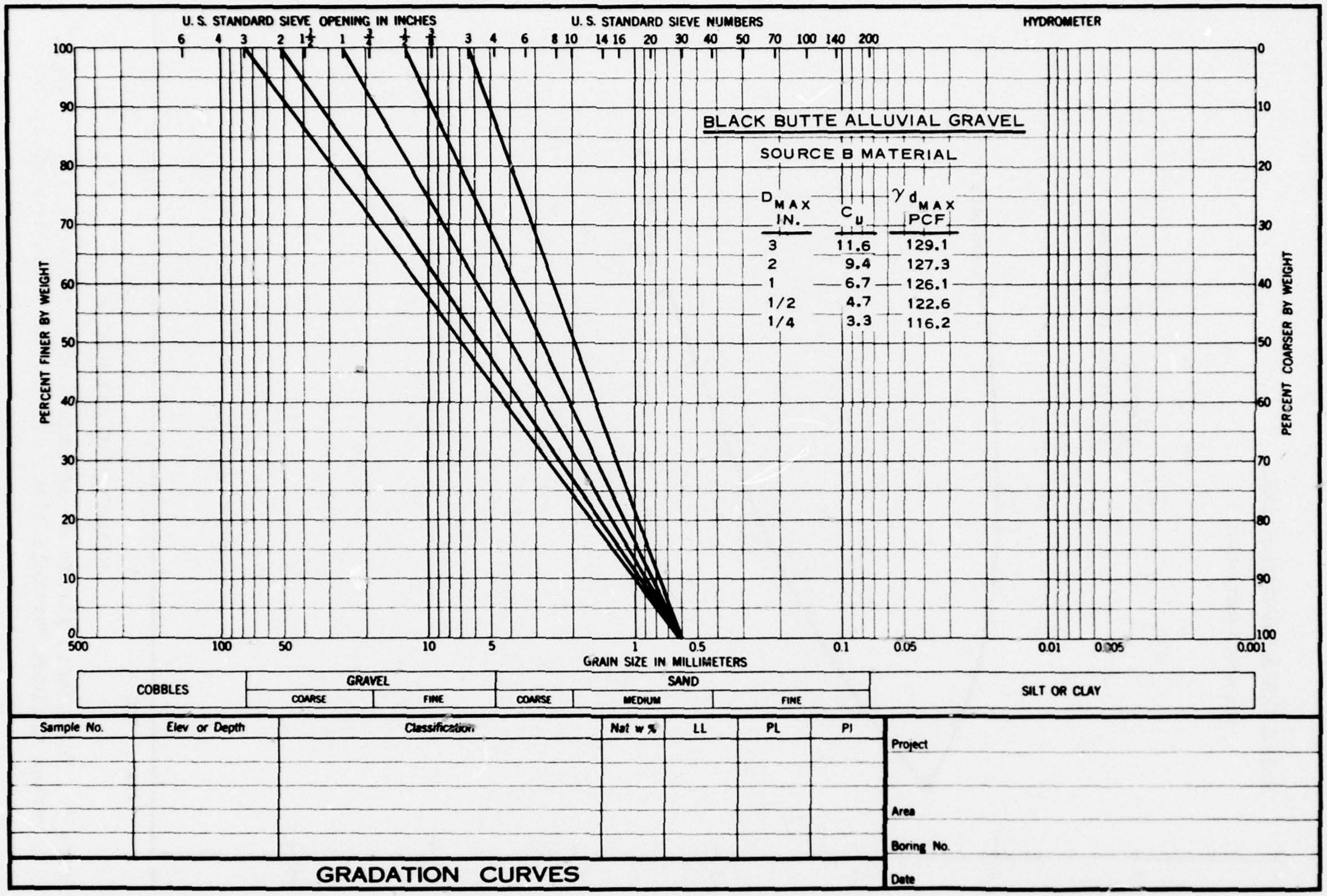

Figure 6. Test gradations for investigation of effects of confining pressure

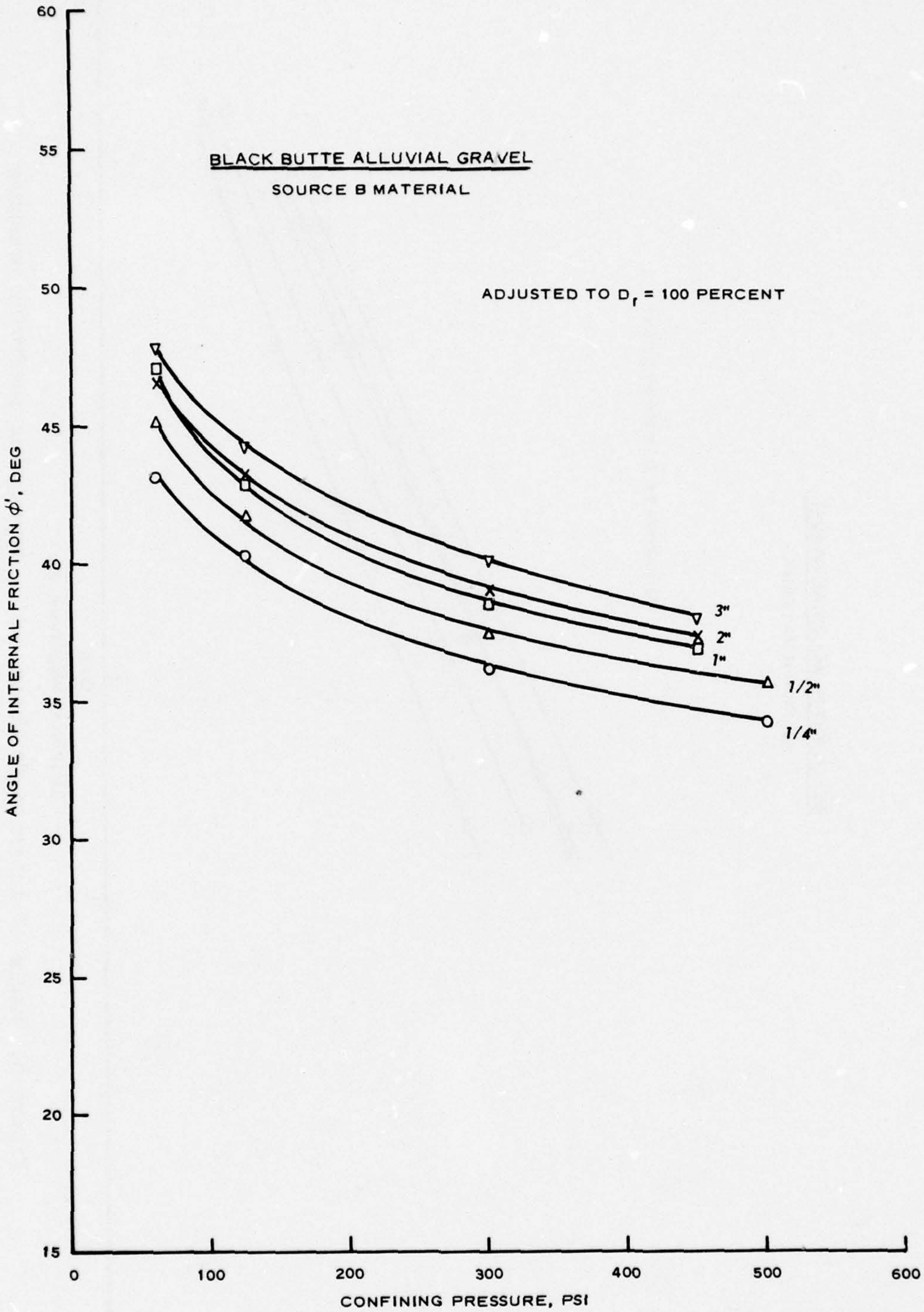

Figure 7. Angle of internal friction, ϕ' , versus confining pressure, effects of confining pressure study

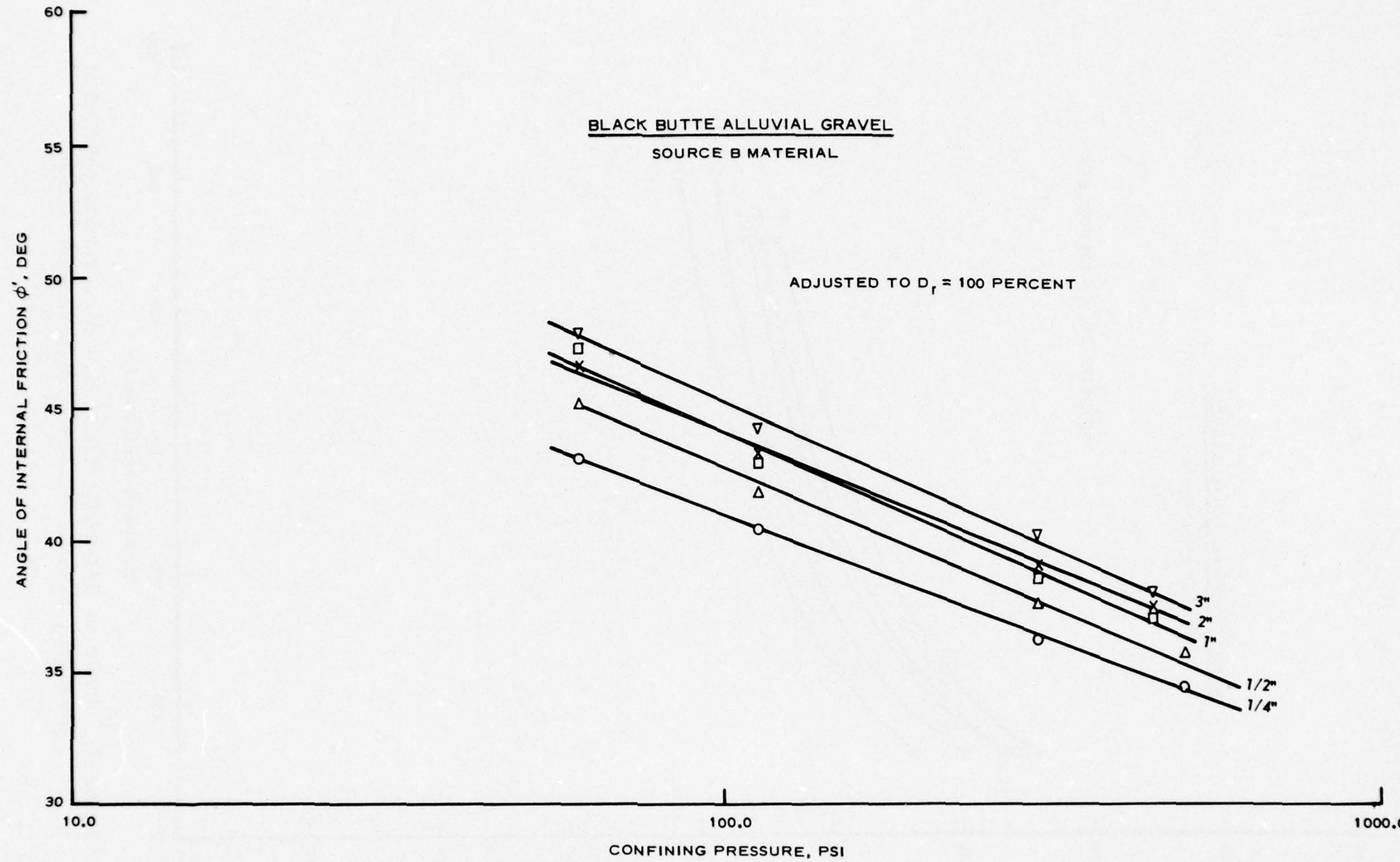

Figure 8. Angle of internal friction, ϕ' , versus log confining pressure effects of confining pressure study

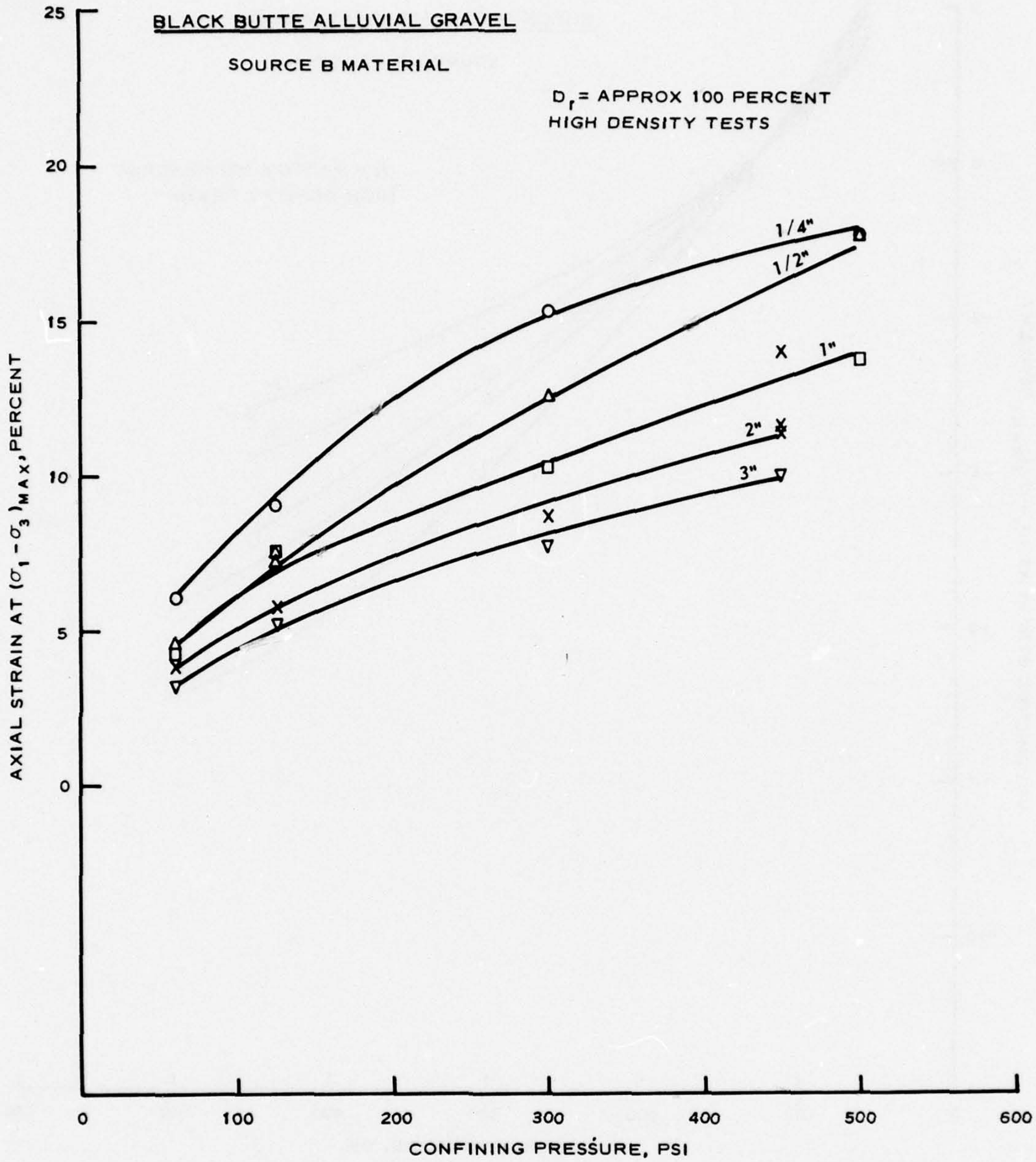

Figure 9. Axial strain at maximum deviator stress $(\sigma_1 - \sigma_3)_{max}$, versus confining pressure, effects of confining pressure study

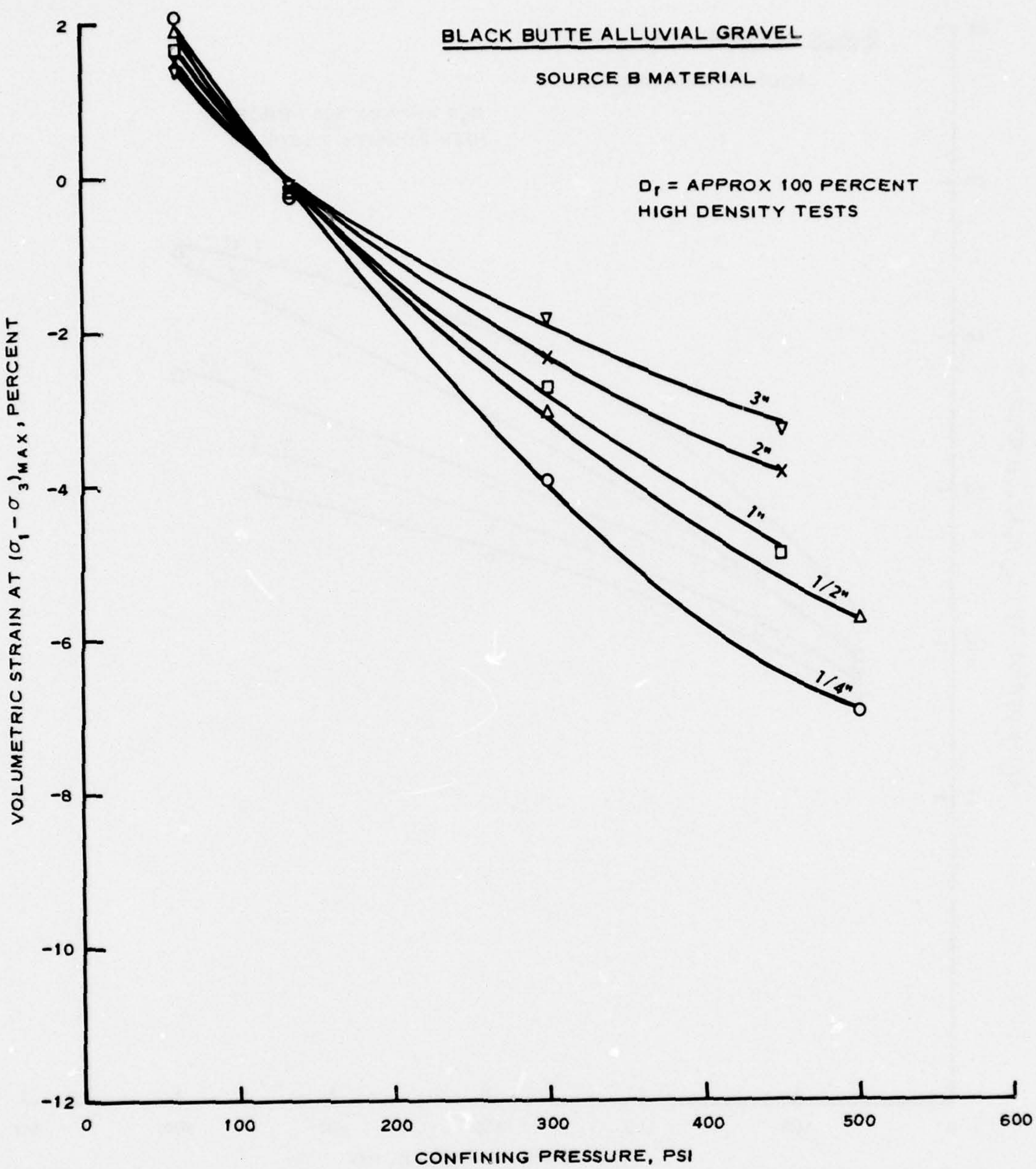

Figure 10. Volumetric strain at maximum deviator stress $(r_1 - r_3)_{max}$, versus confining pressure, effects of confining pressure study

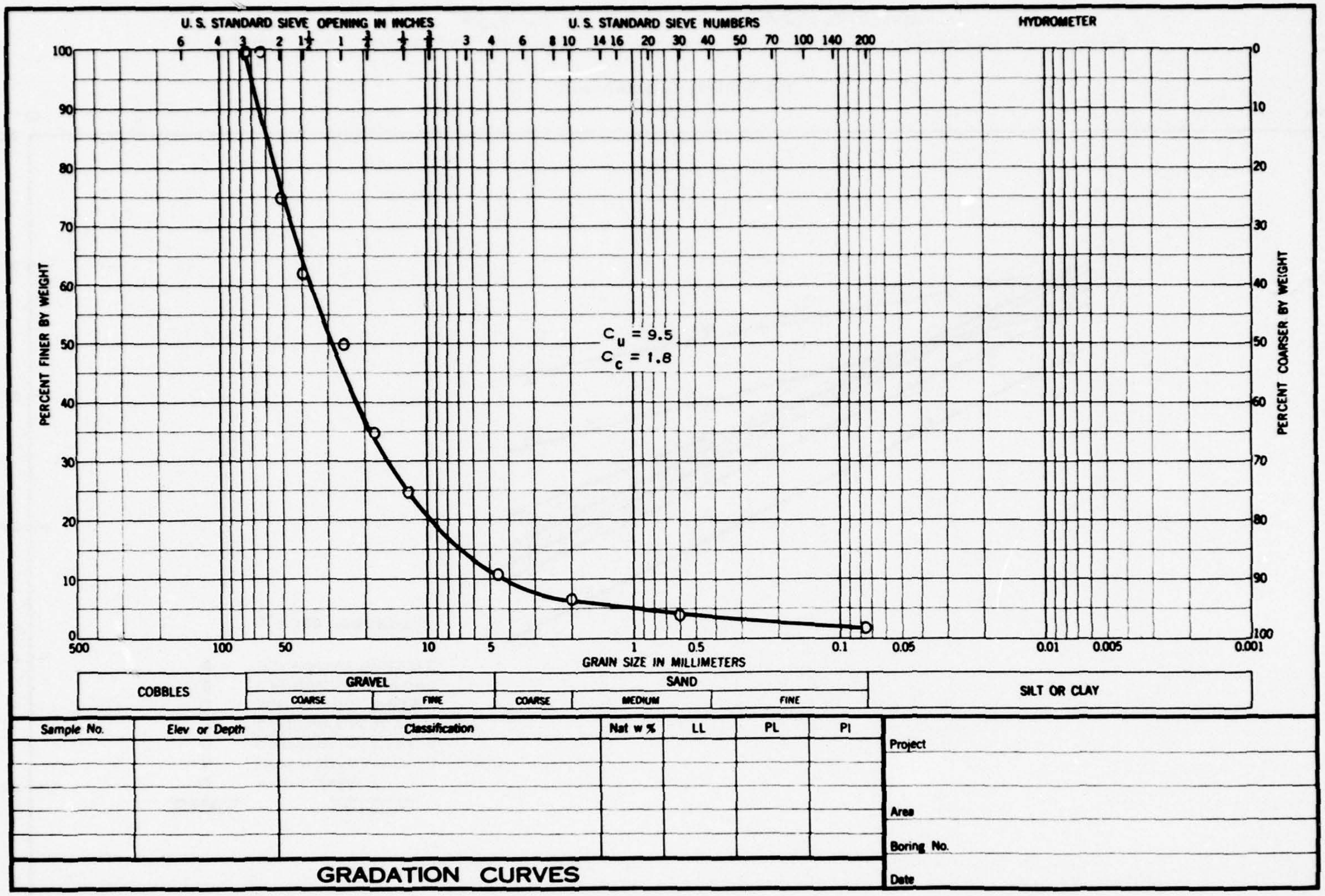

Figure 11. Test gradation for investigation of effects of physical properties

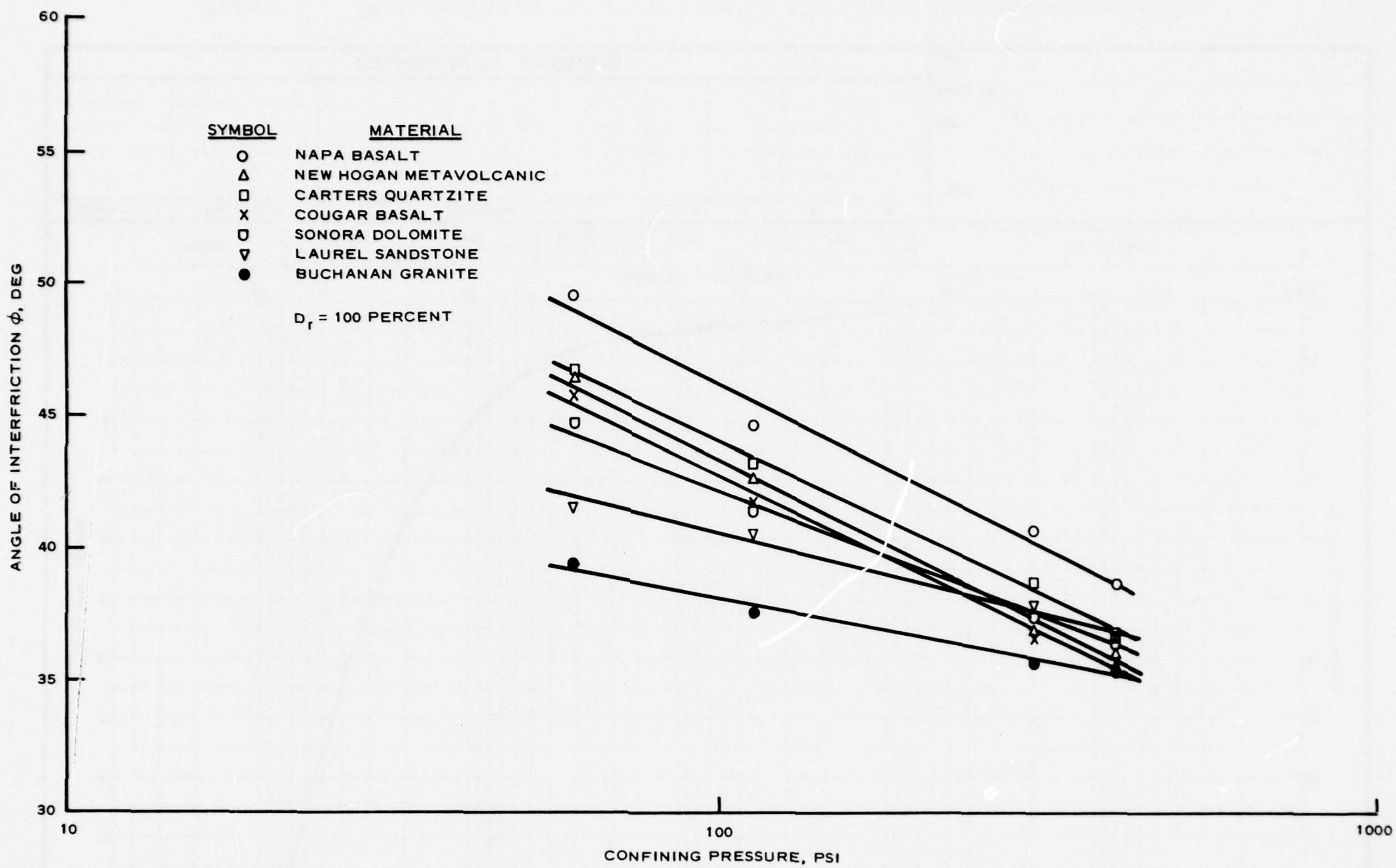

Figure 12. Angle of internal friction, ϕ' , versus confining pressure, effects of physical properties study

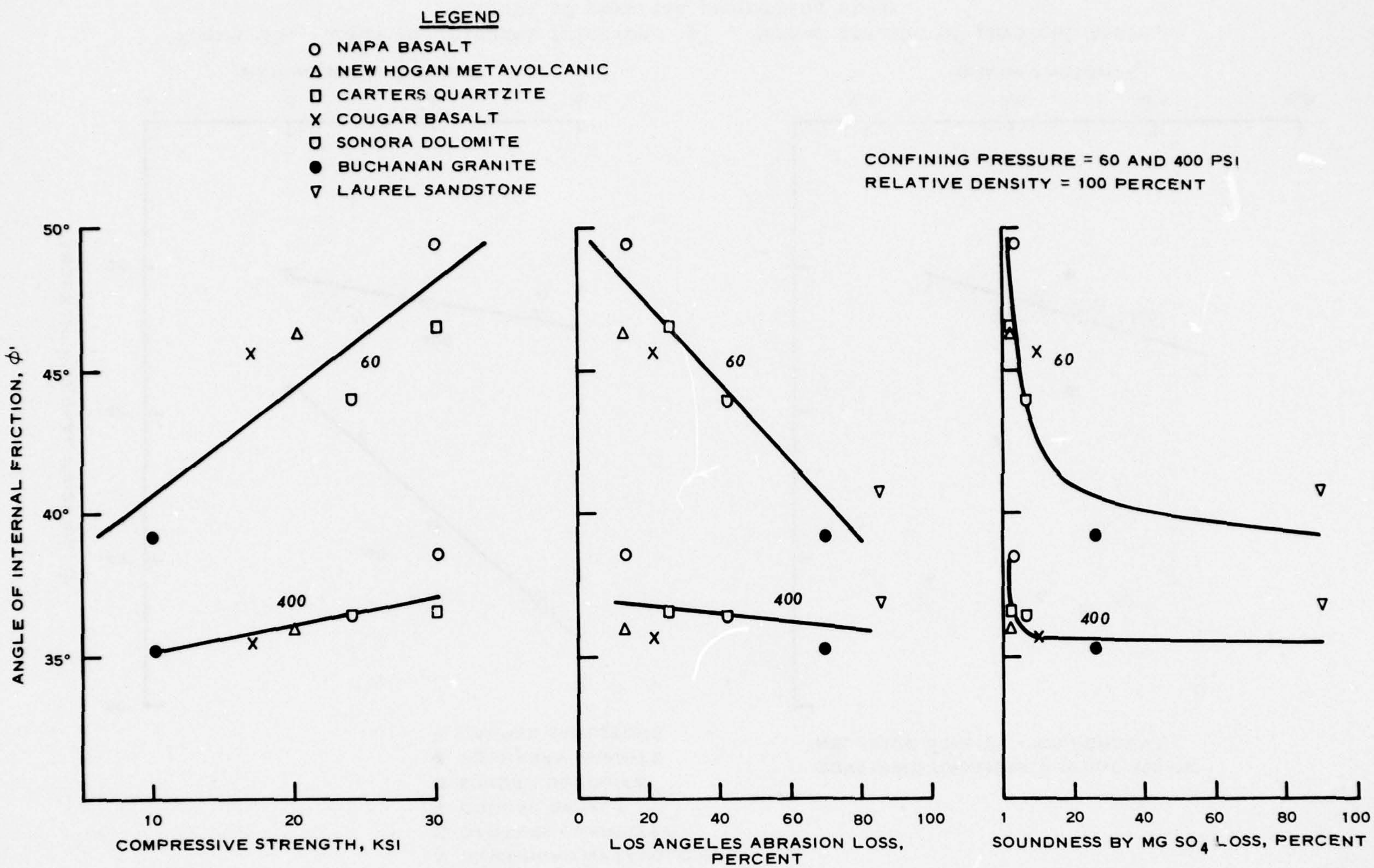

Figure 13. Angle of internal friction, φ' , versus results of physical tests, effects of physical properties study

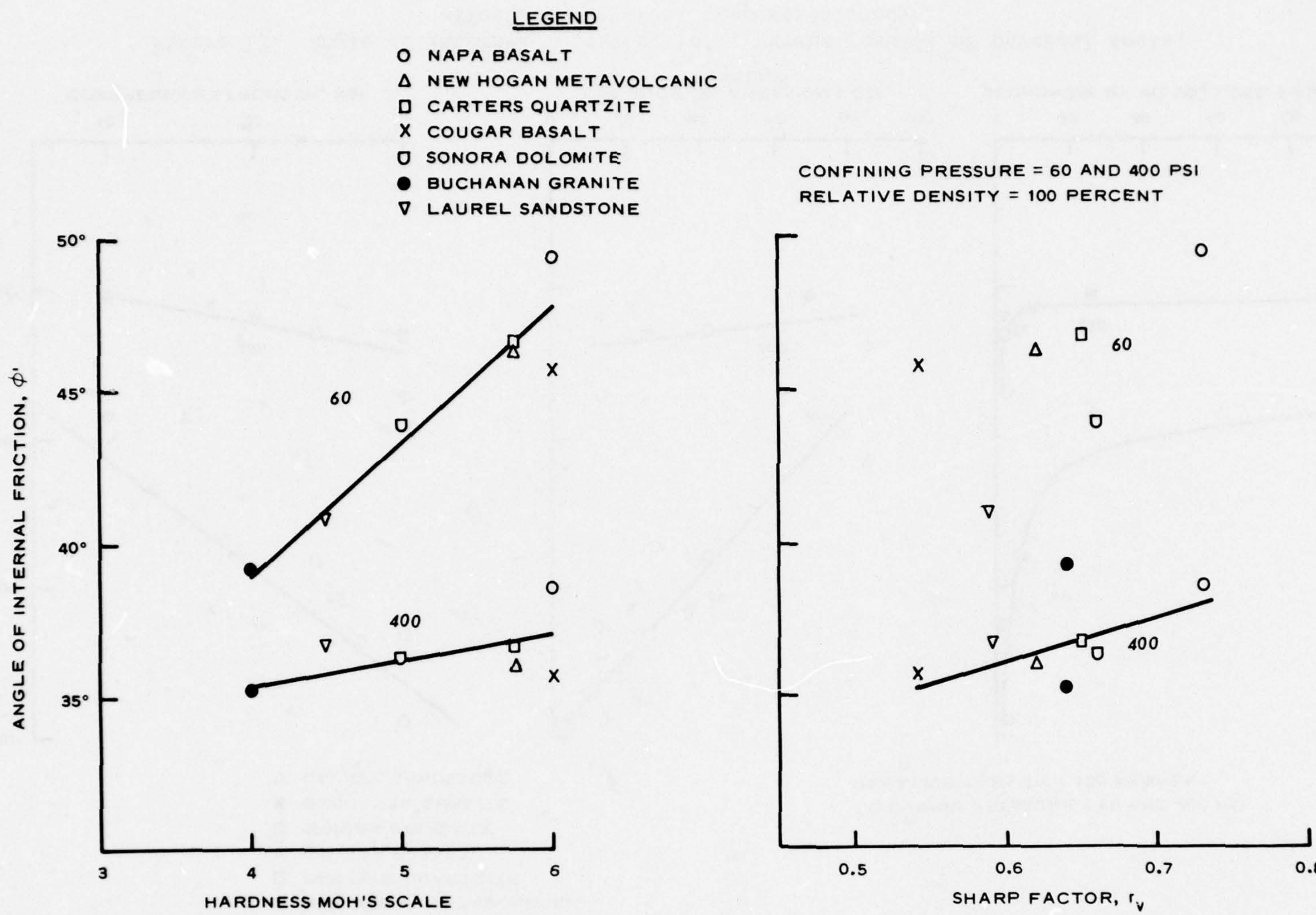

Figure 14. Angle of internal friction, ϕ' , versus results of physical tests, effects of physical properties study

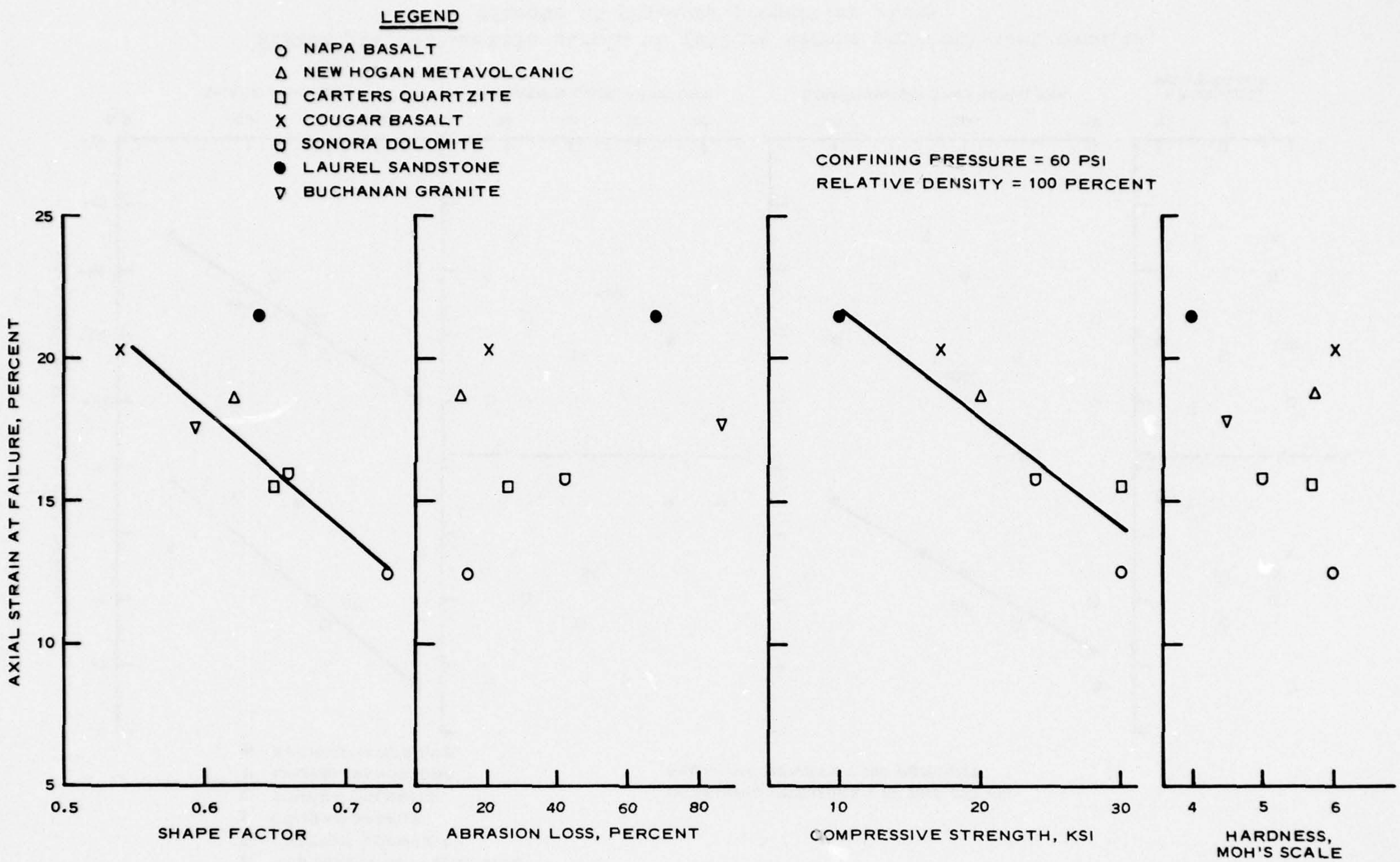

Figure 15. Axial strain at failure versus results of physical tests, effects of physical properties tests

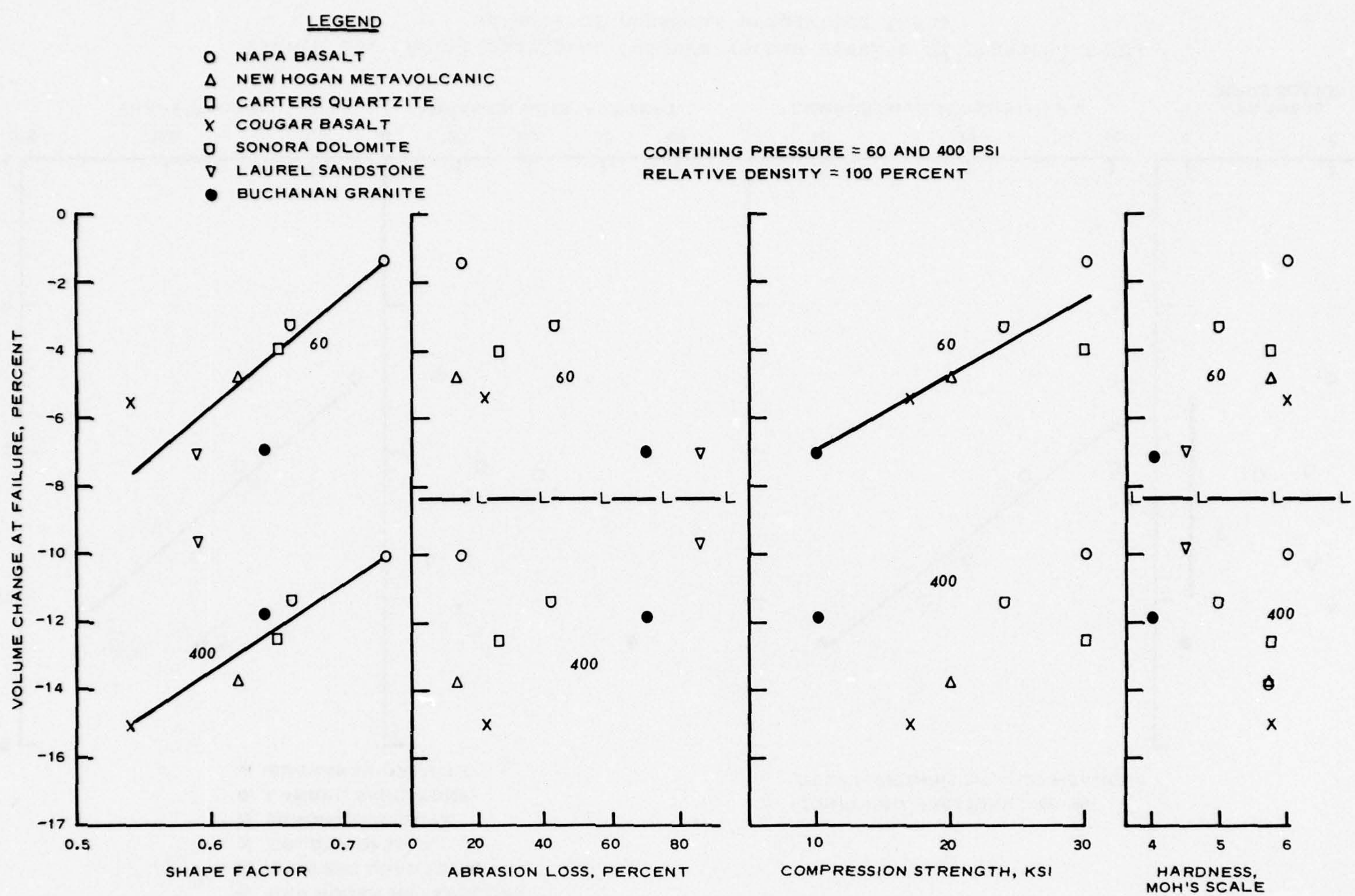

Figure 16. Volumetric strain at failure versus physical test results, effects of physical properties study

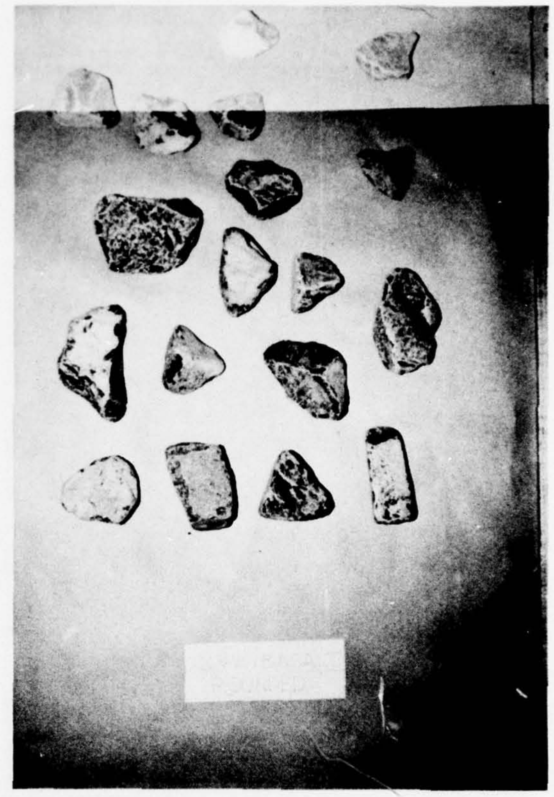

Figure 17. Photographs of pit run and abraided (rounded) samples of Napa basalt

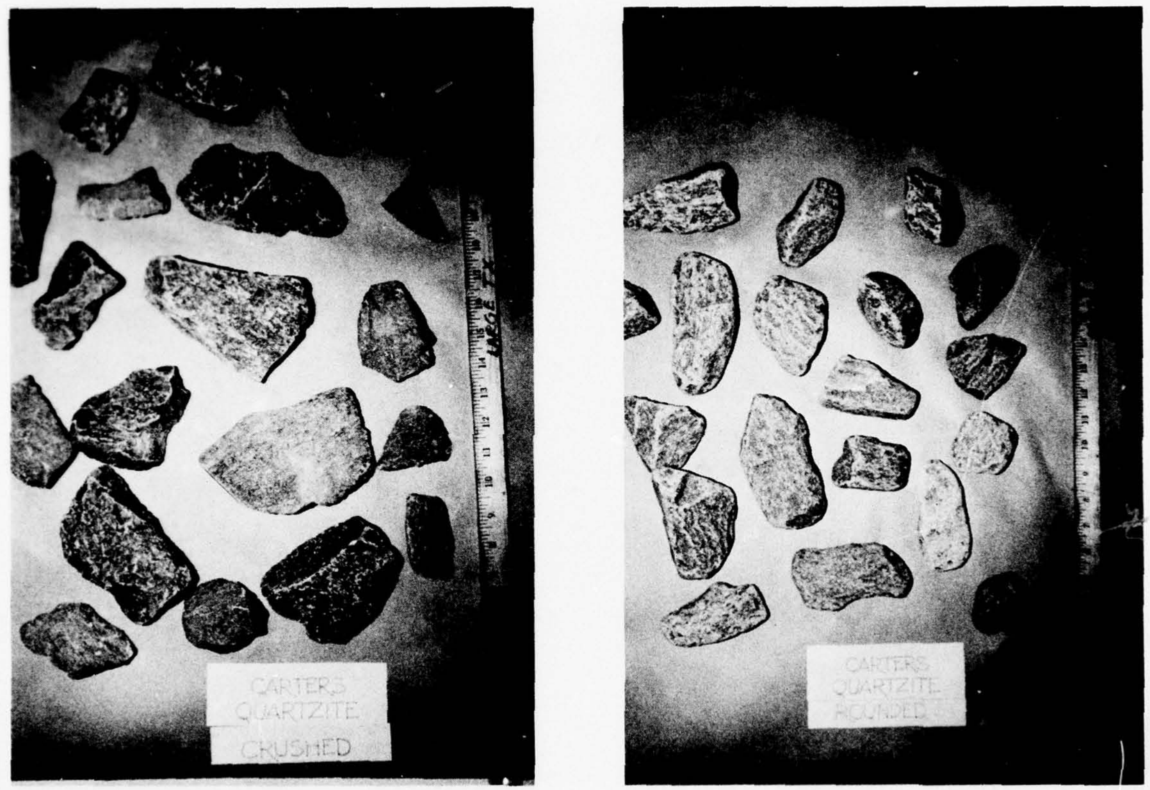

Figure 18. Photographs of crushed and abraided (rounded) samples of Carters Dam quartzite

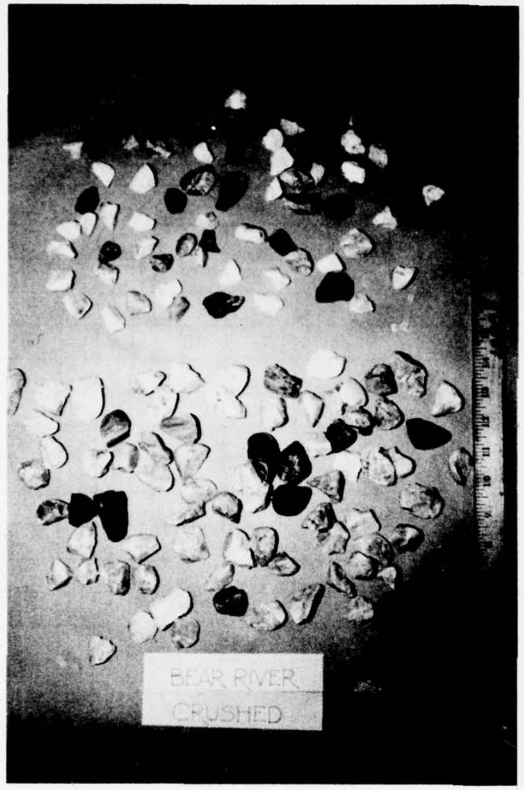

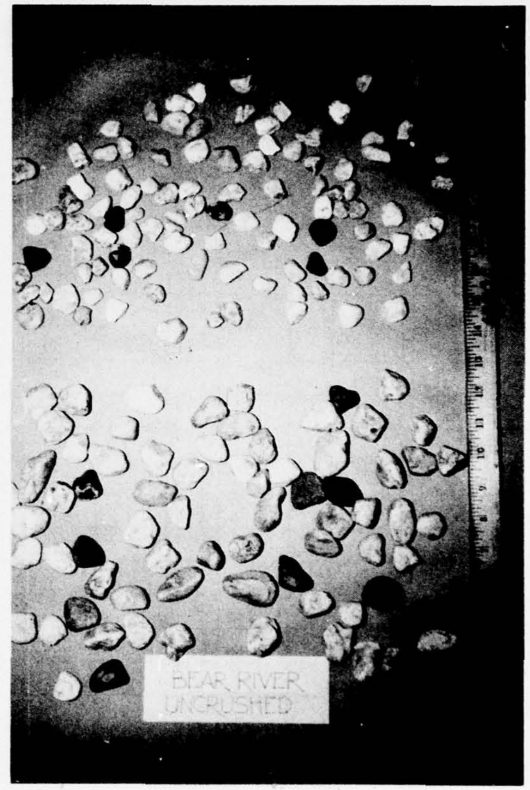

Figure 19. Photographs of crushed and uncrushed samples of Bear River gravel

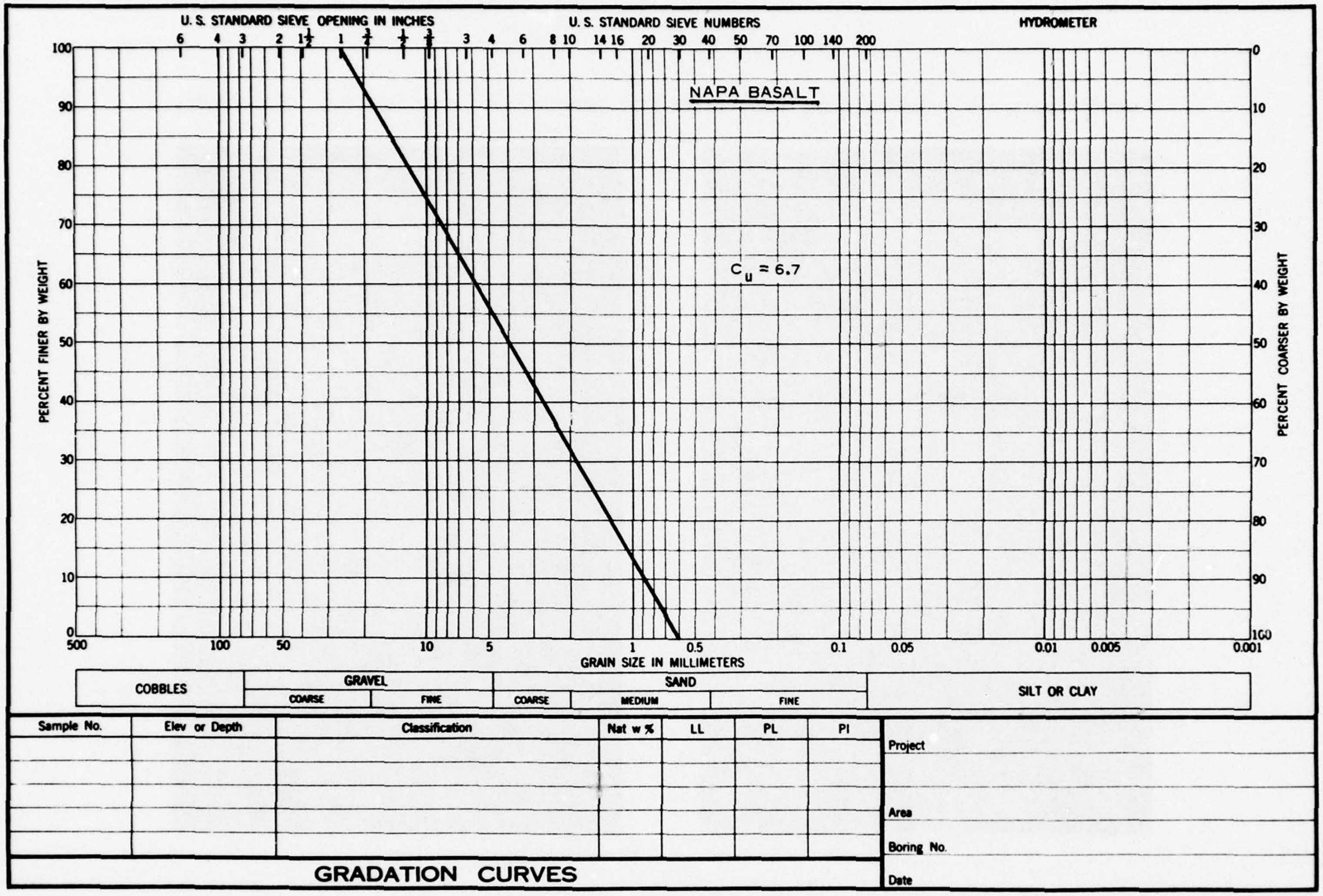

Figure 20. Test gradation for investigation of effects of end restraint

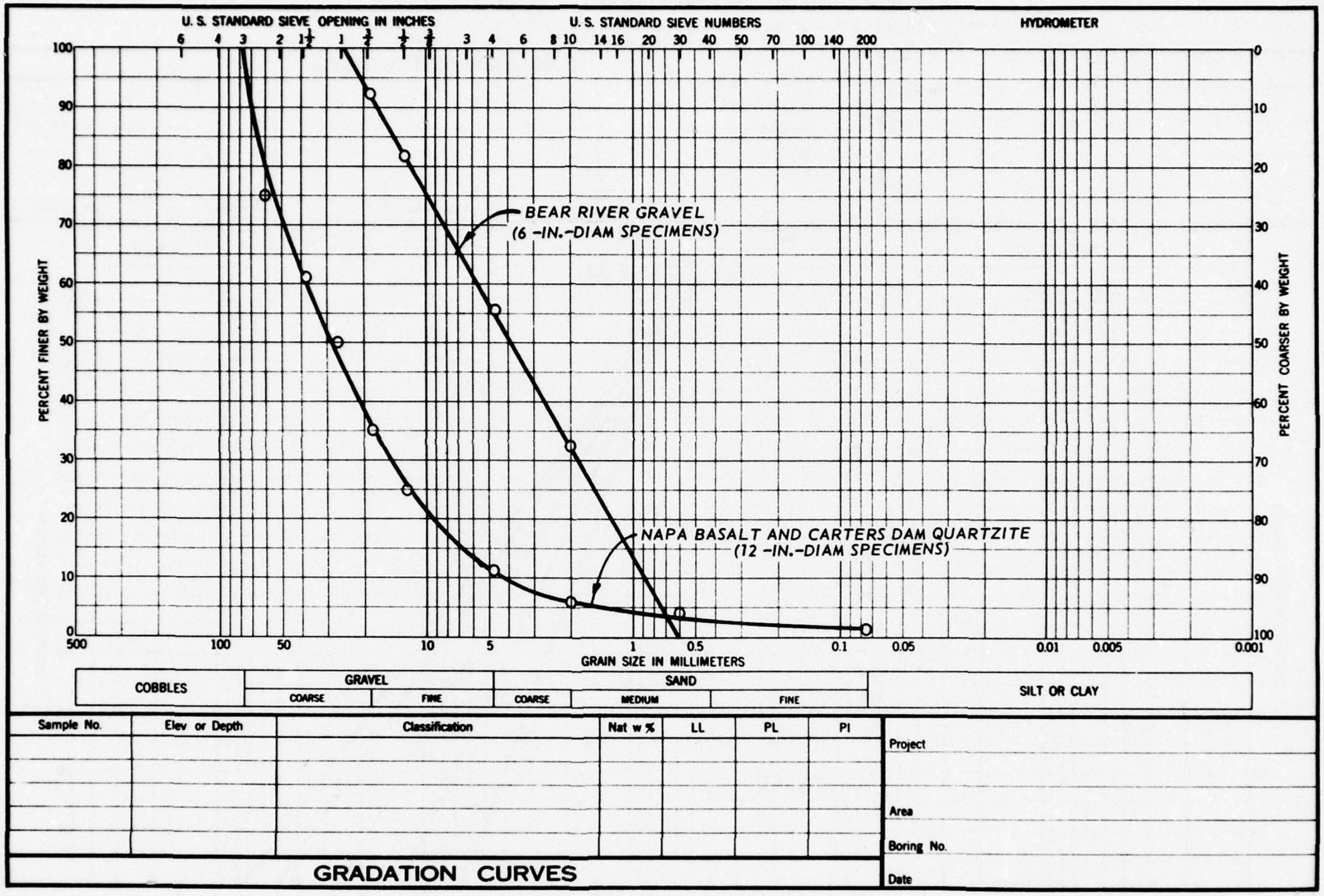

Figure 21. Test gradations for tests to determine effects due to particle shape

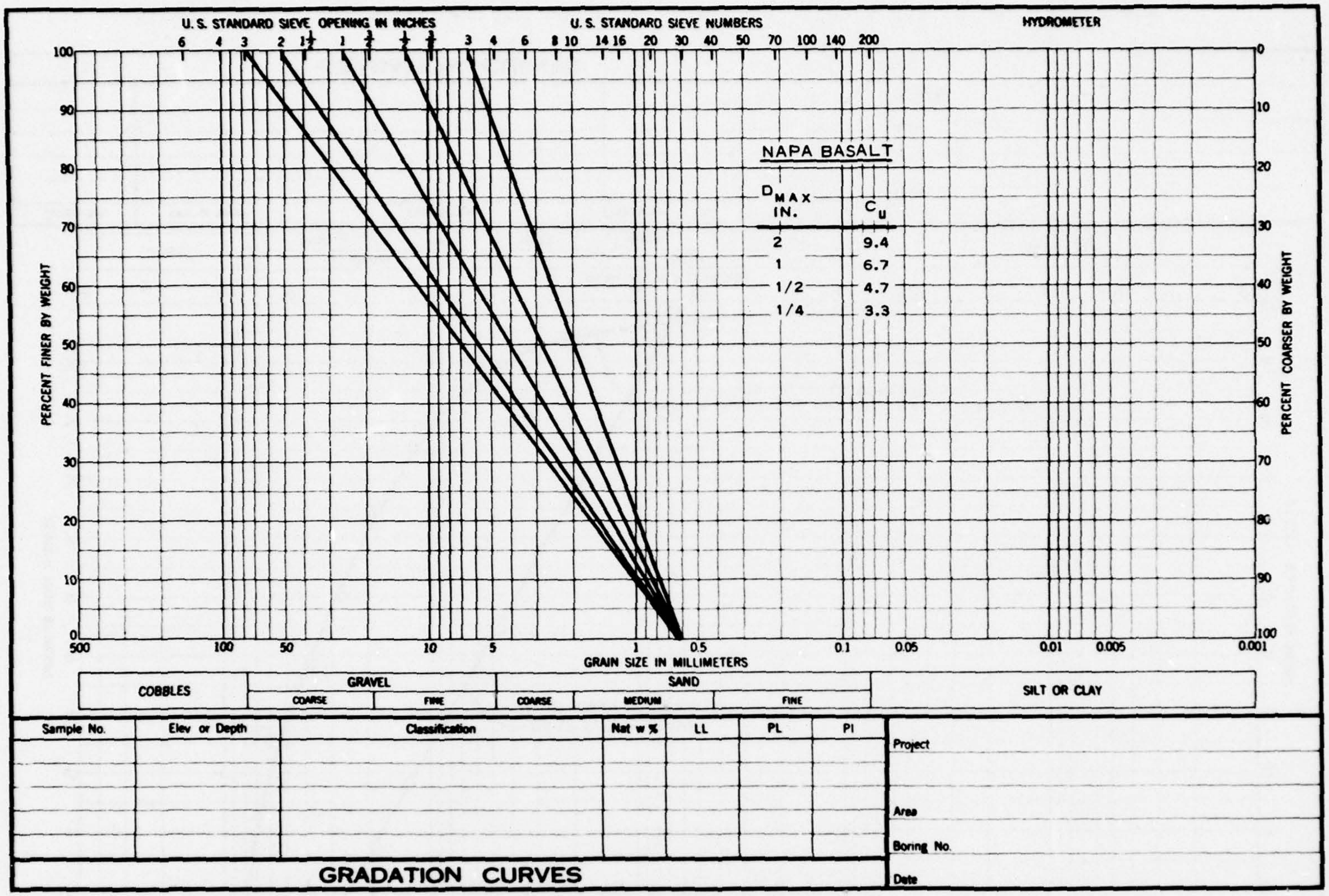

Figure 22. Test gradations to determine effects of particle size on one-dimensional consolidation characteristics

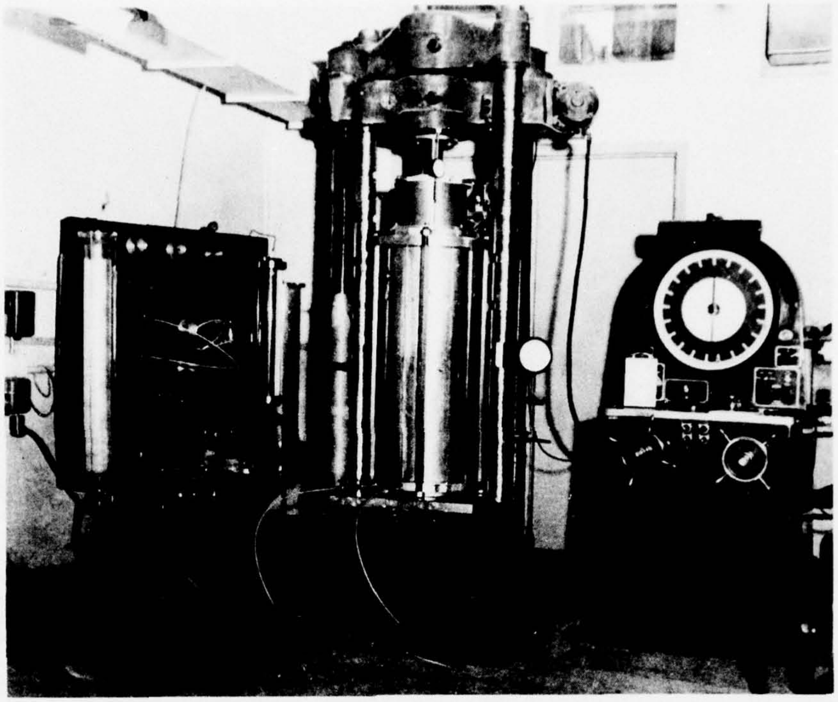

Figure 23. SPD 12-in.-diameter triaxial shear apparatus

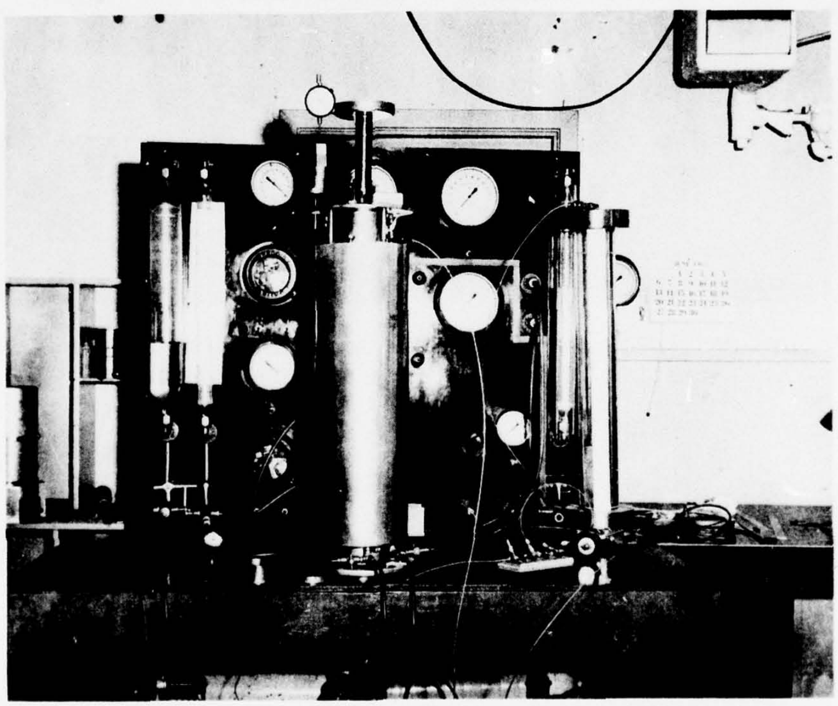

Figure 24. Six-in.-diameter warlam triaxial shear apparatus

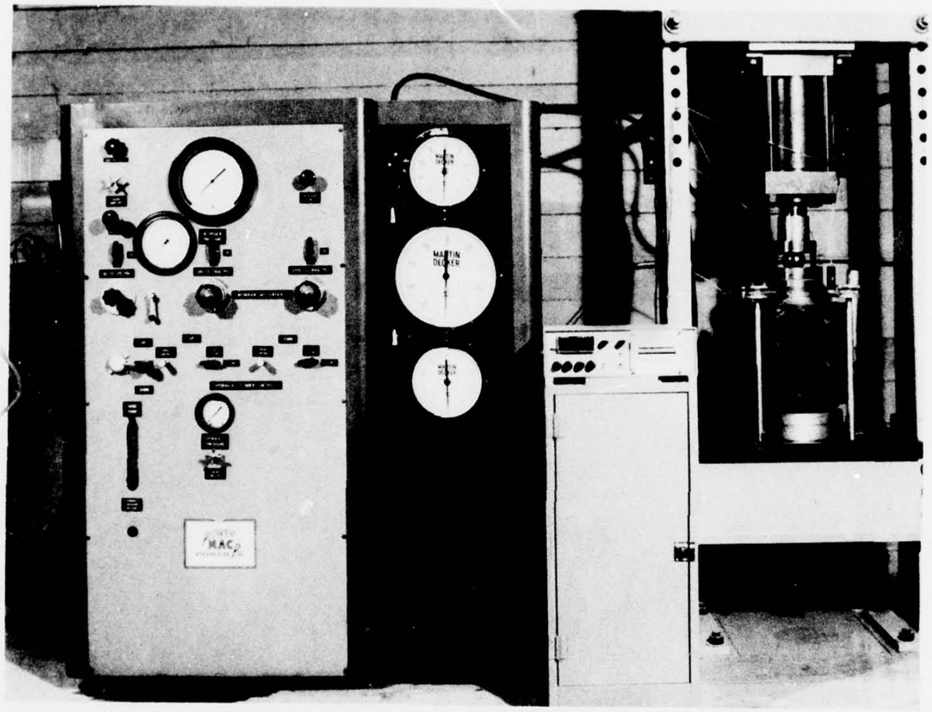

Figure 25. SPD one-dimensional consolidation apparatus for testing 12-in.-diameter rockfill specimens

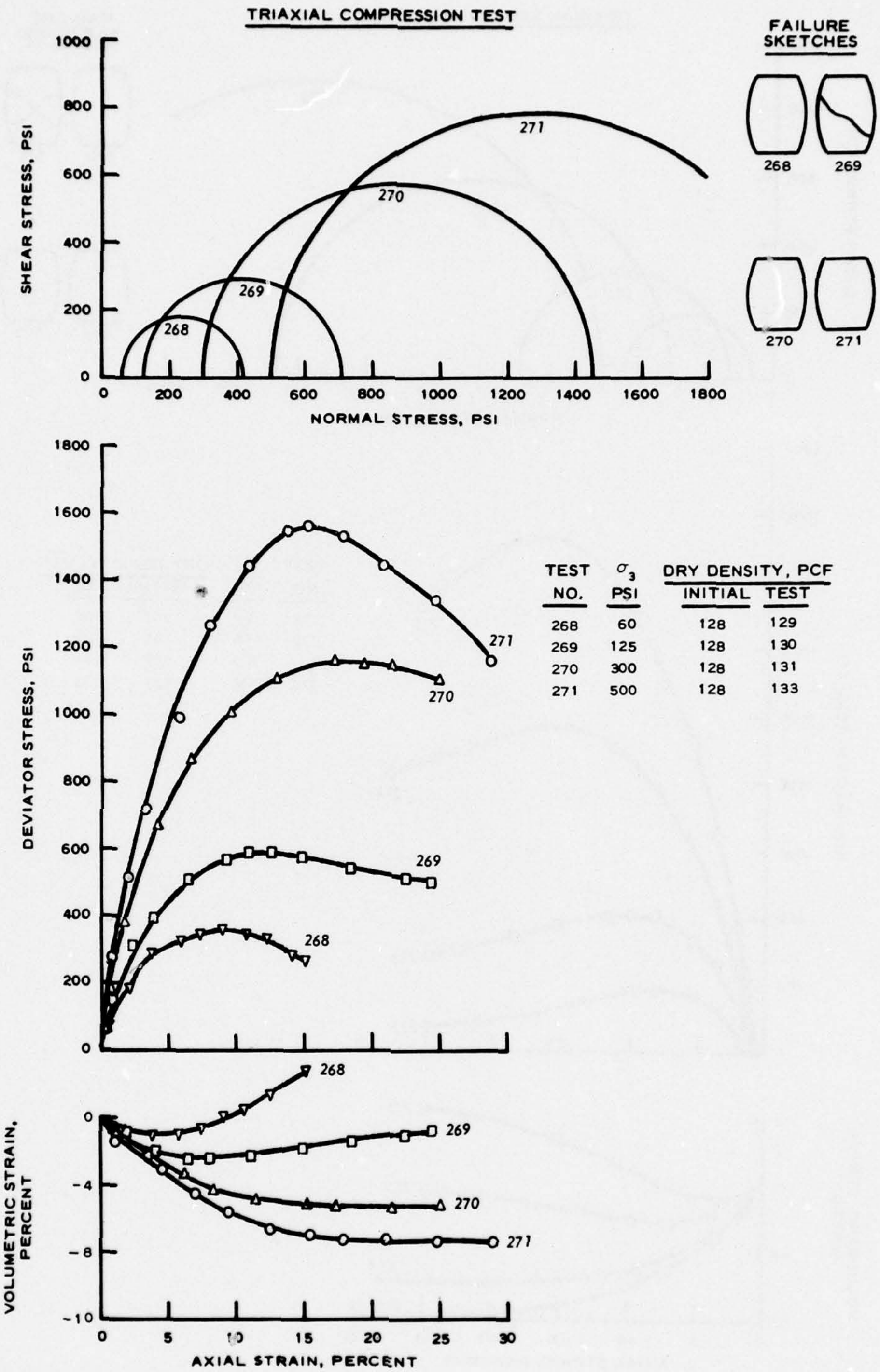

TEST NO.	σ_3 PSI	DRY DENSITY, PCF INITIAL	TEST
268	60	128	129
269	125	128	130
270	300	128	131
271	500	128	133

Figure 26. Test report sheet for Napa basalt high density specimens, 6-in.-diameter, low-friction ends, effects of end restraint

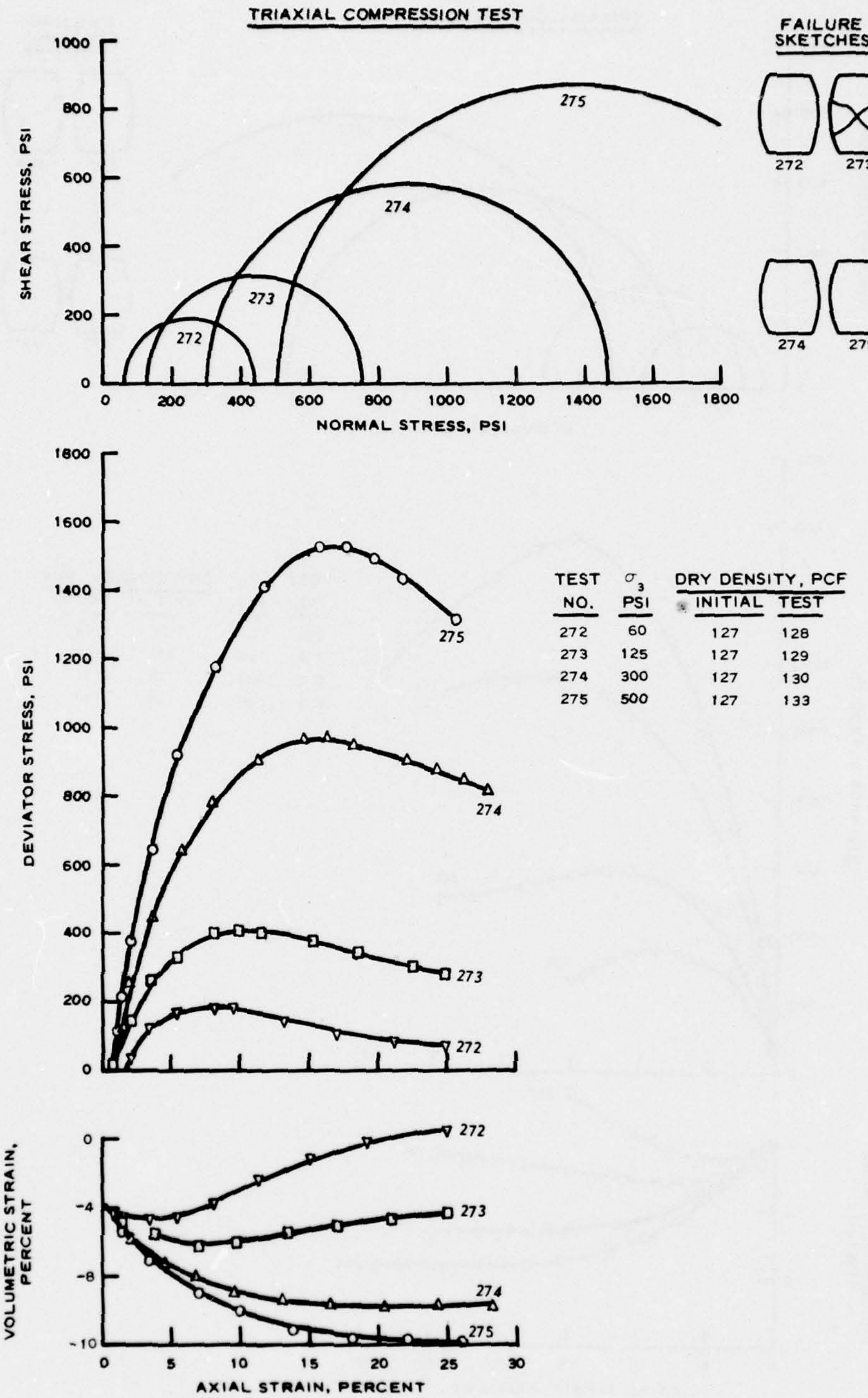

TEST NO.	σ_3 PSI	DRY DENSITY, PCF INITIAL	TEST
272	60	127	128
273	125	127	129
274	300	127	130
275	500	127	133

Figure 27. Test report sheet for Napa basalt high density specimens, 6-in.-diameter, regular ends, effects of end restraint

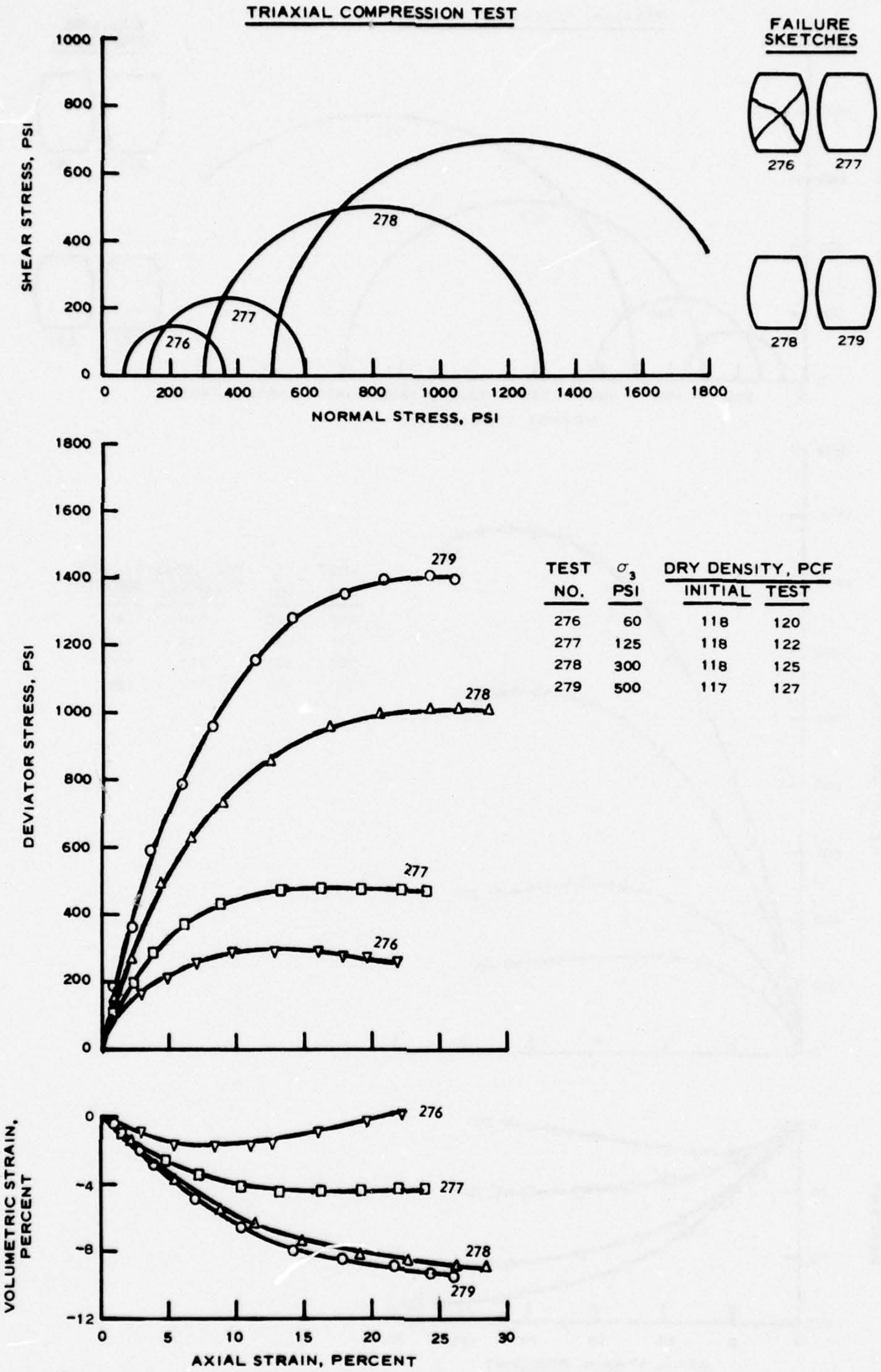

TEST NO.	σ_3 PSI	DRY DENSITY, PCF INITIAL	TEST
276	60	118	120
277	125	118	122
278	300	118	125
279	500	117	127

Figure 28. Test report sheet for Napa basalt medium density specimens, 6-in.-diameter, low-friction ends, effects of end restraint

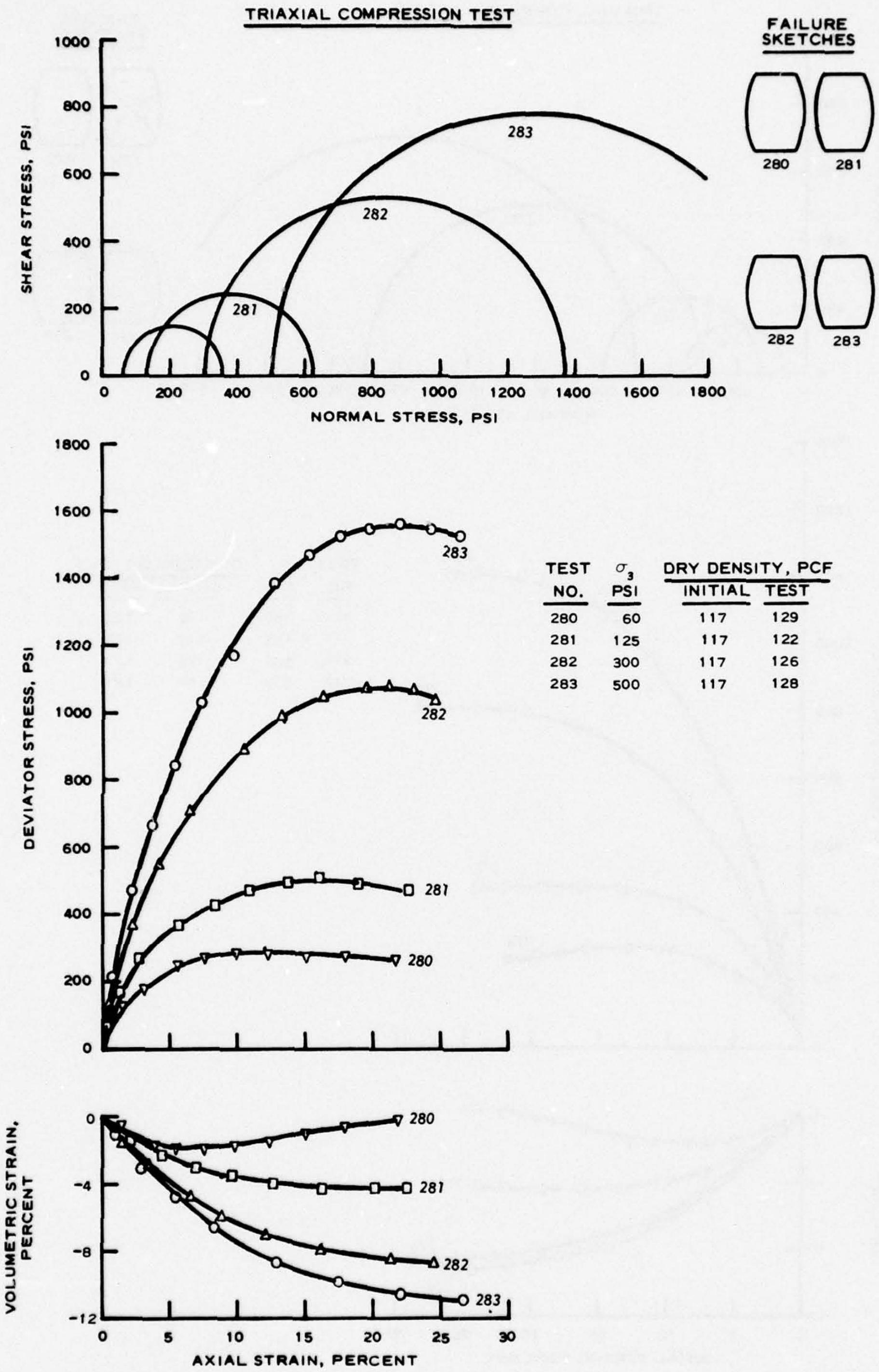

TEST NO.	σ_3 PSI	DRY DENSITY, PCF INITIAL	DRY DENSITY, PCF TEST
280	60	117	129
281	125	117	122
282	300	117	126
283	500	117	128

Figure 29. Test report sheet for Napa basalt medium density specimens, 6-in.-diameter, regular ends, effects of end restraint

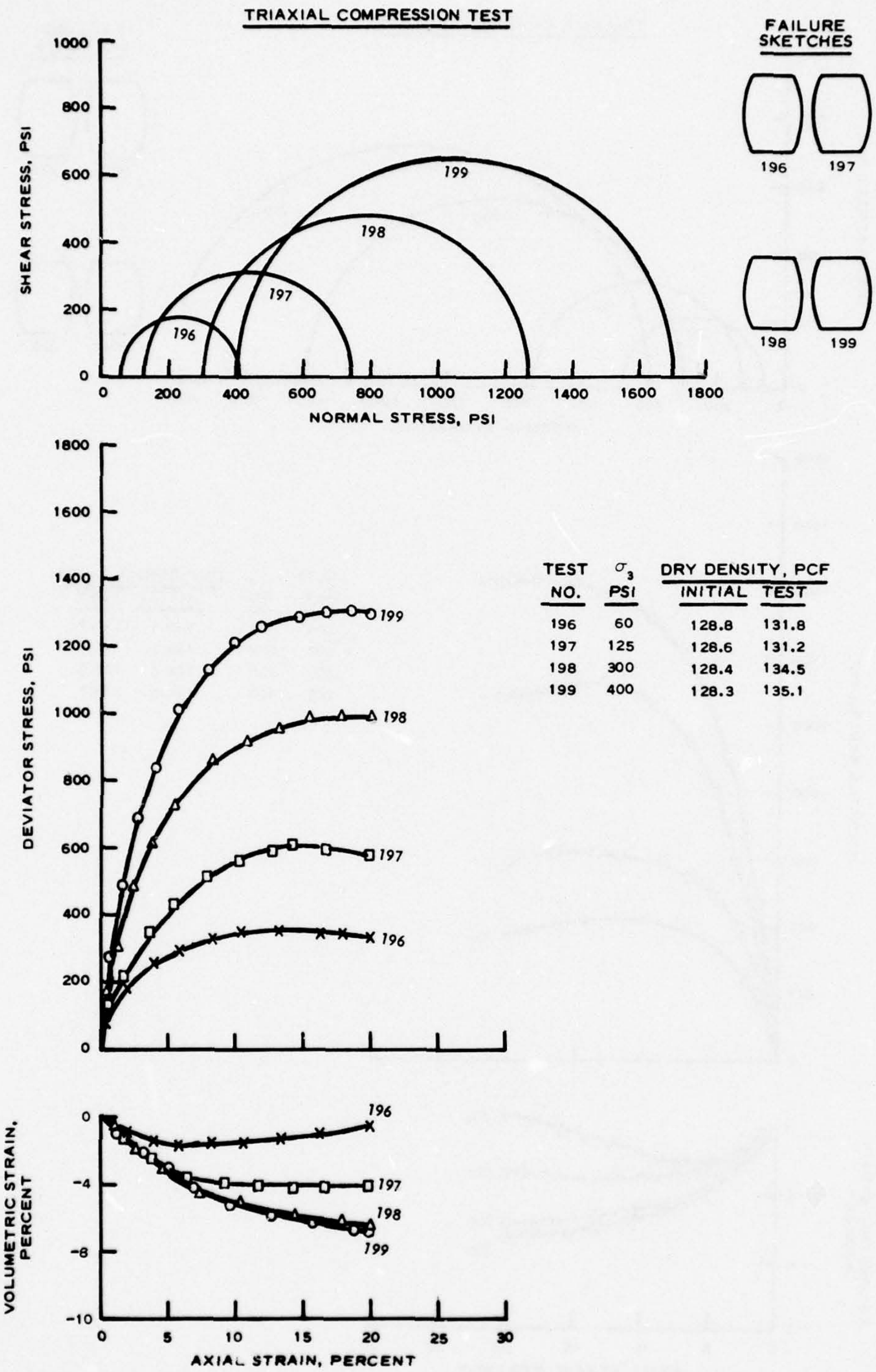

TEST NO.	σ_3 PSI	DRY DENSITY, PCF INITIAL	DRY DENSITY, PCF TEST
196	60	128.8	131.8
197	125	128.6	131.2
198	300	128.4	134.5
199	400	128.3	135.1

Figure 30. Test report sheet for Napa basalt high density specimens, less angular particles, effects of particle shape

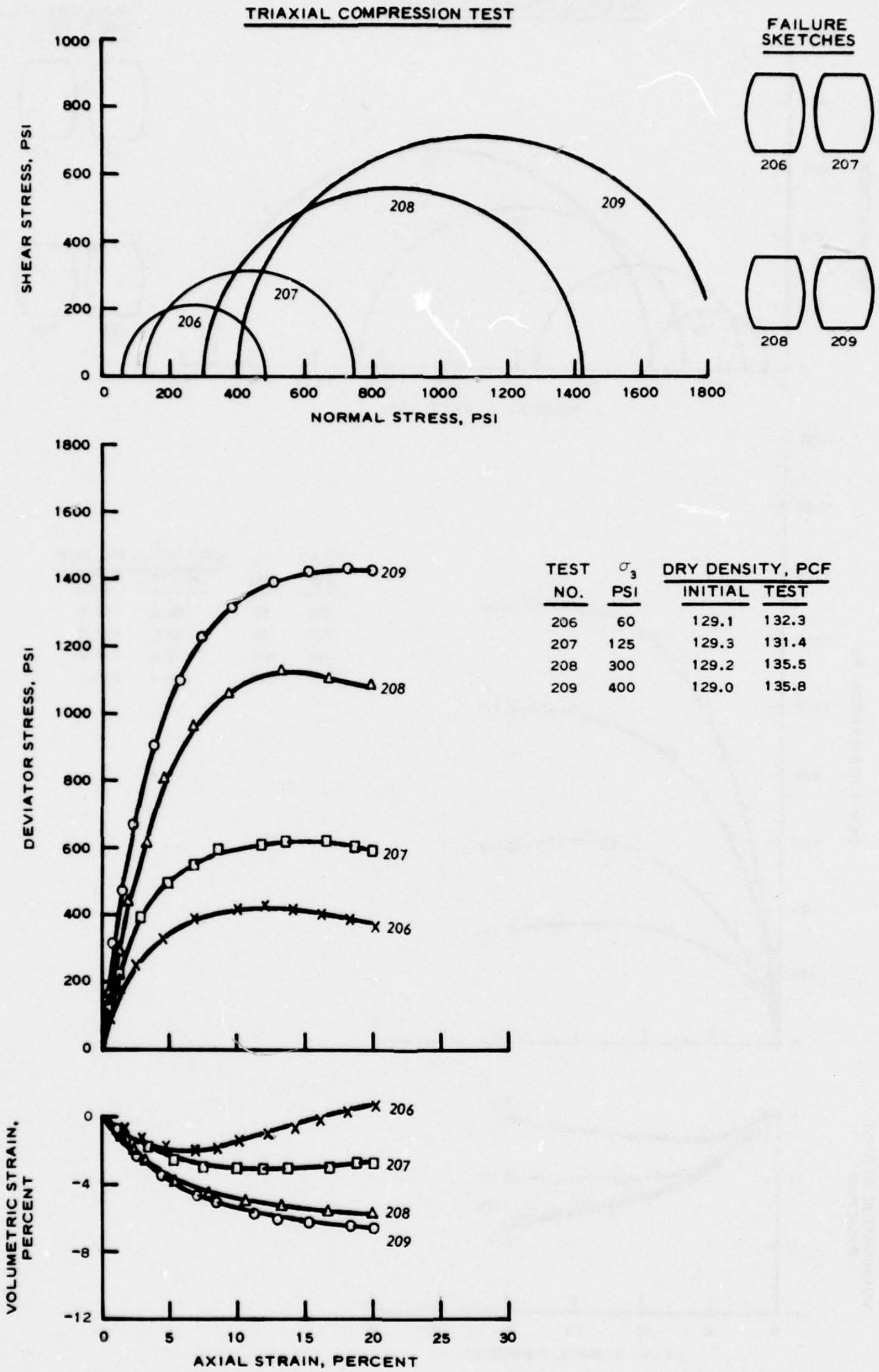

TEST NO.	σ_3 PSI	DRY DENSITY, PCF INITIAL	TEST
206	60	129.1	132.3
207	125	129.3	131.4
208	300	129.2	135.5
209	400	129.0	135.8

Figure 31. Test report sheet for Napa basalt high density specimens, more angular specimens, effects of particle shape

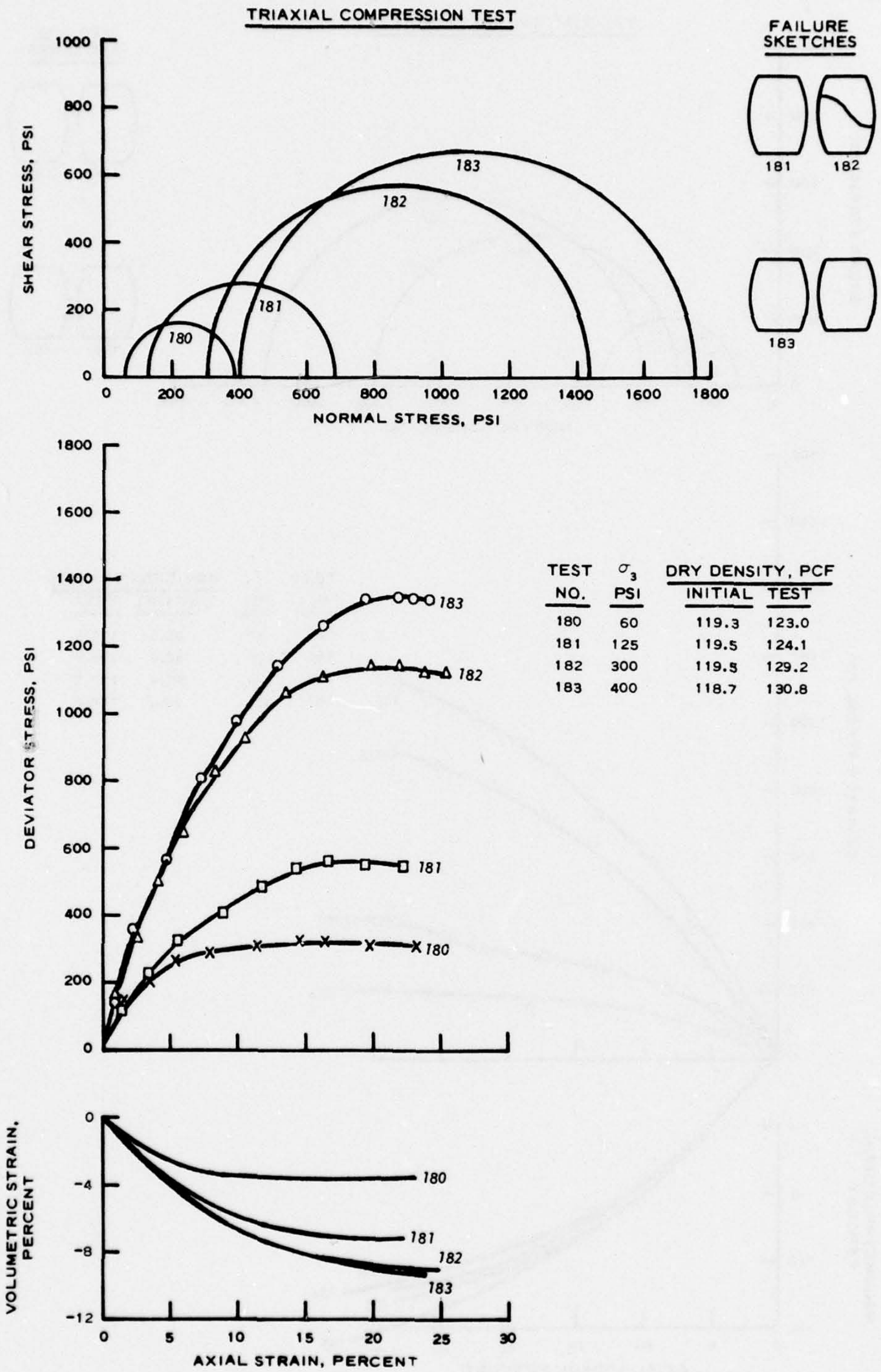

Figure 32. Test report sheet for Carters Dam quartzite high density specimens, more angular particles, effects of particles shape

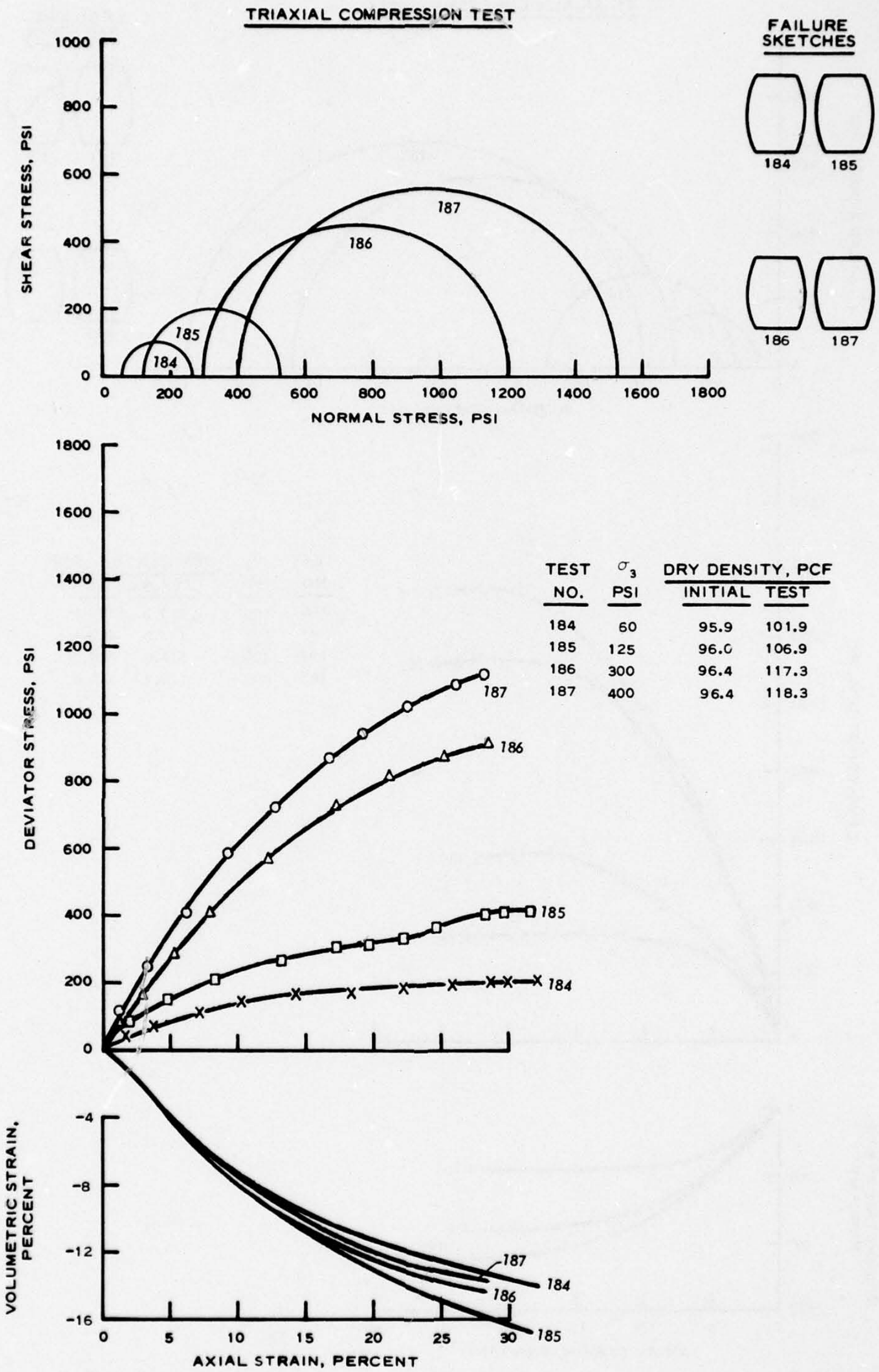

Figure 33. Test report sheet for Carters Dam quartzite low density specimens, more angular particles, effects of particle shape

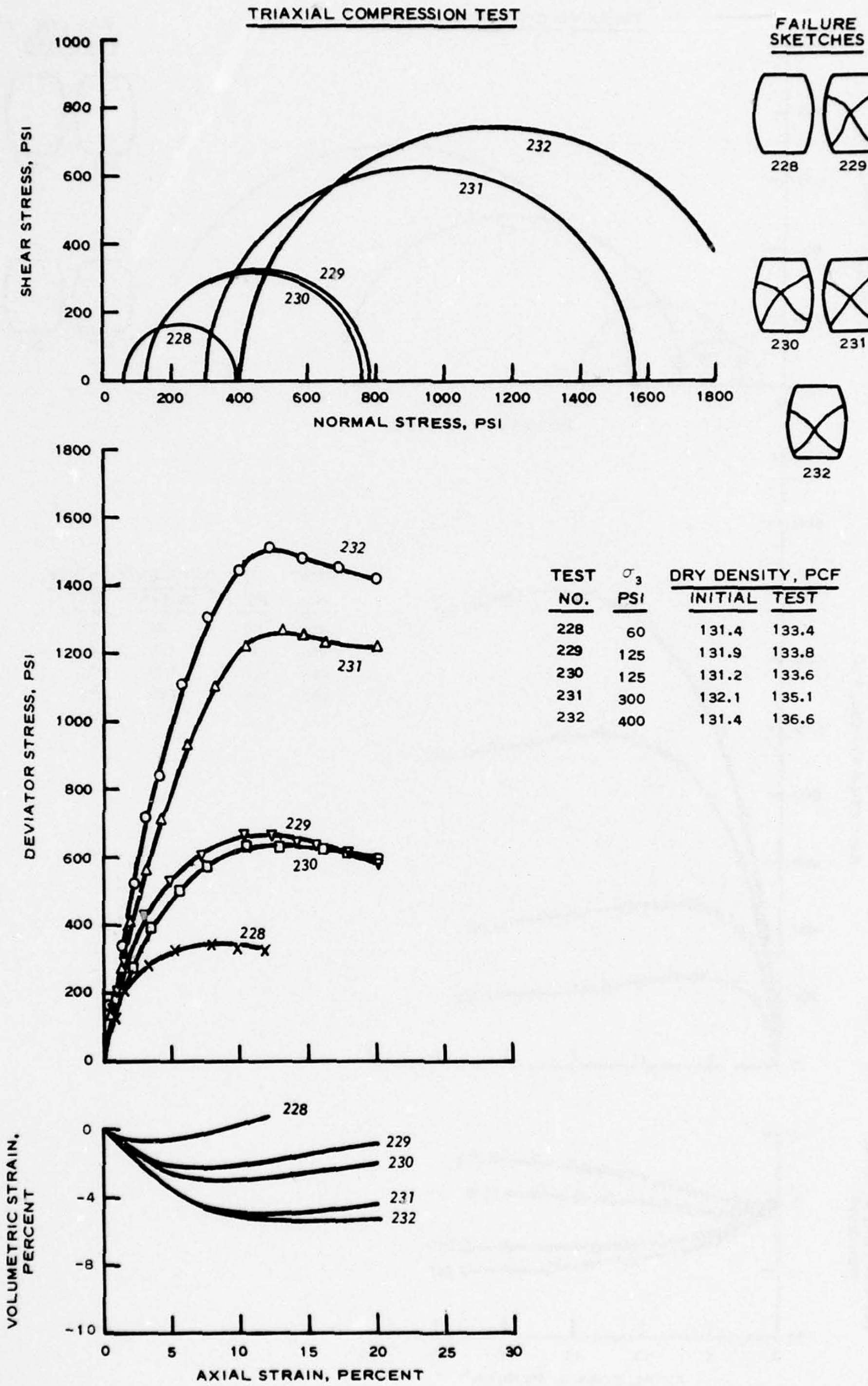

TEST NO.	σ_3 PSI	DRY DENSITY, PCF INITIAL	TEST
228	60	131.4	133.4
229	125	131.9	133.8
230	125	131.2	133.6
231	300	132.1	135.1
232	400	131.4	136.6

Figure 34. Test report sheet for Carters Dam quartzite high density specimens, less angular particles, effects of particle shape

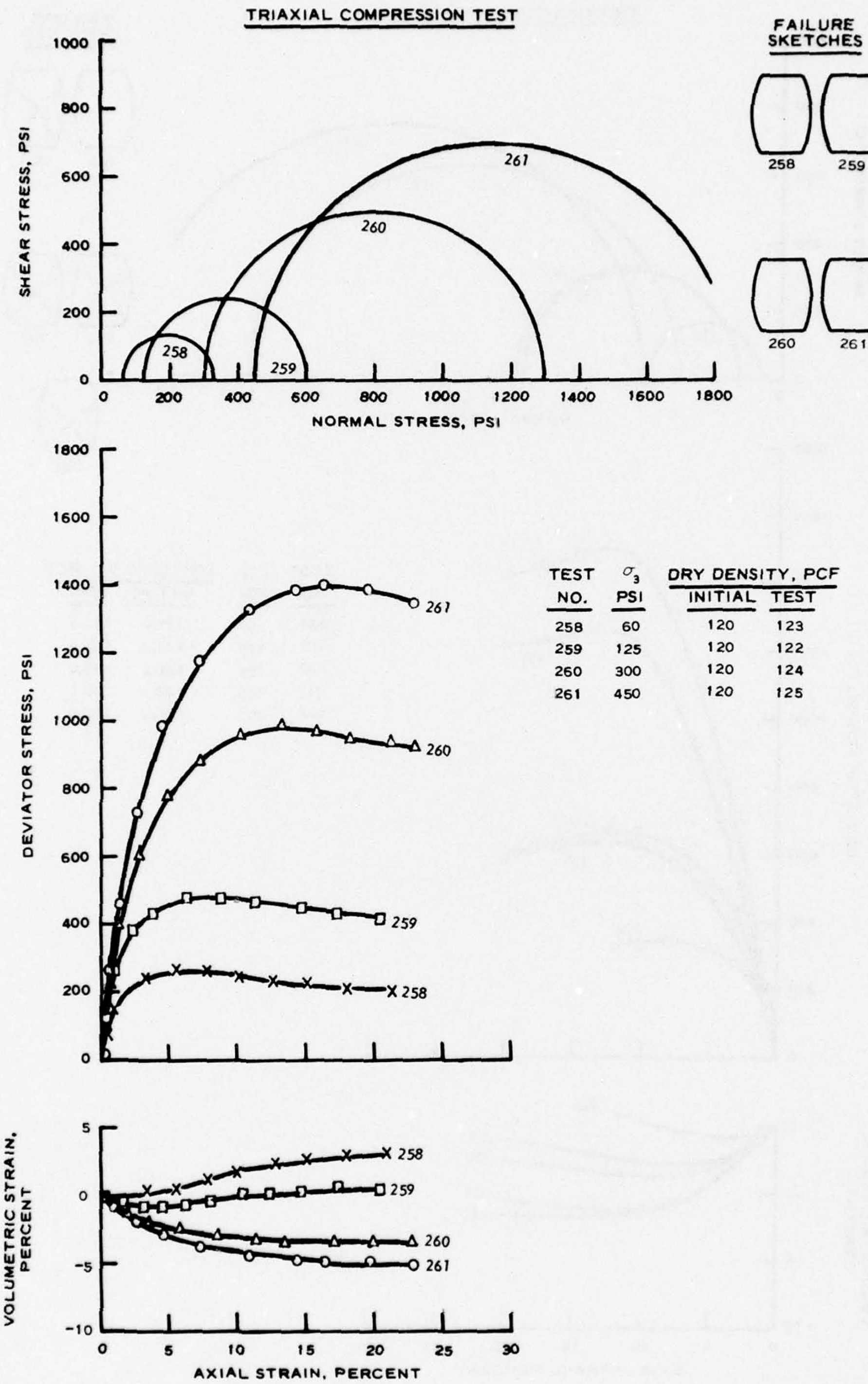

TEST NO.	σ_3 PSI	DRY DENSITY, PCF INITIAL	TEST
258	60	120	123
259	125	120	122
260	300	120	124
261	450	120	125

Figure 35. Test report sheet for Bear River gravel high density specimens, 1-in. to No. 30, more angular particles, effects of particle shape

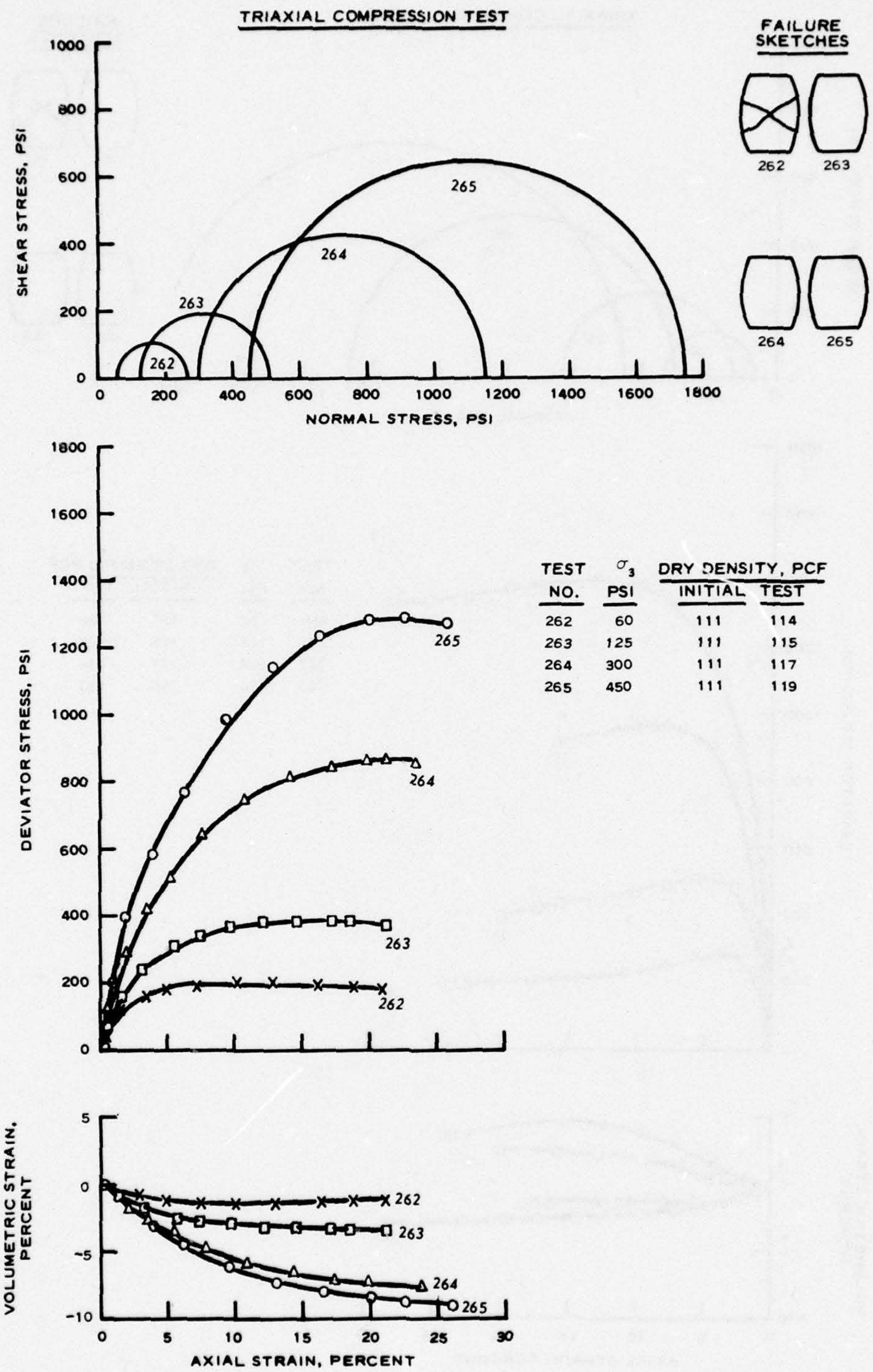

Figure 36. Test report sheet for Bear River gravel medium density specimens, 1-in. to No. 30, more angular particles, effects of particle shape

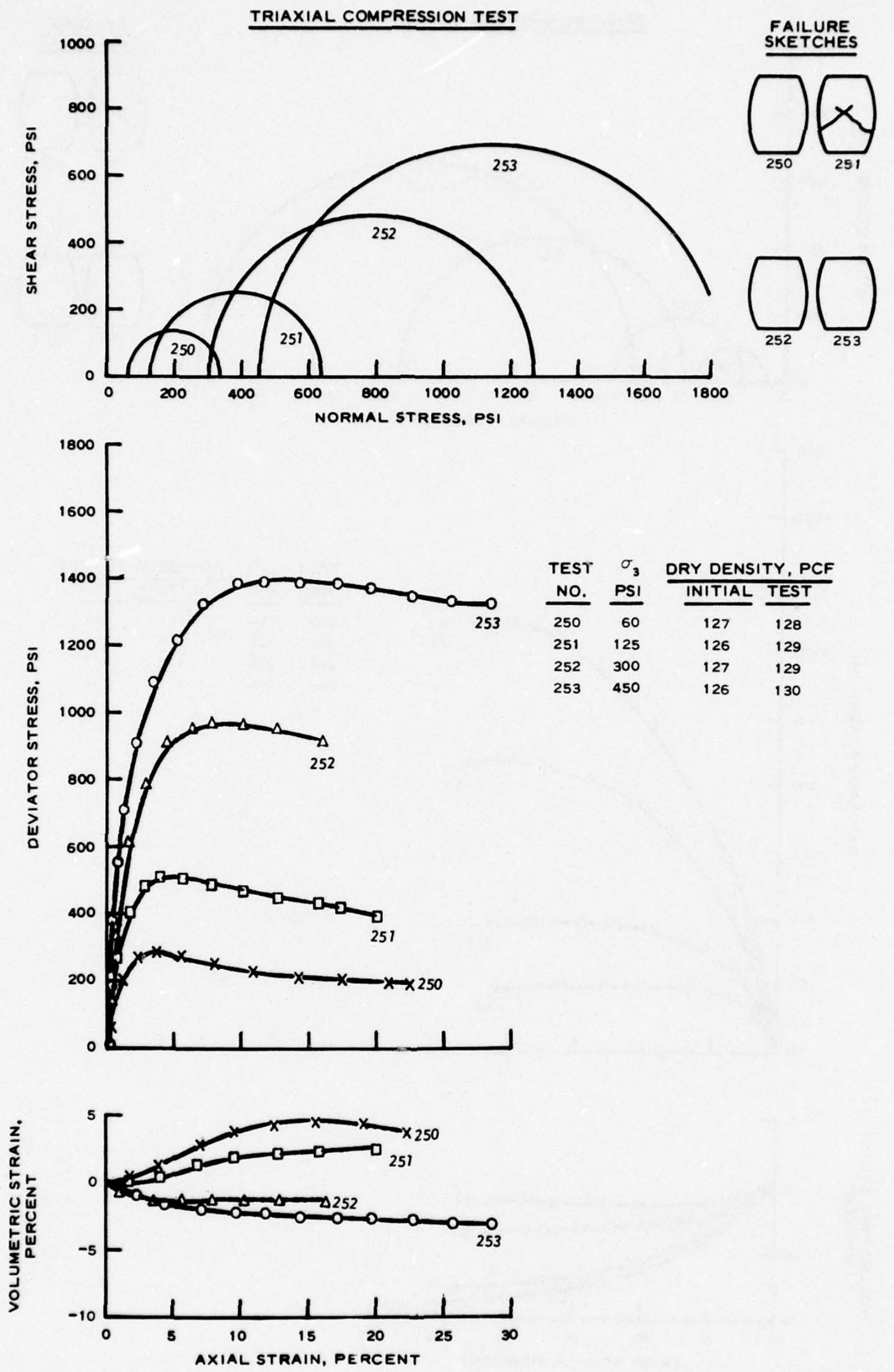

Figure 37. Test report sheet for Bear River gravel high density specimens, 1-in. to No. 30, less angular particles, effects of particle shape

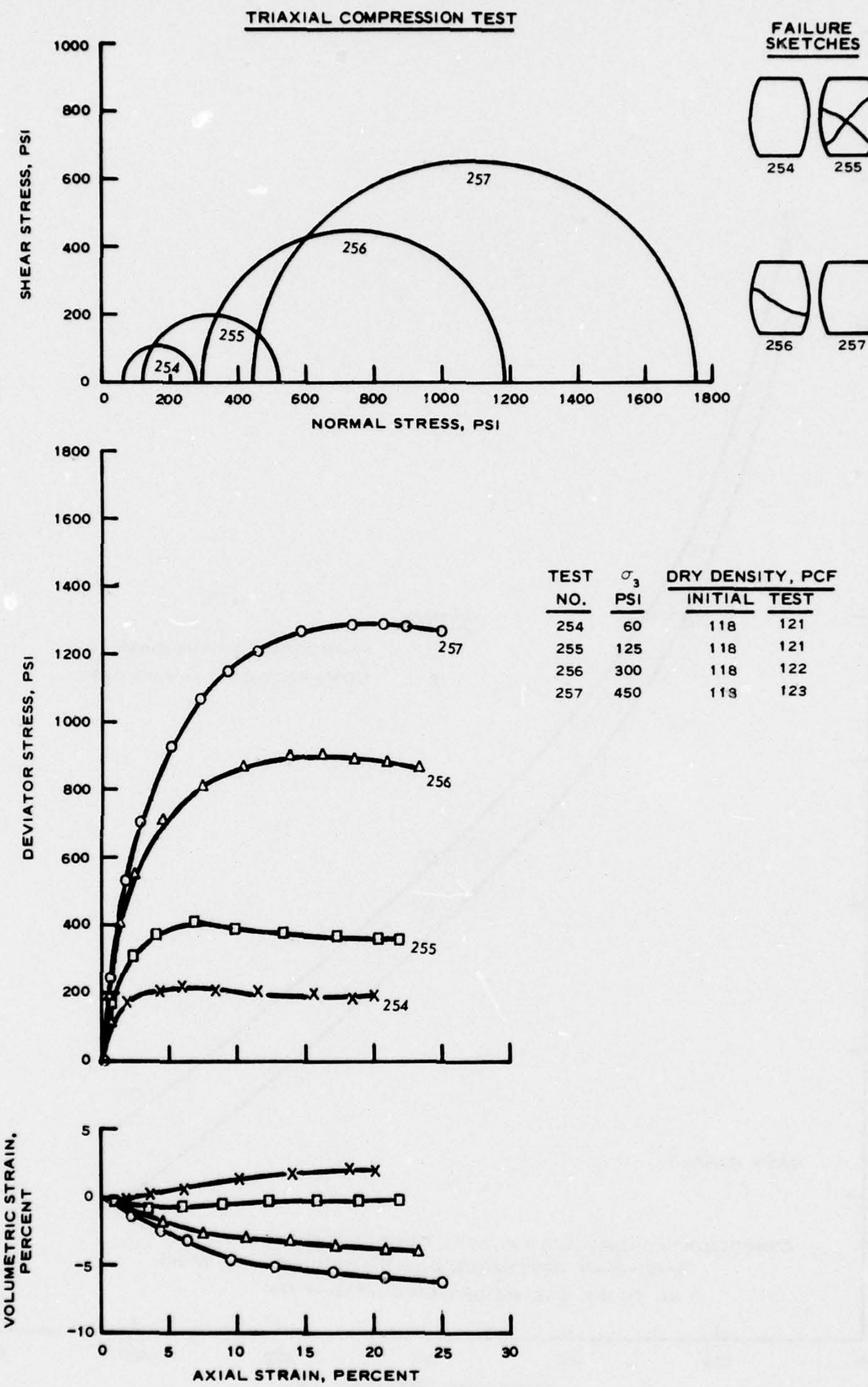

TEST NO.	σ_3 PSI	DRY DENSITY, PCF INITIAL	TEST
254	60	118	121
255	125	118	121
256	300	118	122
257	450	118	123

Figure 38. Test report sheet for Bear River gravel medium density specimens, 1-in. to No. 30, less angular particles, effects of particle shape

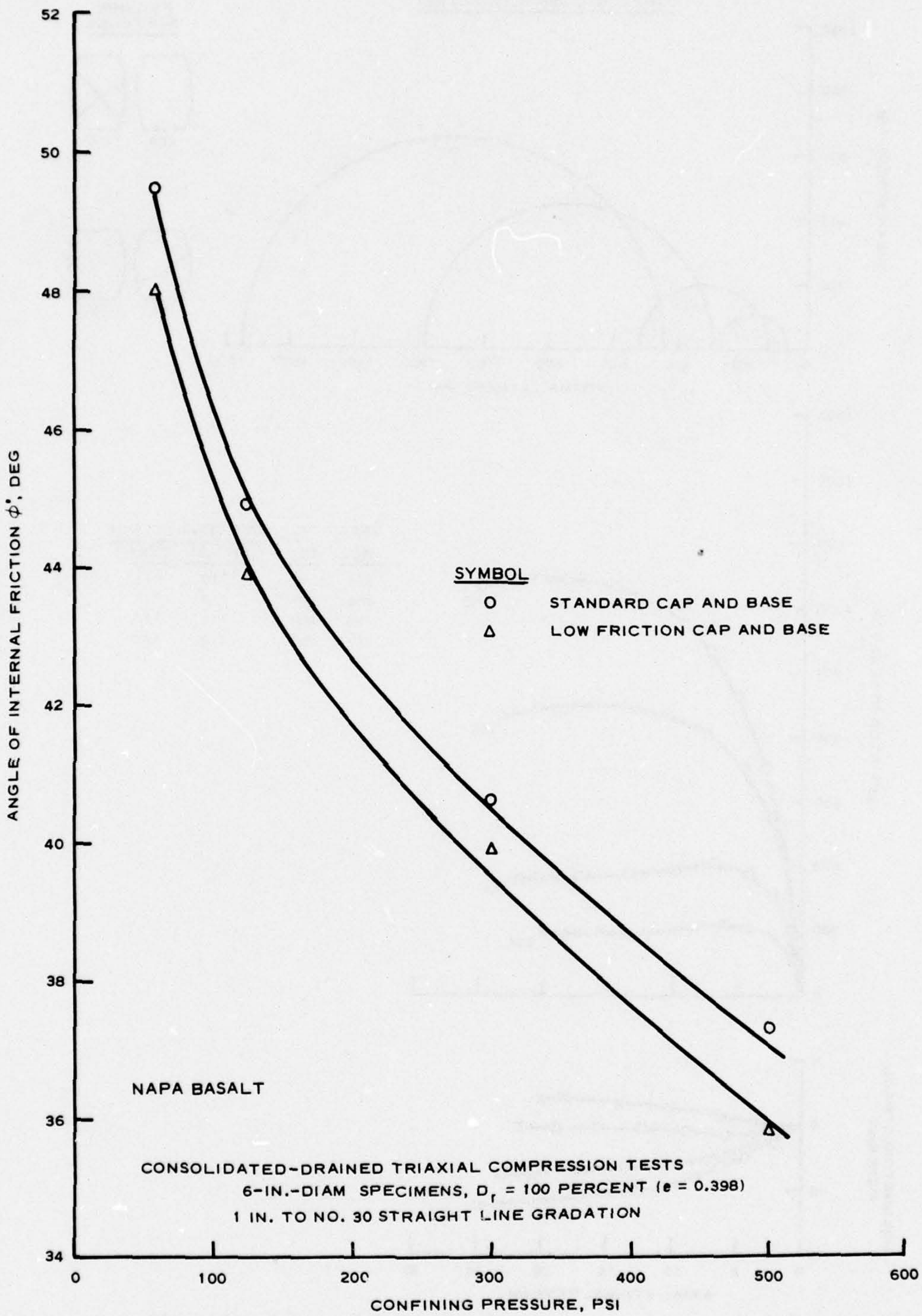

Figure 39. Angle of internal friction, ϕ', versus confining pressure, effects of end restraint

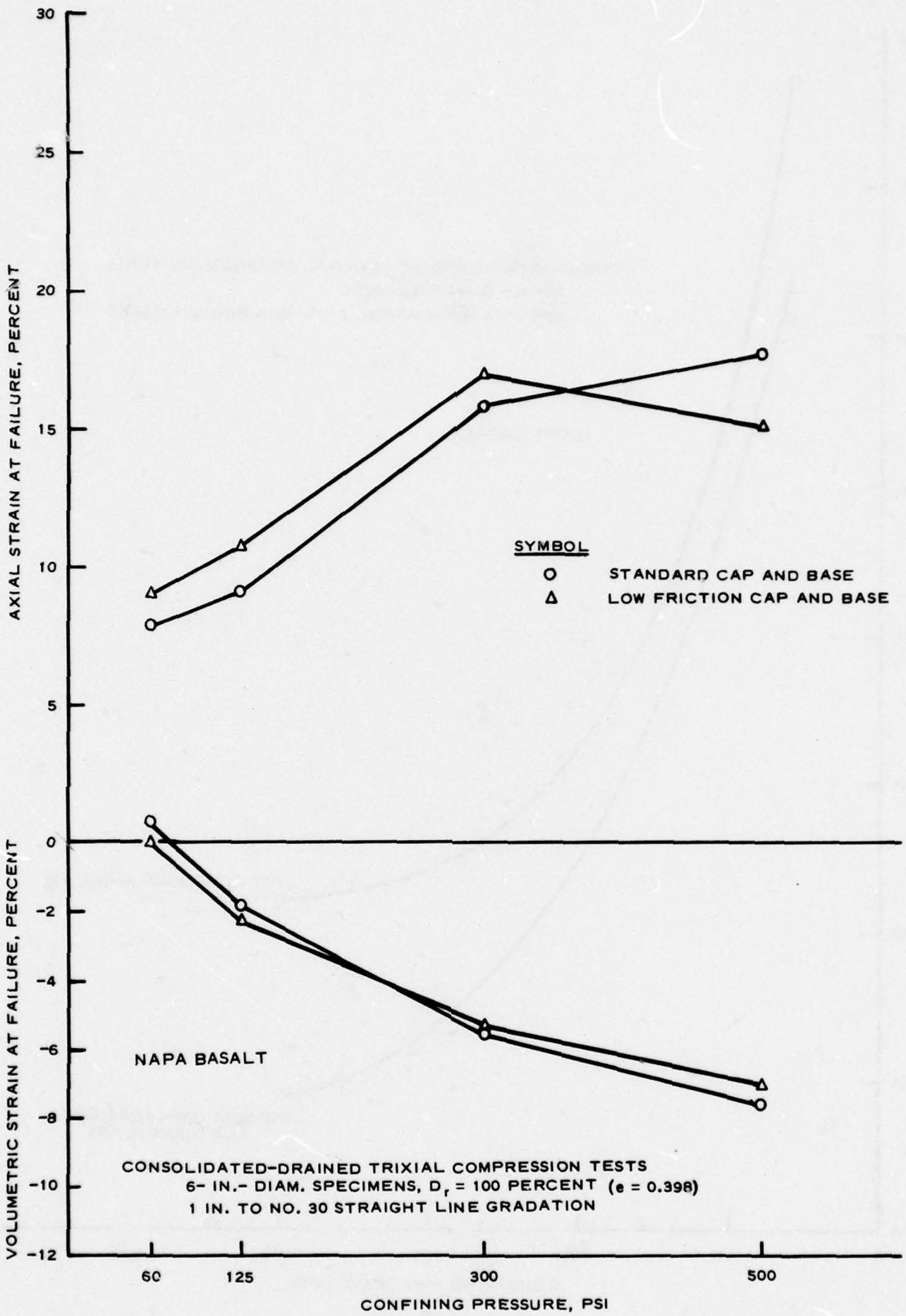

Figure 40. Axial and volumetric strains at failure versus confining pressure, effects of end restraint

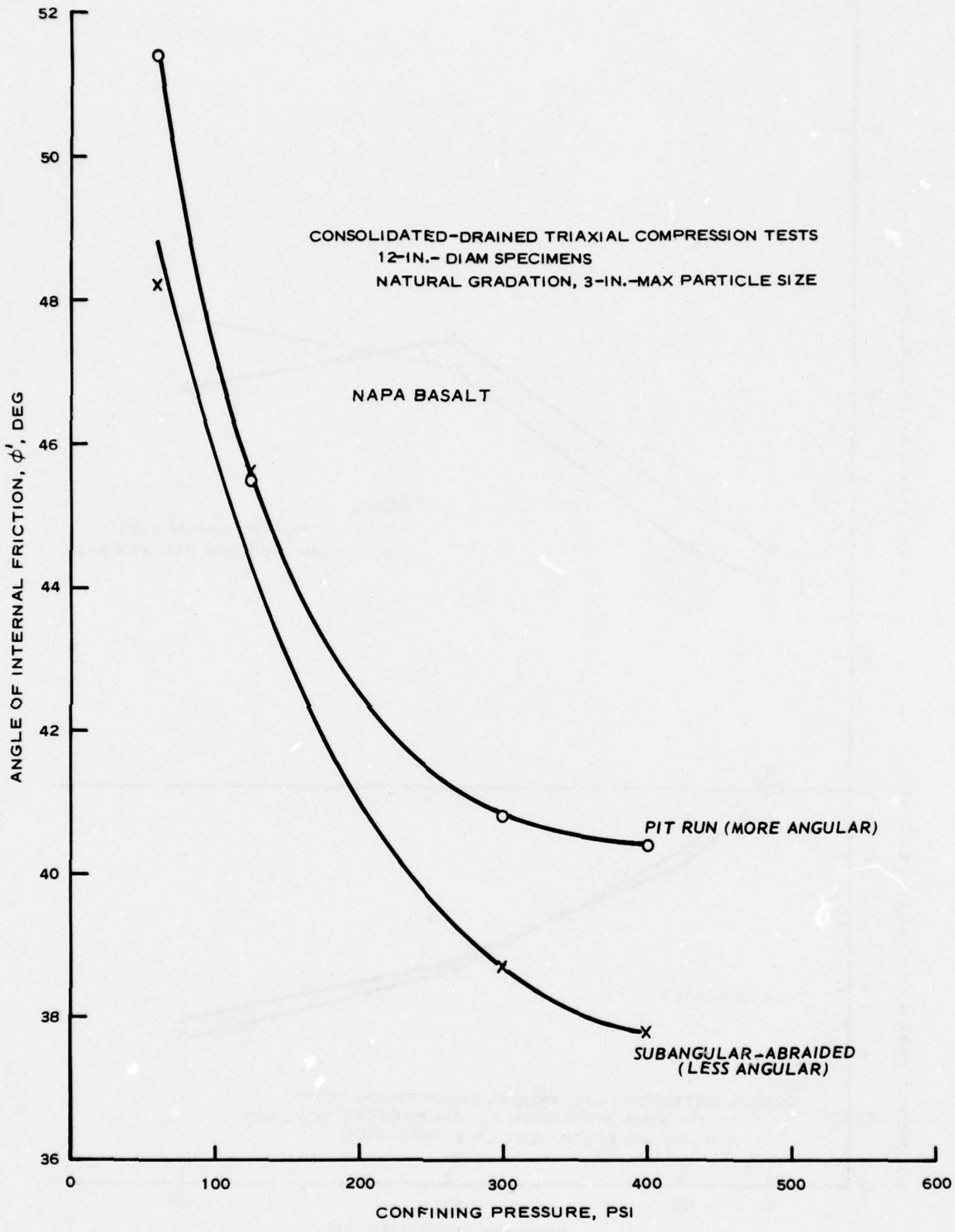

Figure 41. Angle of internal friction, φ' , versus confining pressure, Napa basalt, effects of particle shape

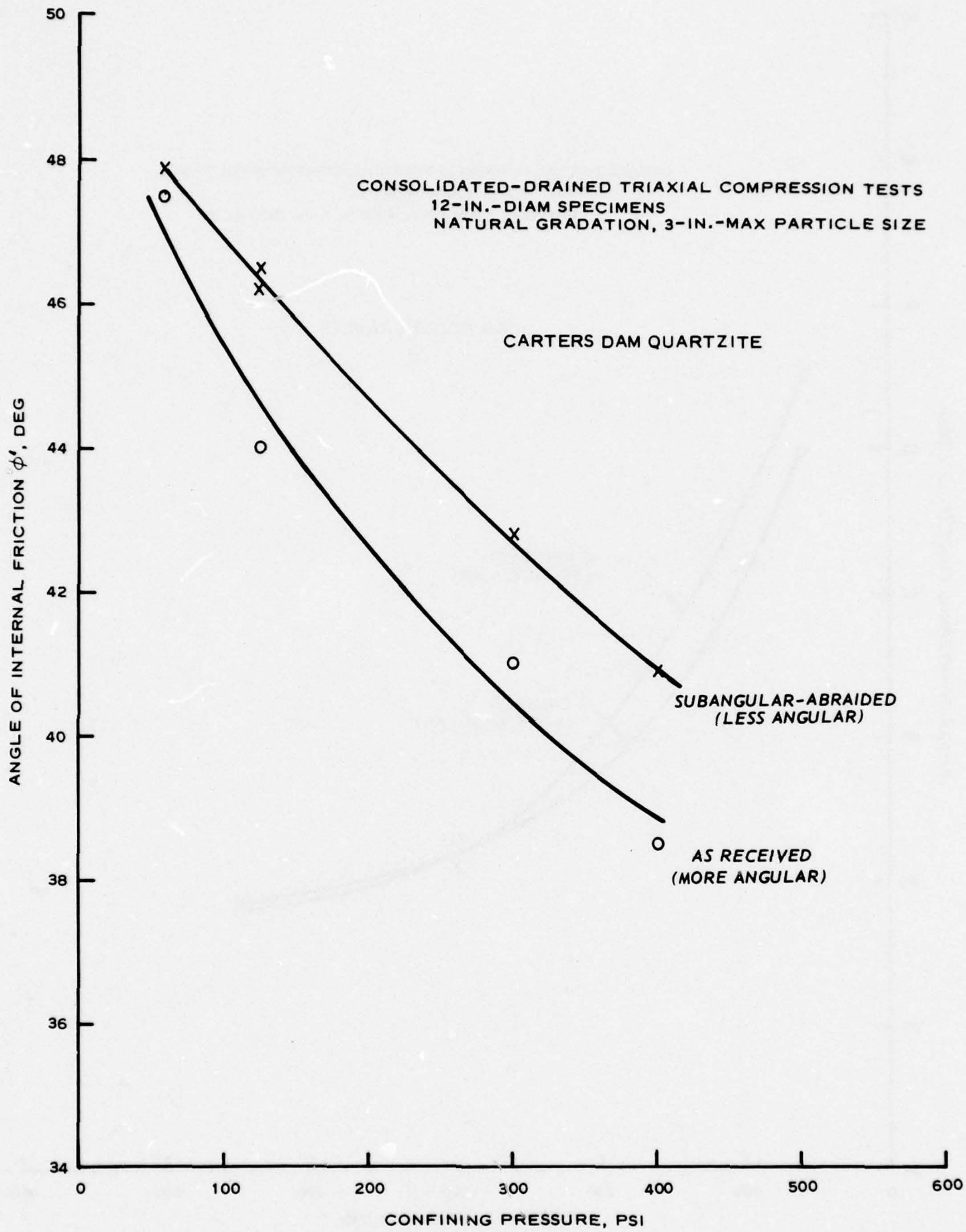

Figure 42. Angle of internal friction, ϕ' , versus confining pressure, Carters Dam quartzite, effects of particle shape

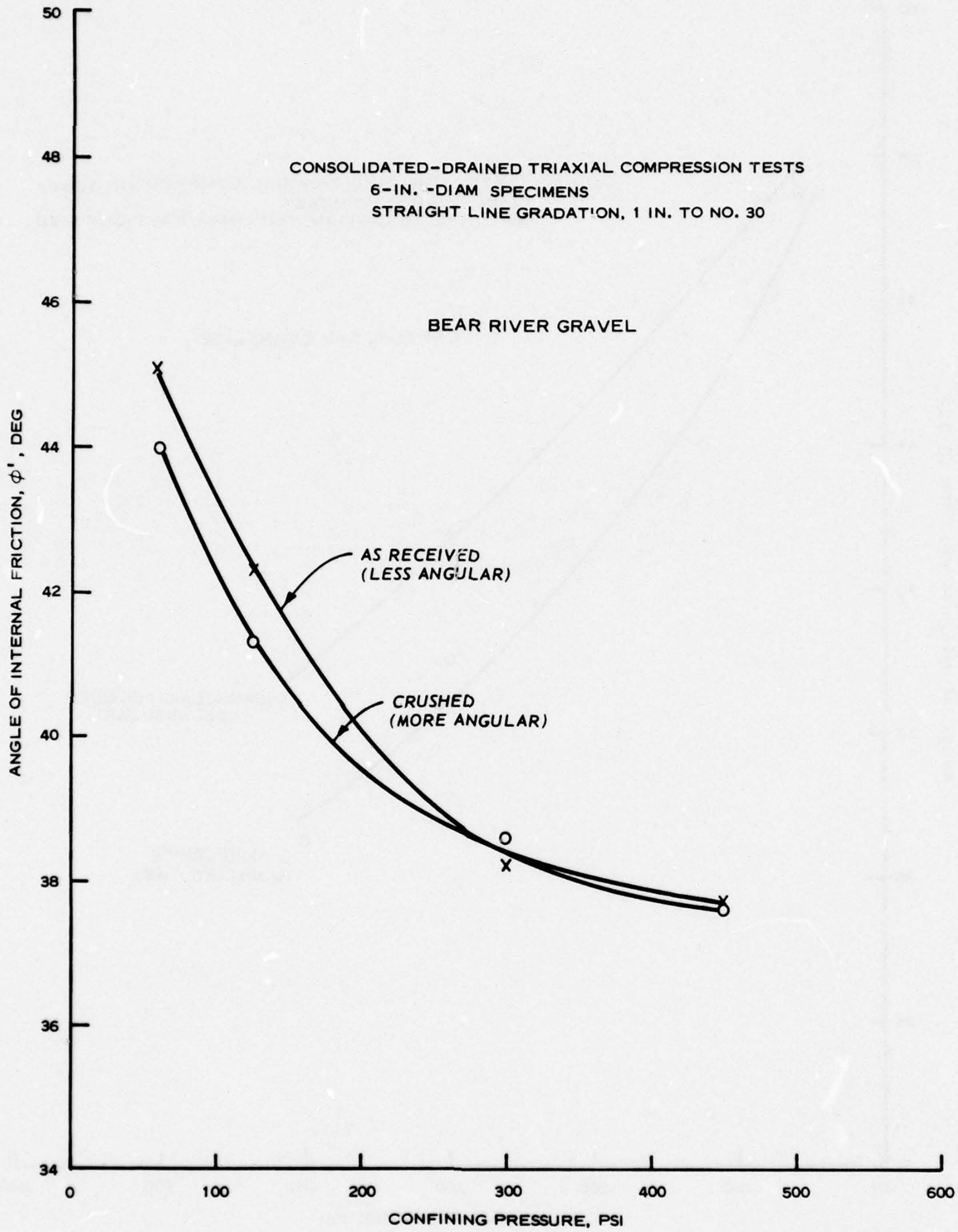

Figure 43. Angle of internal friction, ϕ' , versus confining pressure, Bear River gravel, effects of particle shape

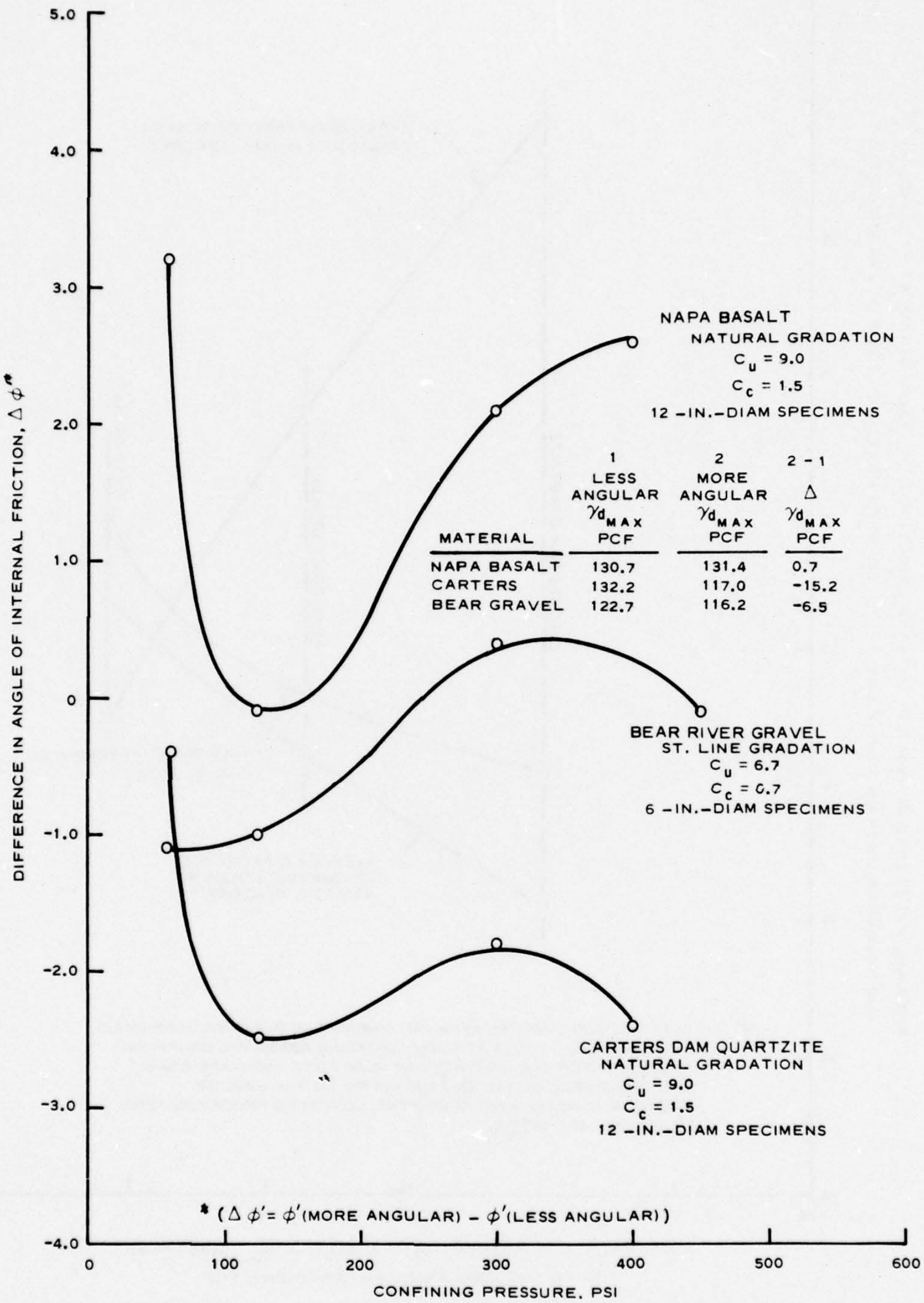

MATERIAL	1 LESS ANGULAR $\gamma_{d_{MAX}}$ PCF	2 MORE ANGULAR $\gamma_{d_{MAX}}$ PCF	2 - 1 Δ $\gamma_{d_{MAX}}$ PCF
NAPA BASALT	130.7	131.4	0.7
CARTERS	132.2	117.0	-15.2
BEAR GRAVEL	122.7	116.2	-6.5

Figure 44. Change in angle of internal friction due to increased particle angularity versus confining pressure, effects of particle shape

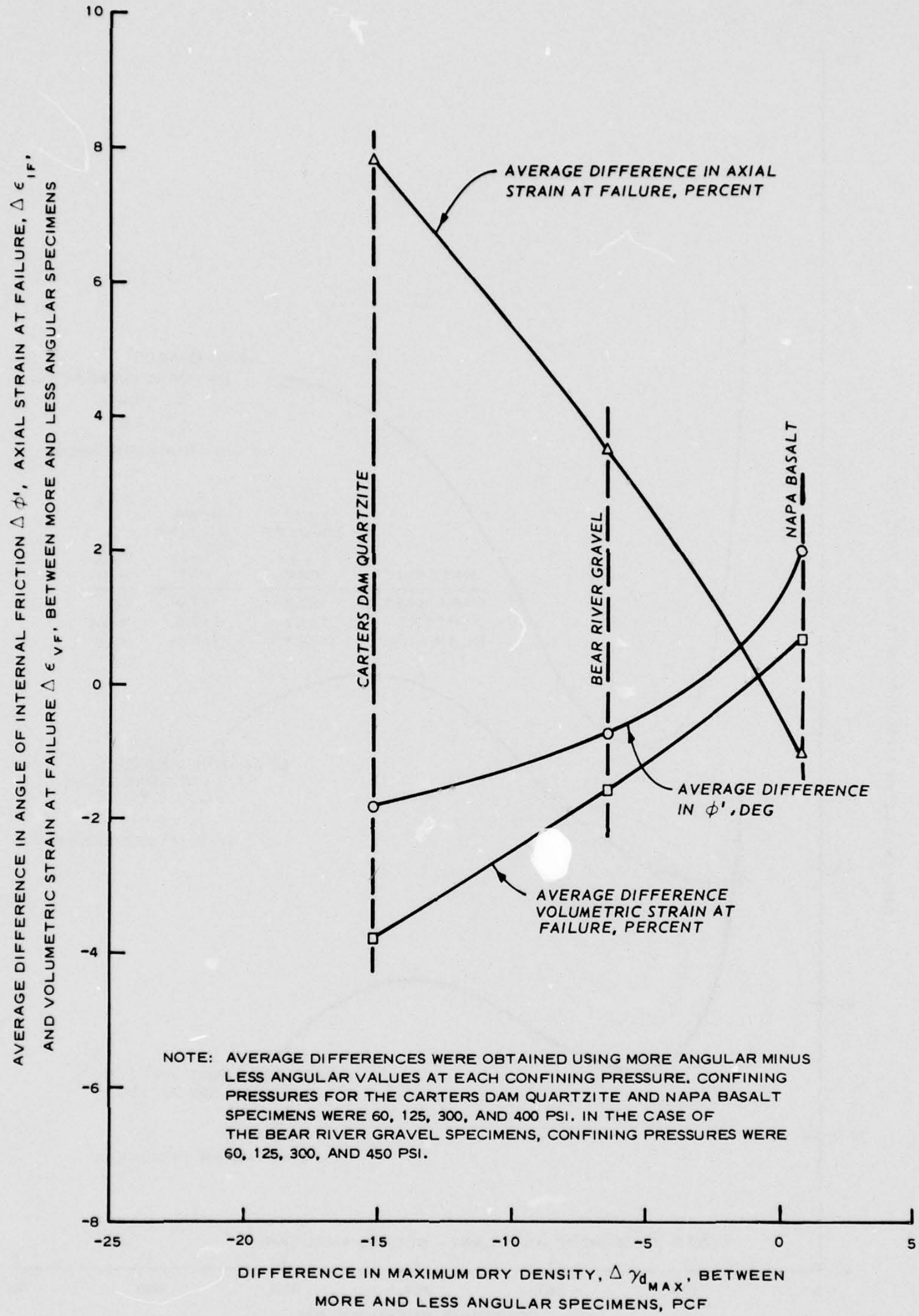

Figure 45. Average difference in angle of internal friction, $\Delta\phi'$, axial strain at failure, $\Delta\varepsilon_{1f}$, and volumetric strain at failure, $\Delta\varepsilon_{vf1}$ between more and less angular specimens versus the average difference in maximum dry density, $\Delta\delta d_{max}$, between more and less angular specimens, effects of particle shape

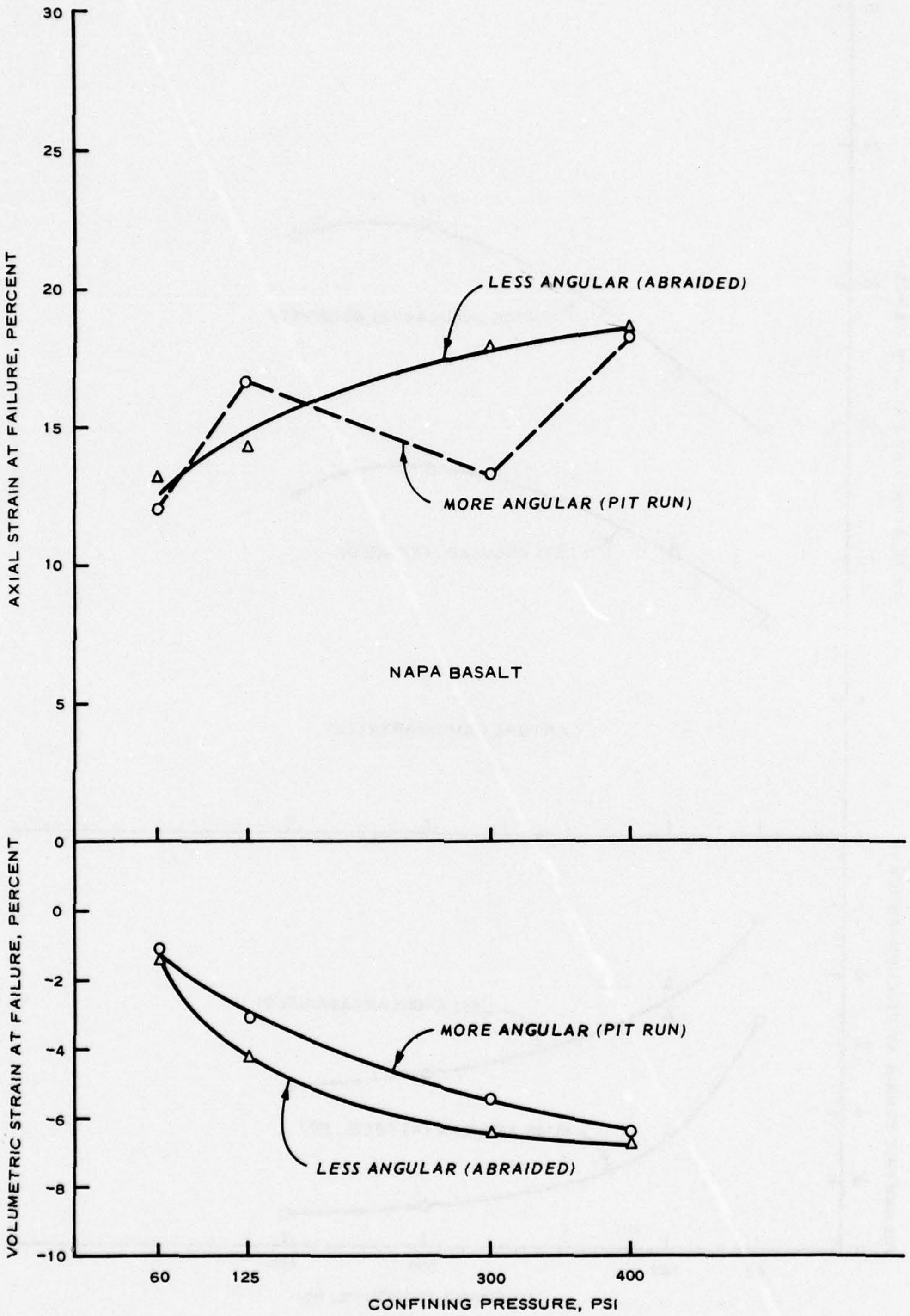

Figure 46. Axial and volumetric strain at failure versus confining pressure, Napa basalt, effects of particle shape

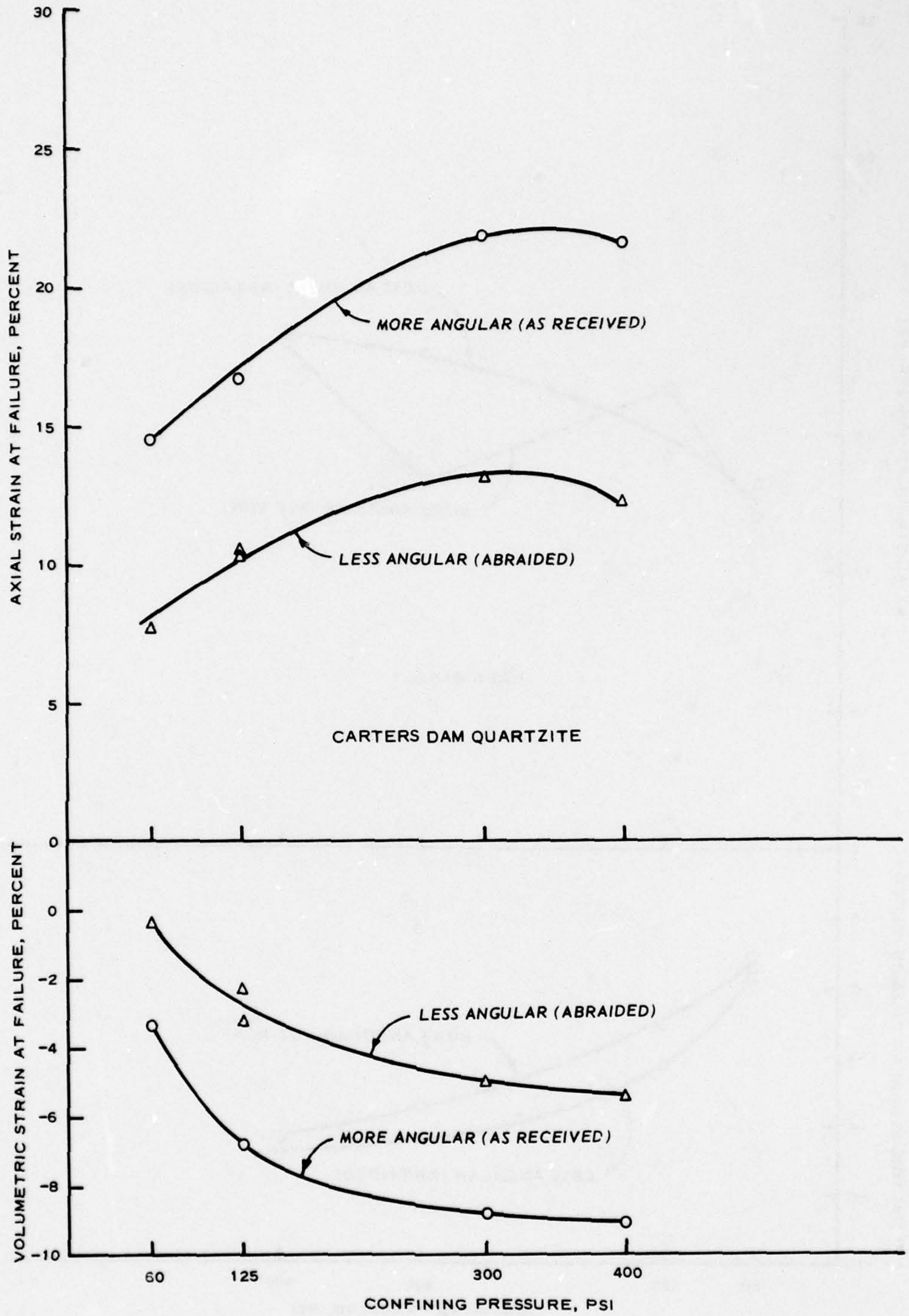

Figure 47. Axial and volumetric strain at failure versus confining pressure, Carters Dam quartzite, effects of particle shape

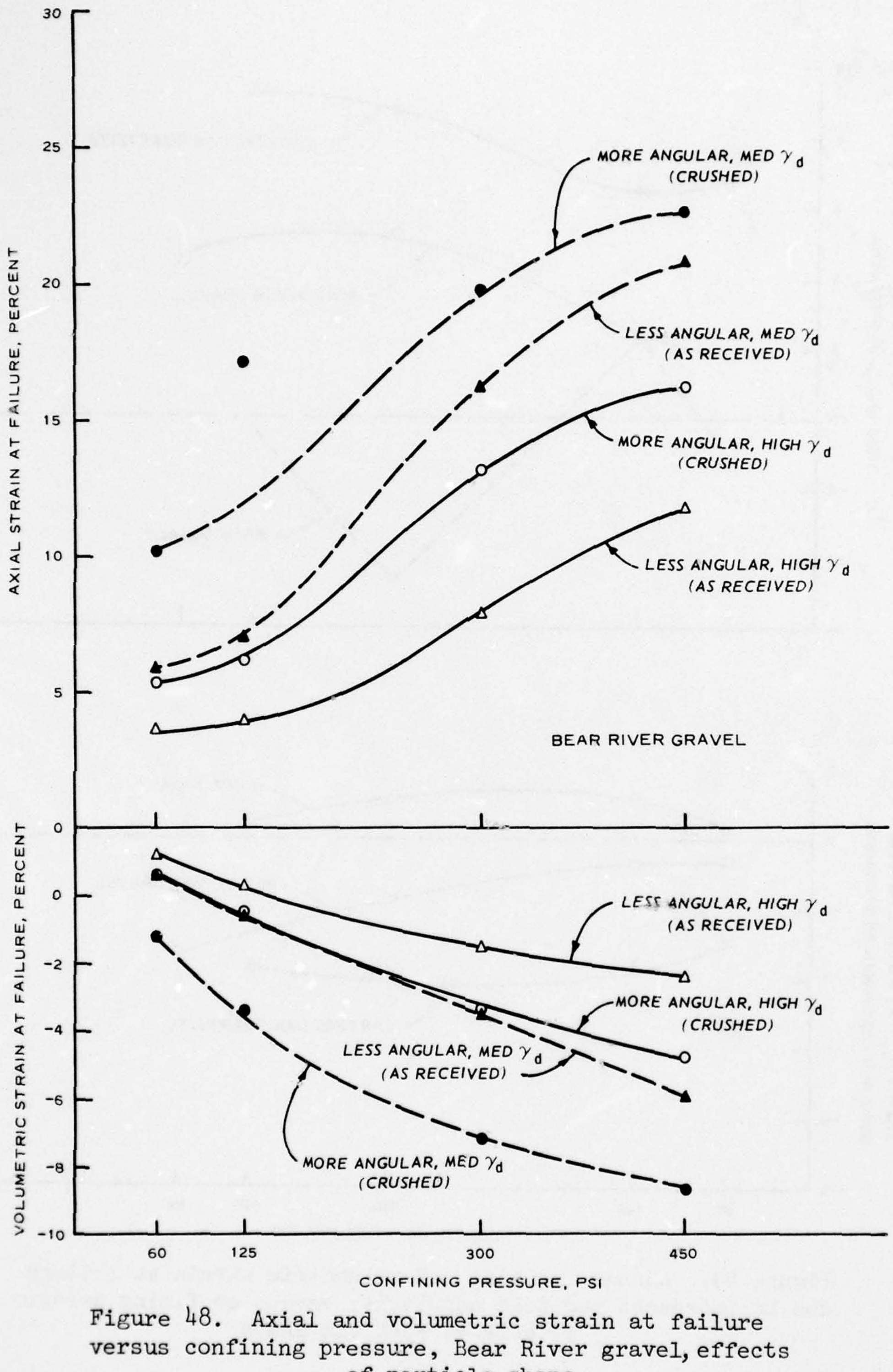

Figure 48. Axial and volumetric strain at failure versus confining pressure, Bear River gravel, effects of particle shape

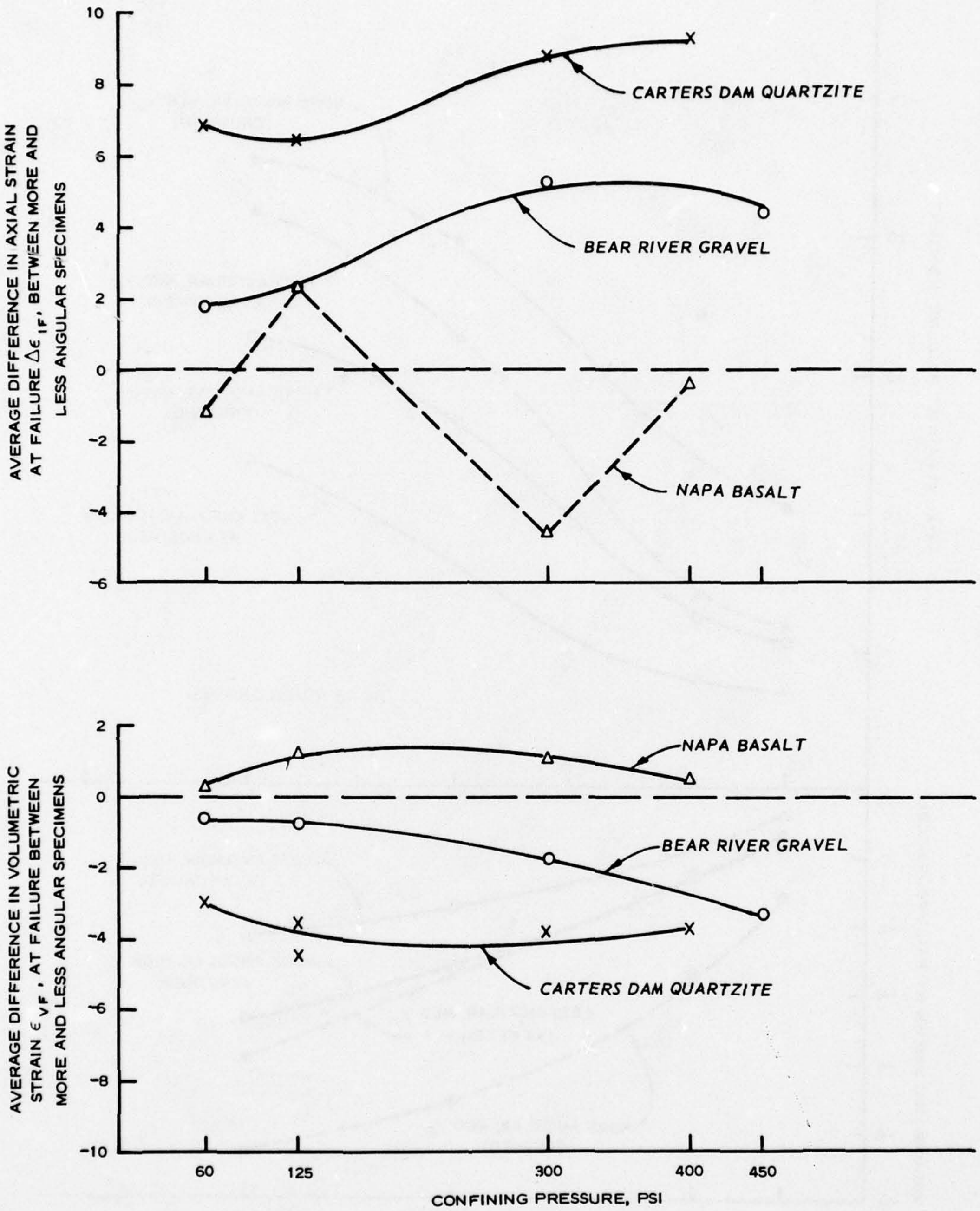

Figure 49. Change in axial and volumetric strain at failure due to increased particle angularity versus confining pressure, effects of particle shape

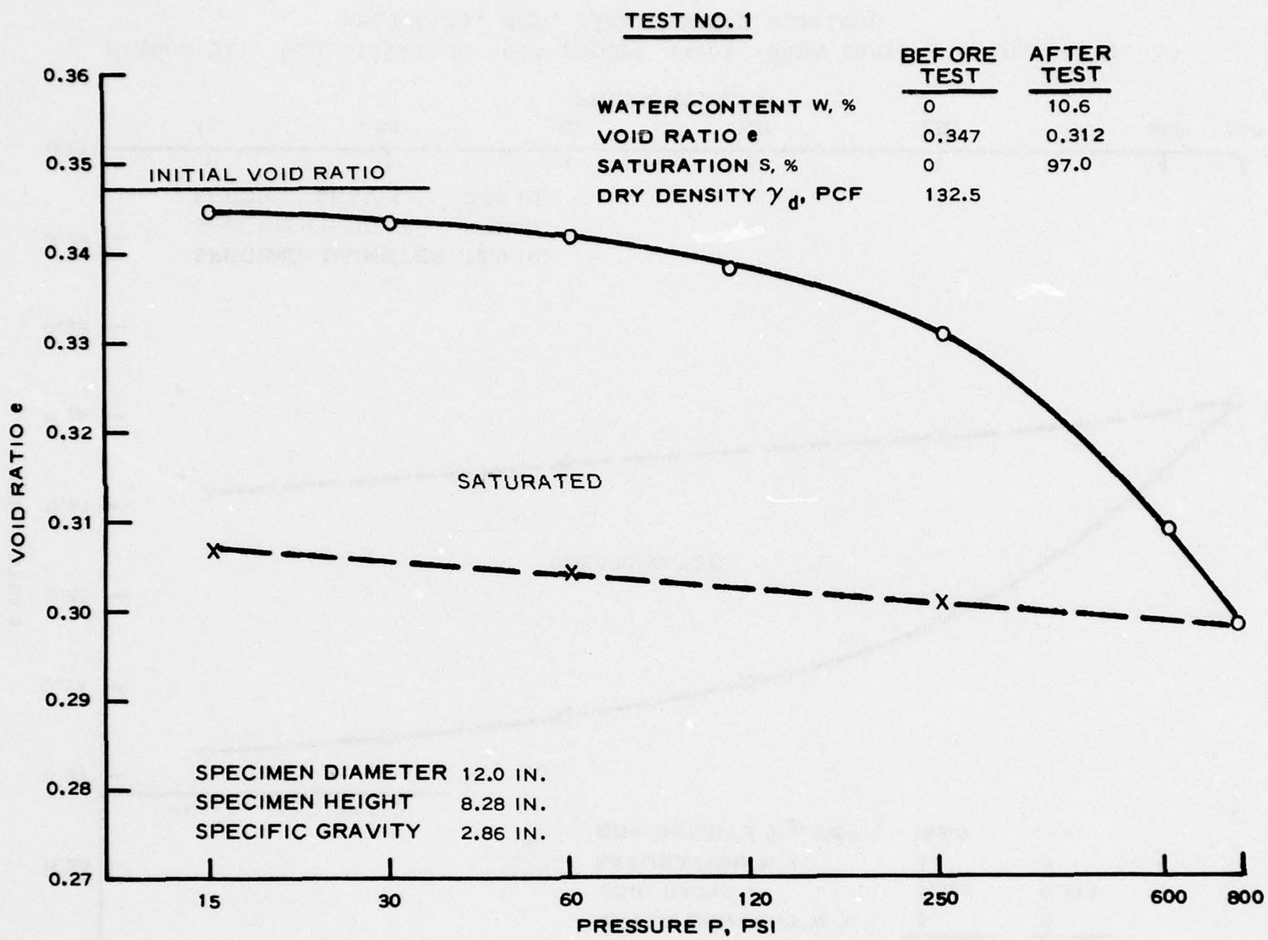

Figure 50. Consolidation test report sheet, Napa basalt, 3 in. to No. 30 gradation, inundated, high density specimen

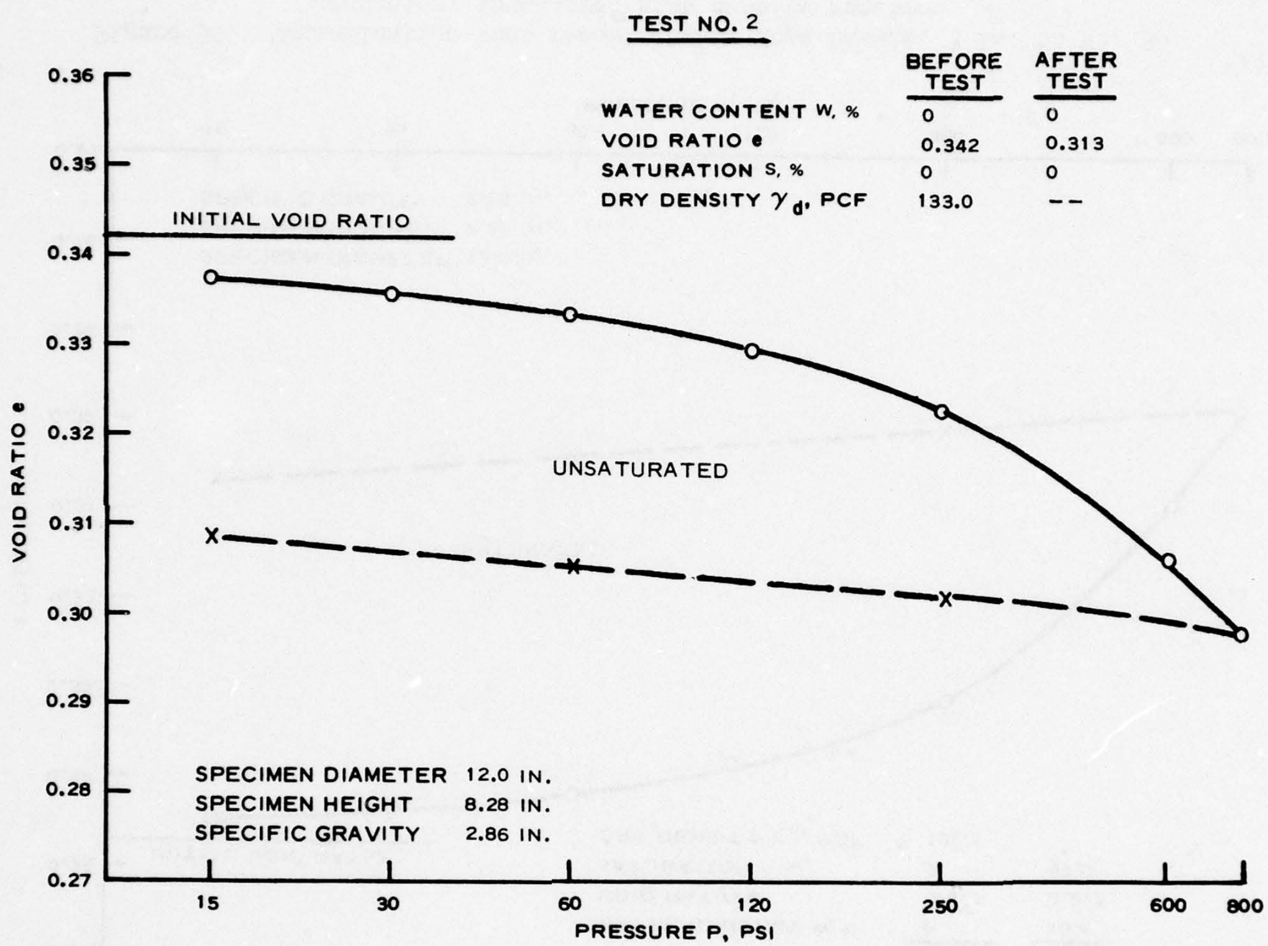

Figure 51. Consolidation test report sheet, Napa basalt, 3 in. to No. 30 gradation, dry, high density specimen

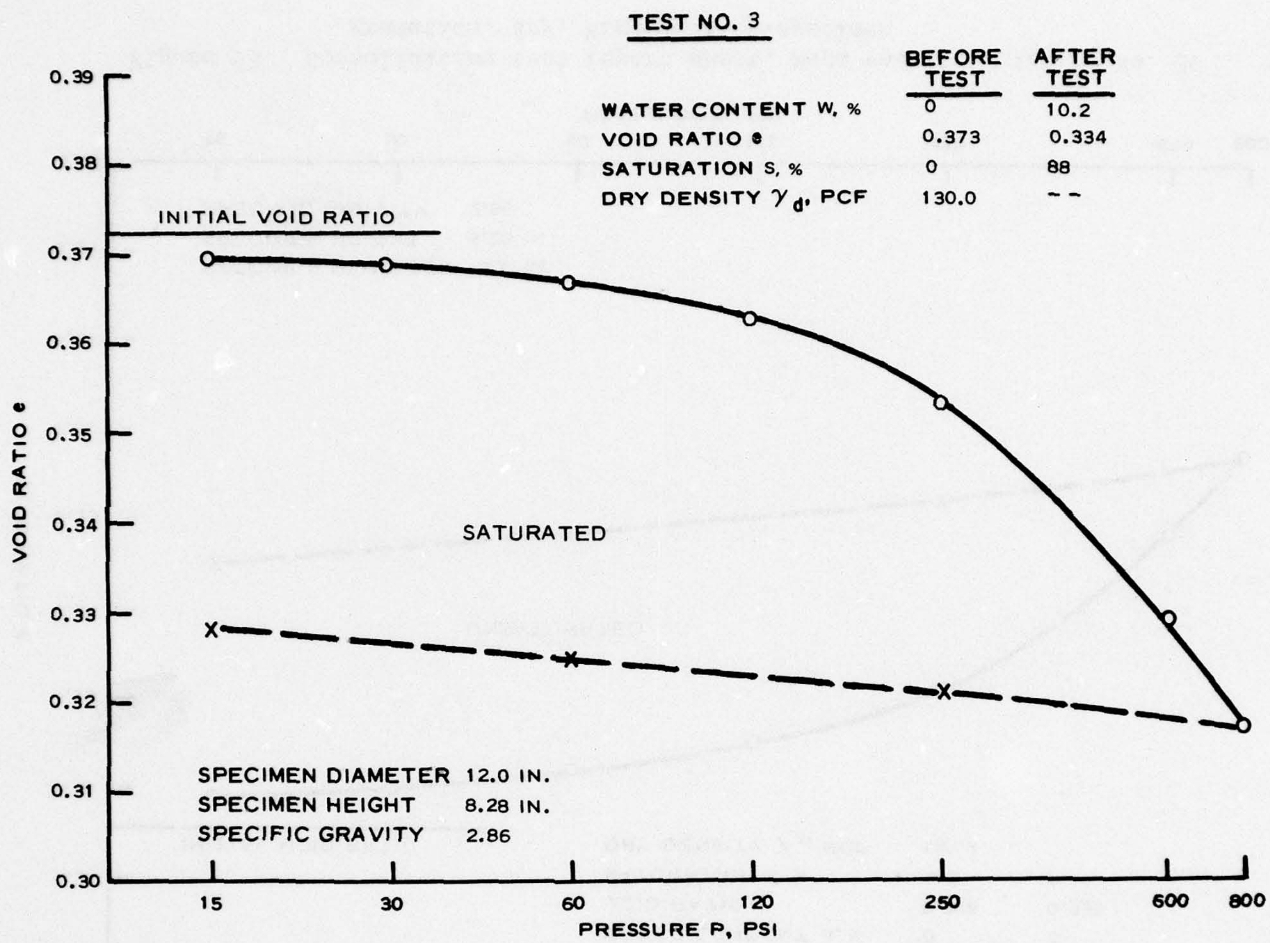

Figure 52. Consolidation test report sheet, Napa basalt, 2 in. to No. 30 gradation, inundated, high density specimen

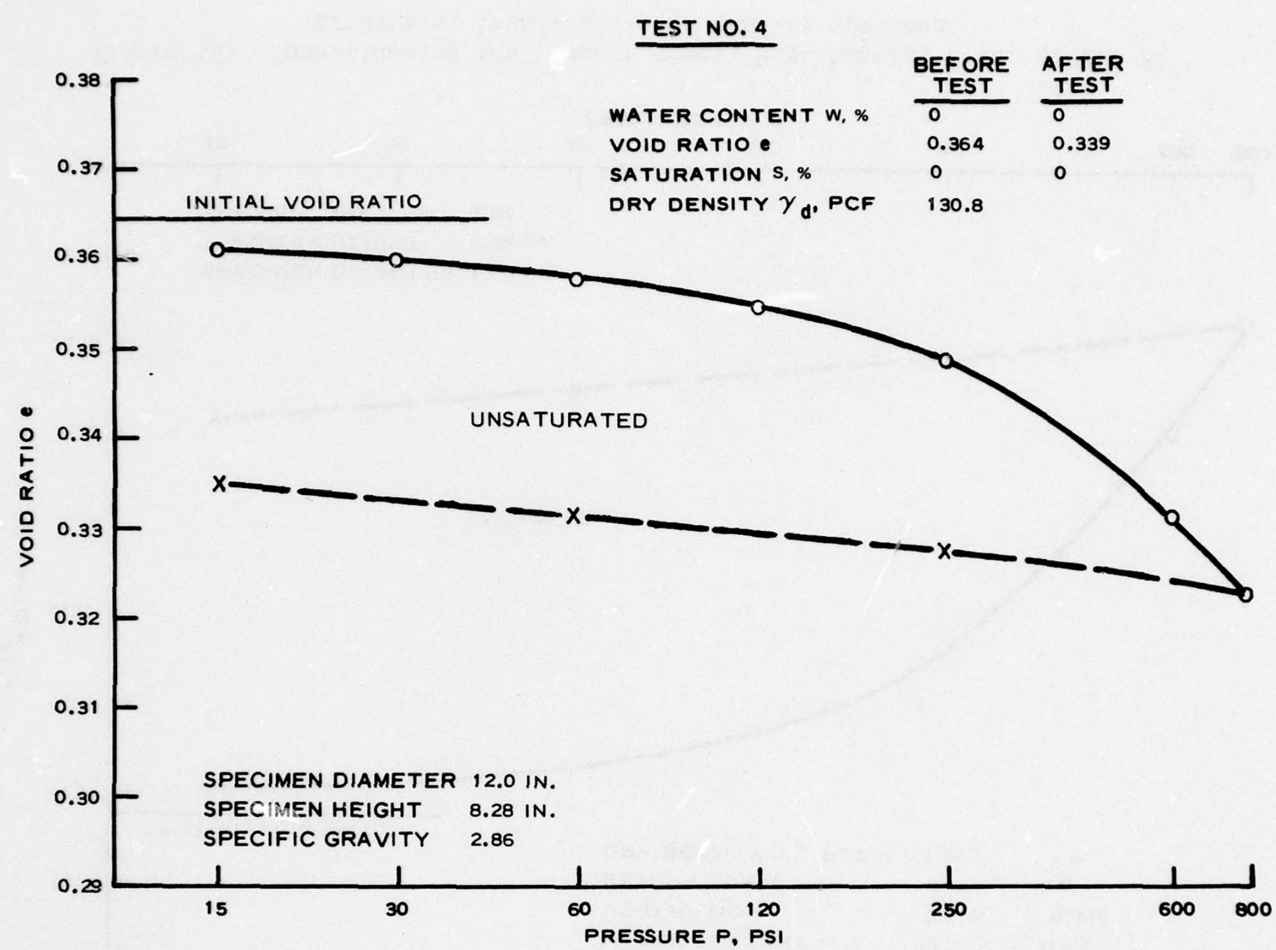

Figure 53. Consolidation test report sheet, Napa basalt, 2 in. to No. 30 gradation, dry, high density specimen

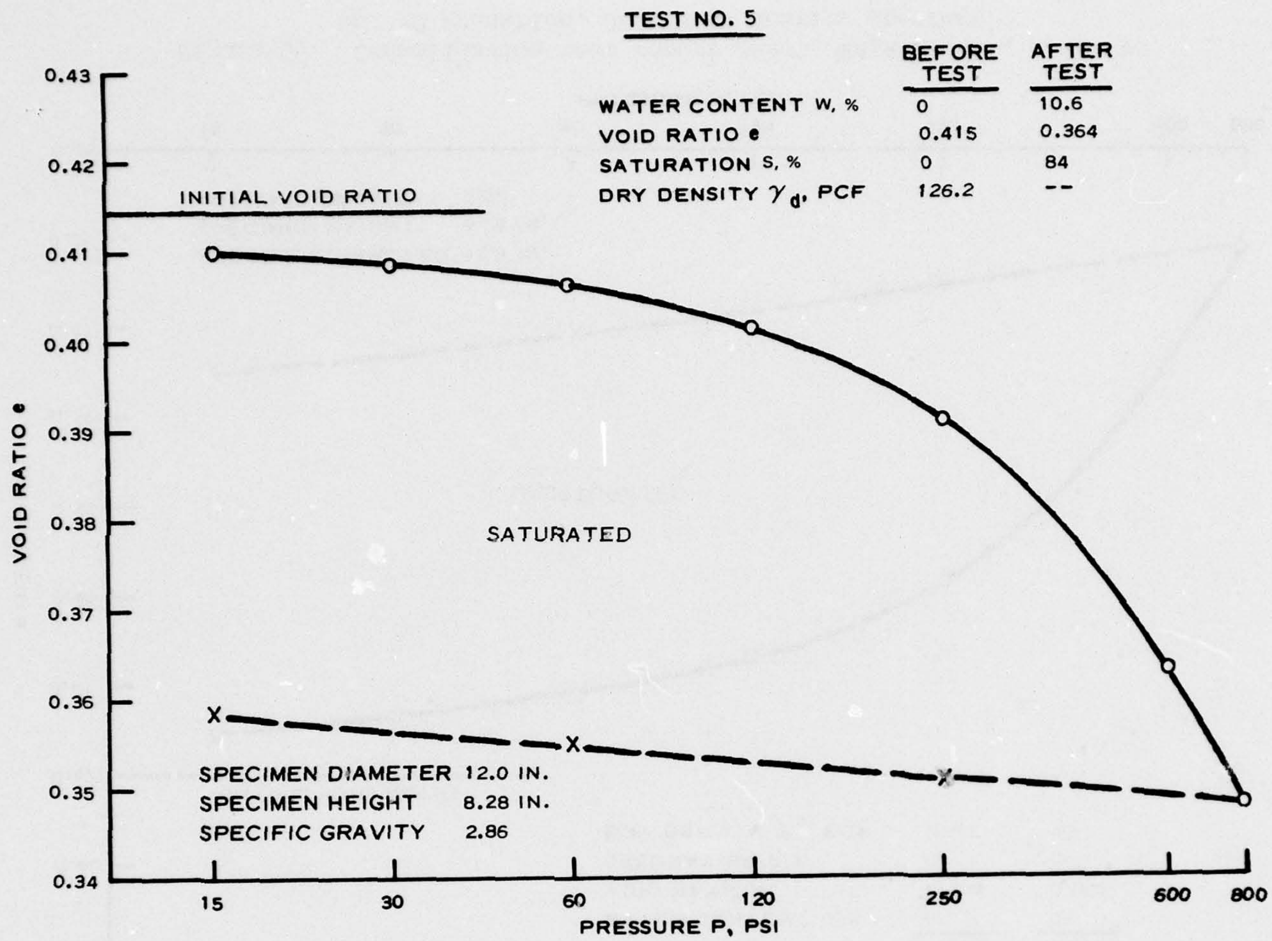

Figure 54. Consolidation test report sheet, Napa basalt, 1 in. to No. 30 gradation, inundated, high density specimen

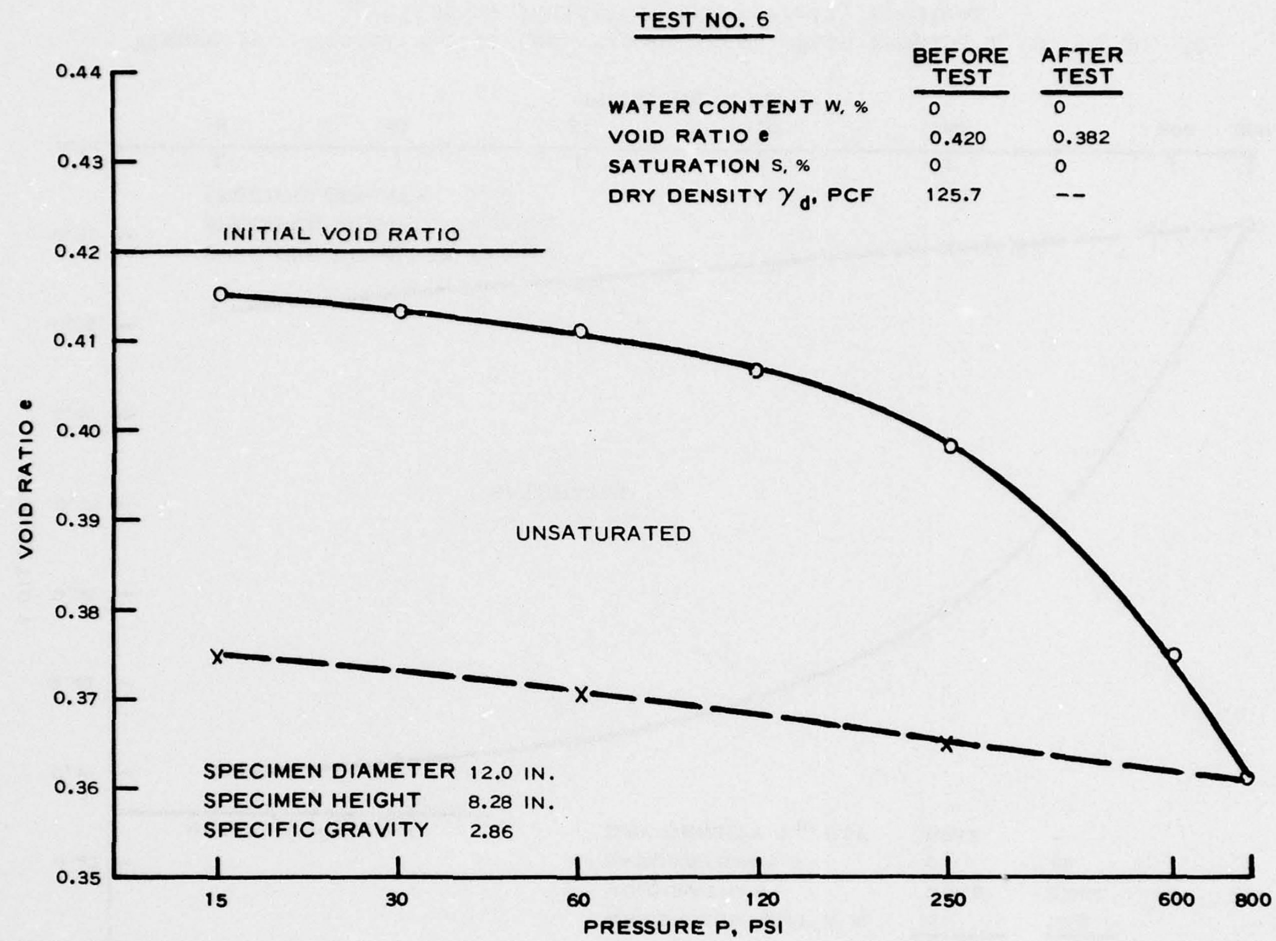

Figure 55. Consolidation test report sheet, Napa basalt, 1 in. to No. 30 gradation, dry, high density specimen

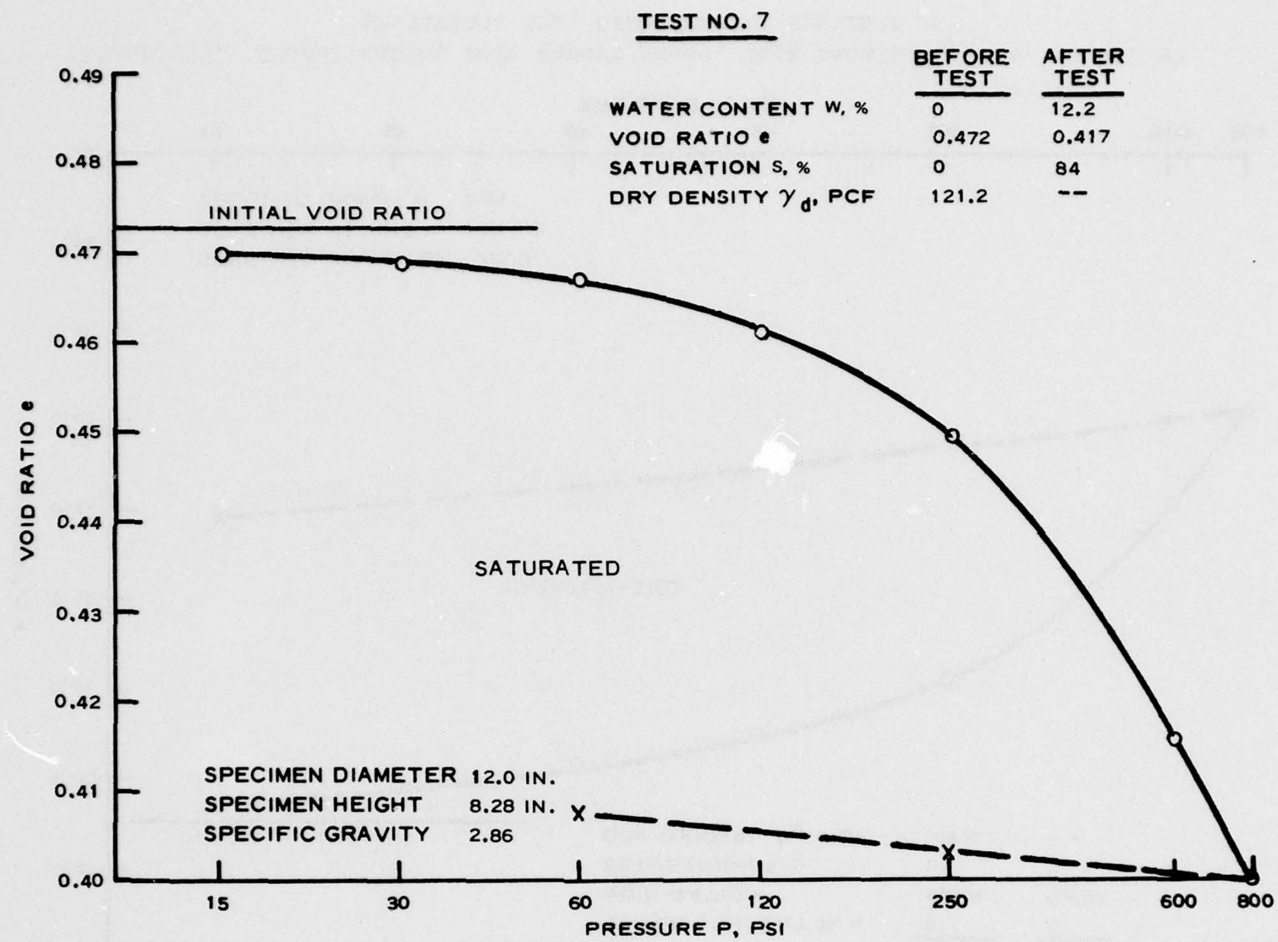

Figure 56. Consolidation test report sheet, Napa basalt, 1/2 in. to No. 30 gradation, inundated, high density specimen

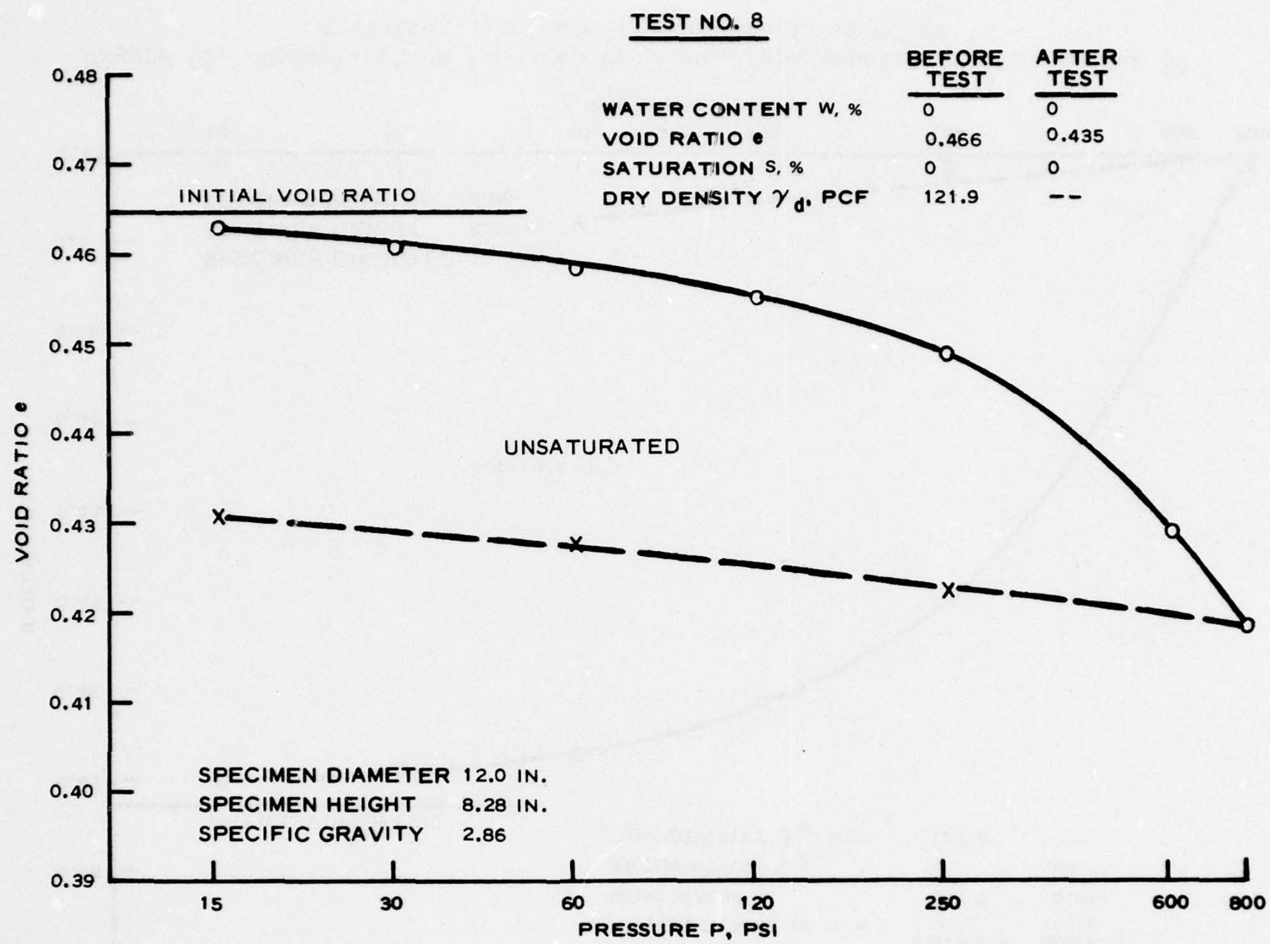

Figure 57. Consolidation test report sheet, Napa basalt, 1/2 in. to No. 30 gradation, dry, high density specimen

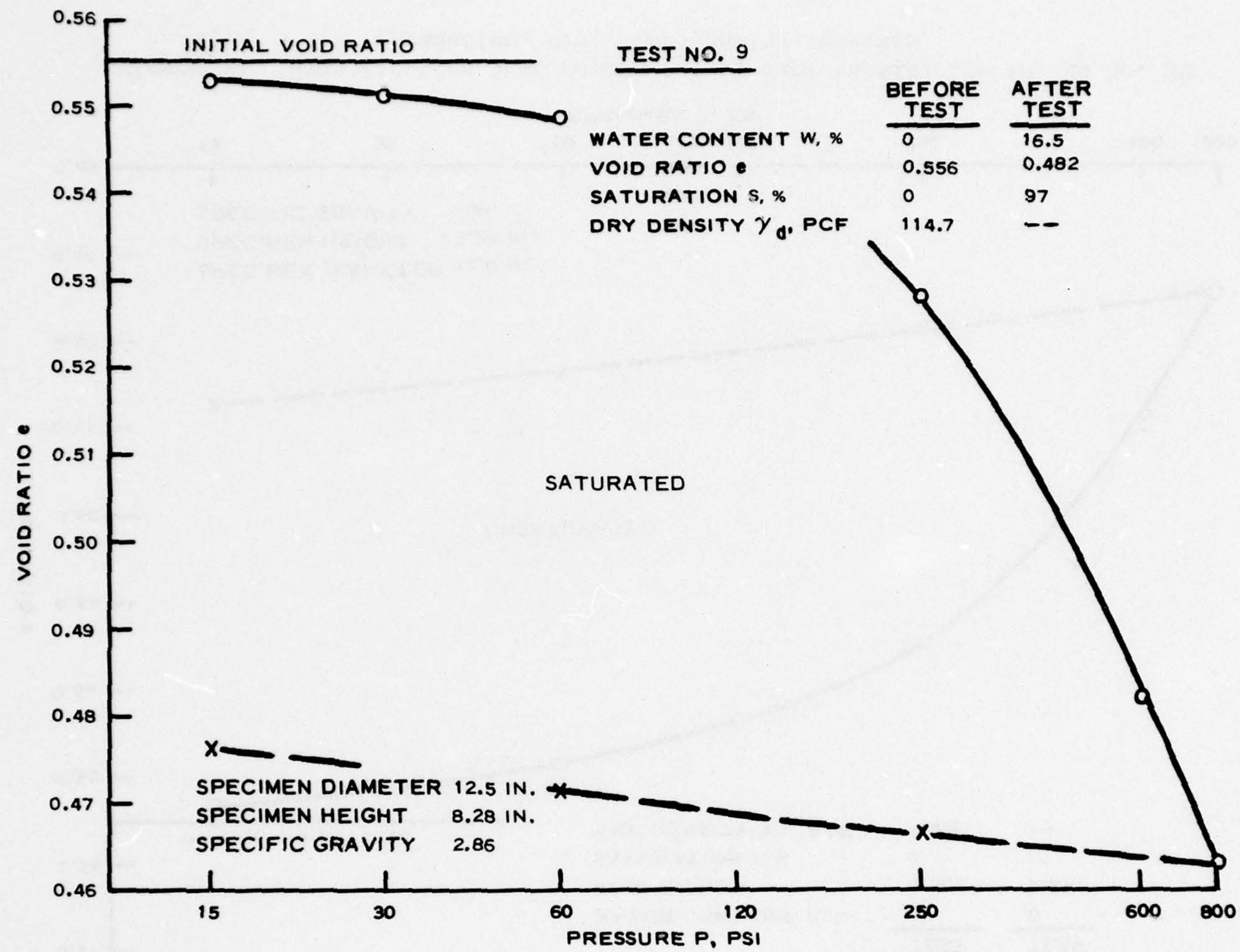

Figure 58. Consolidation test report sheet, Napa basalt, 1/4 in. to No. 30 gradation, inundated, high density specimen

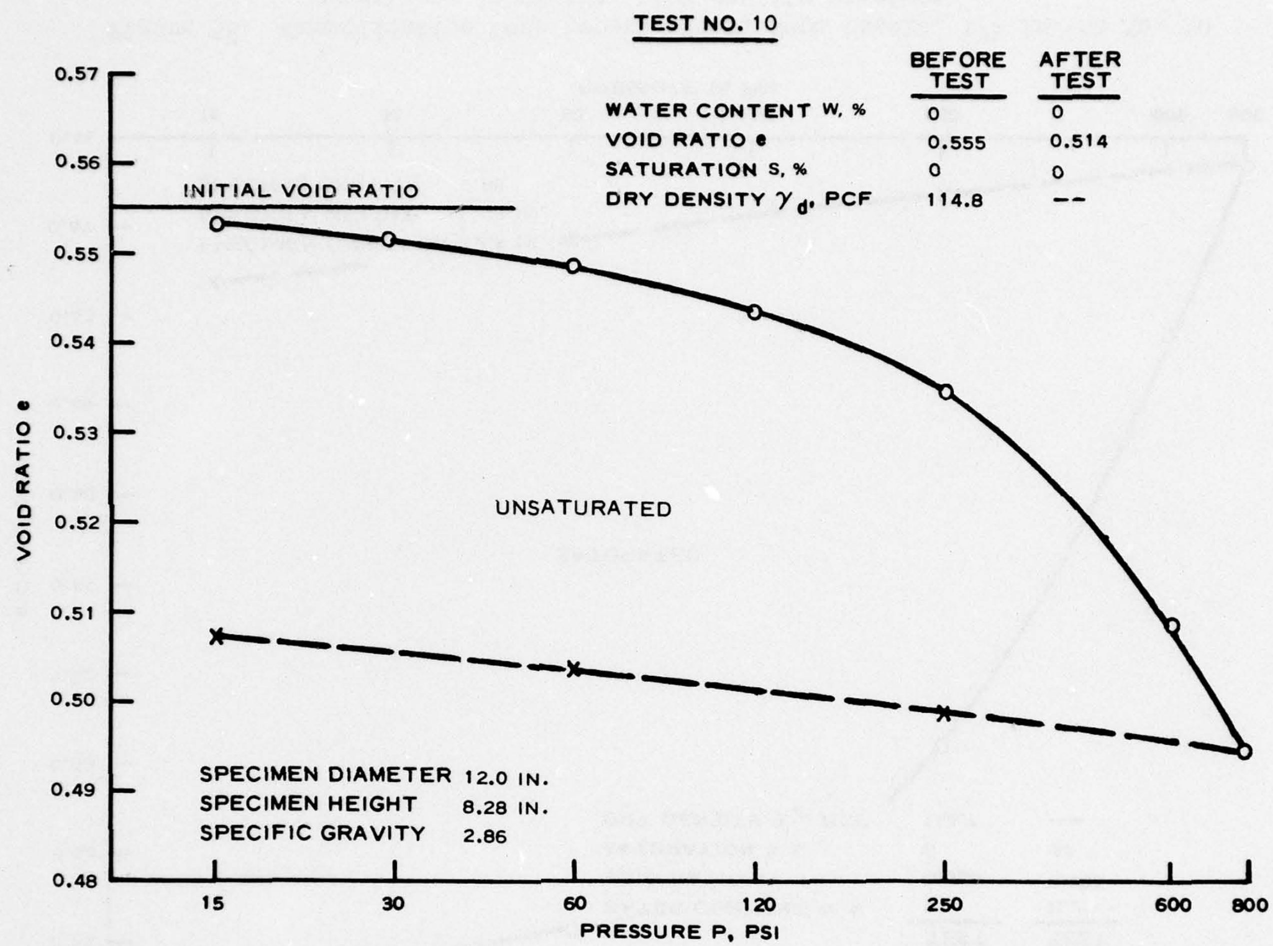

Figure 59. Consolidation test report sheet, Napa basalt, 1/4 in. to No. 30 gradation, dry, high density specimen

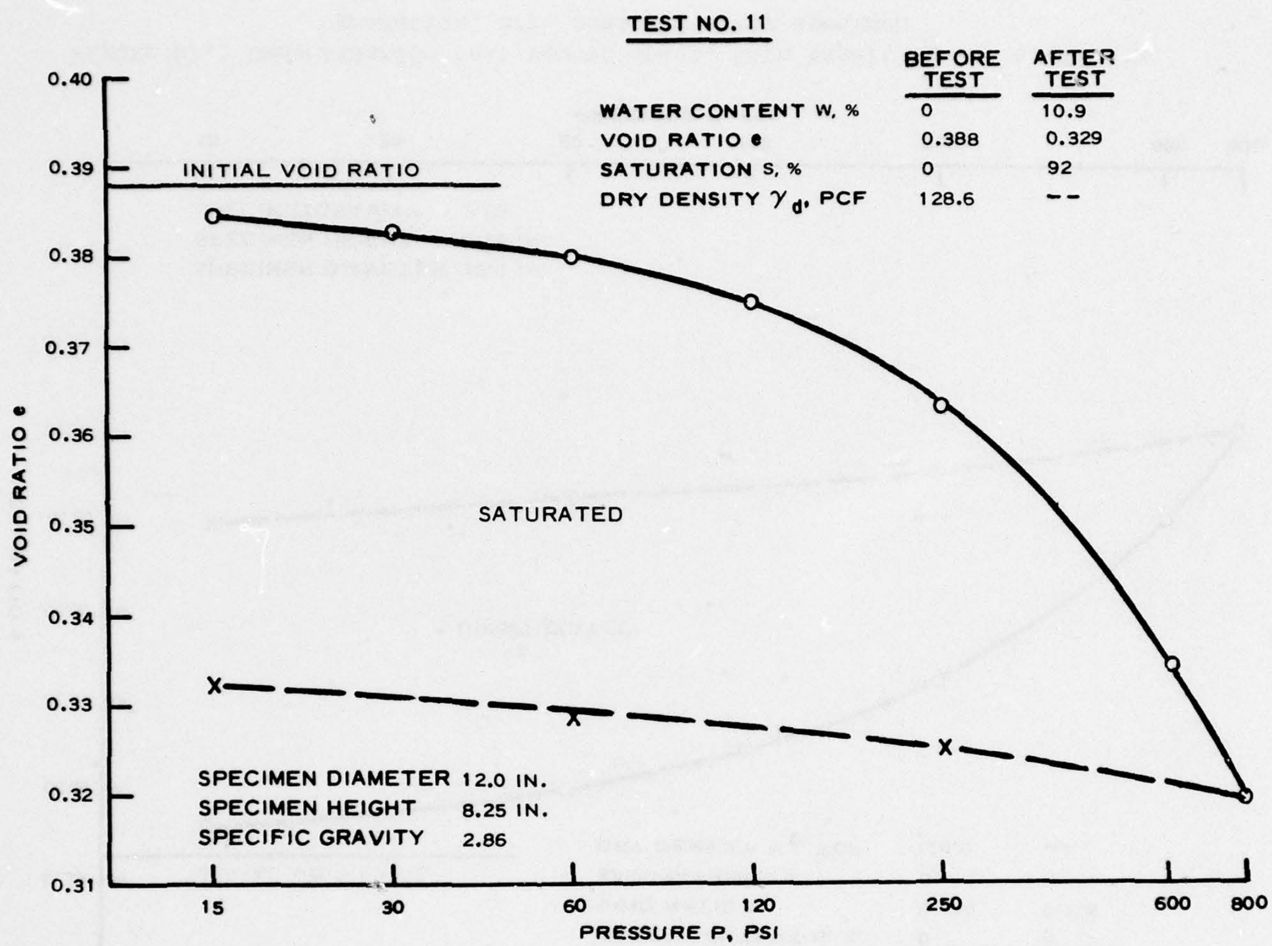

Figure 60. Consolidation test report sheet, Napa basalt, 3 in. to No. 30 gradation, inundated, medium density specimen

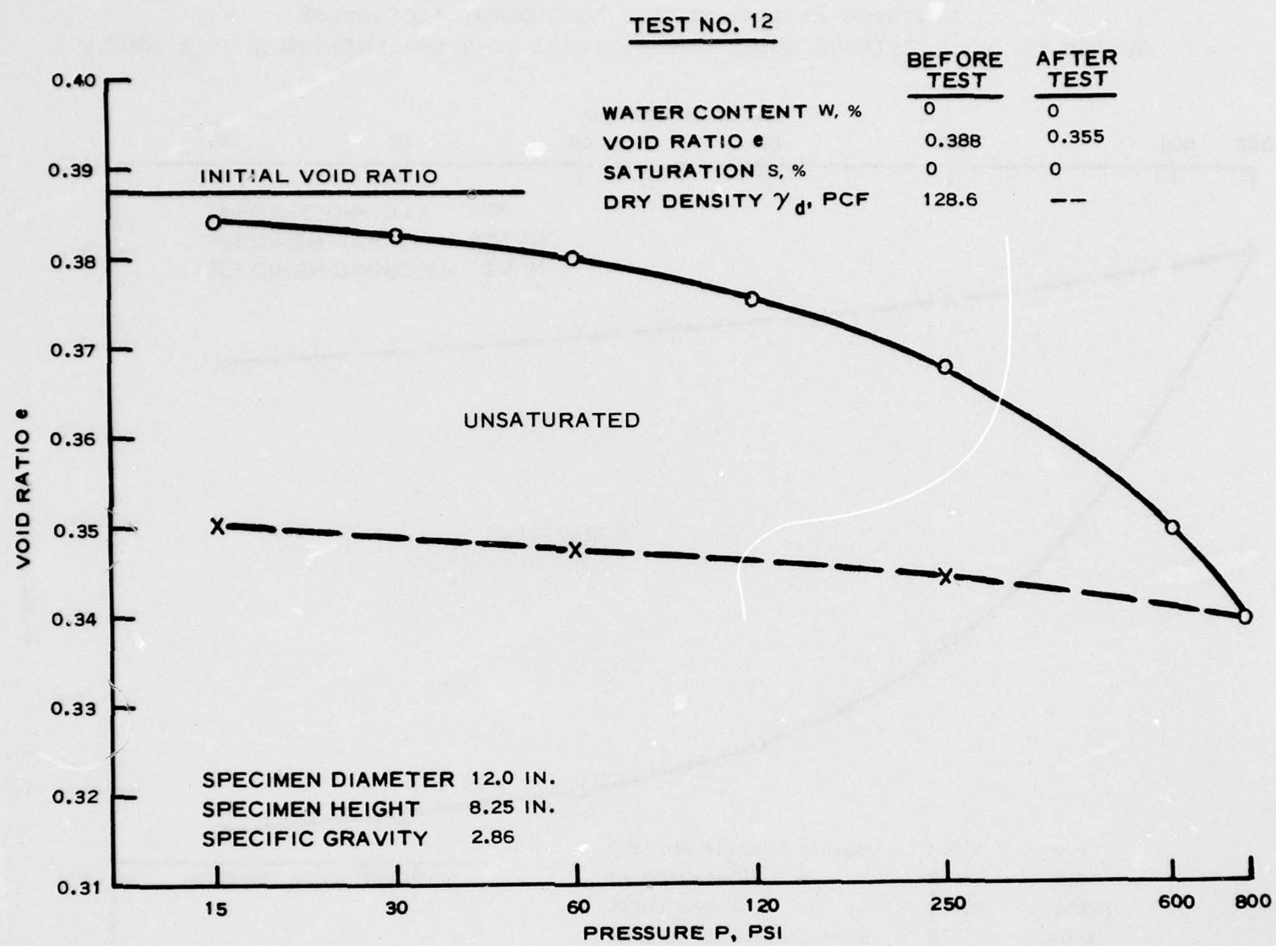

Figure 61. Consolidation test report sheet, Napa basalt, 3 in. to No. 30 gradation, dry, medium density specimen

AD-A051 795 ARMY ENGINEER WATERWAYS EXPERIMENT STATION VICKSBURG MISS F/G 13/2
STRENGTH AND DEFORMATION PROPERTIES OF ROCK FILL.(U)
JAN 78 R T DONAGHE, M W COHEN

UNCLASSIFIED WES-TR-S-78-1 NL

2 OF 2
AD
A051 795





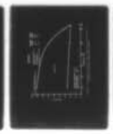




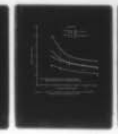

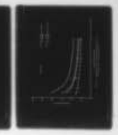
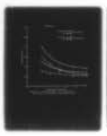

END
DATE
FILMED
4-78
DDC

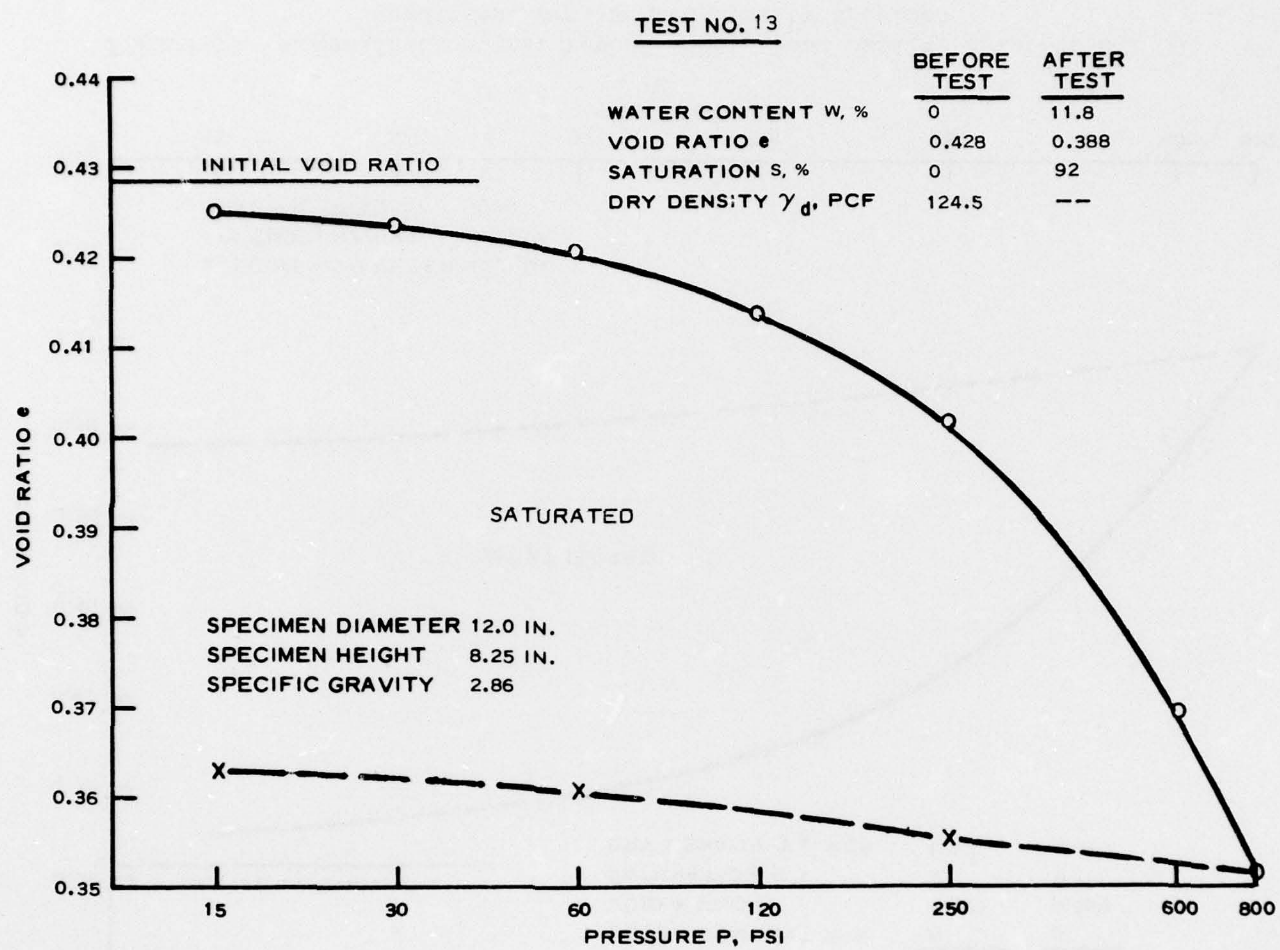

Figure 62. Consolidation test report sheet, Napa basalt, 2 in. to No. 30 gradation, inundated, medium density specimen

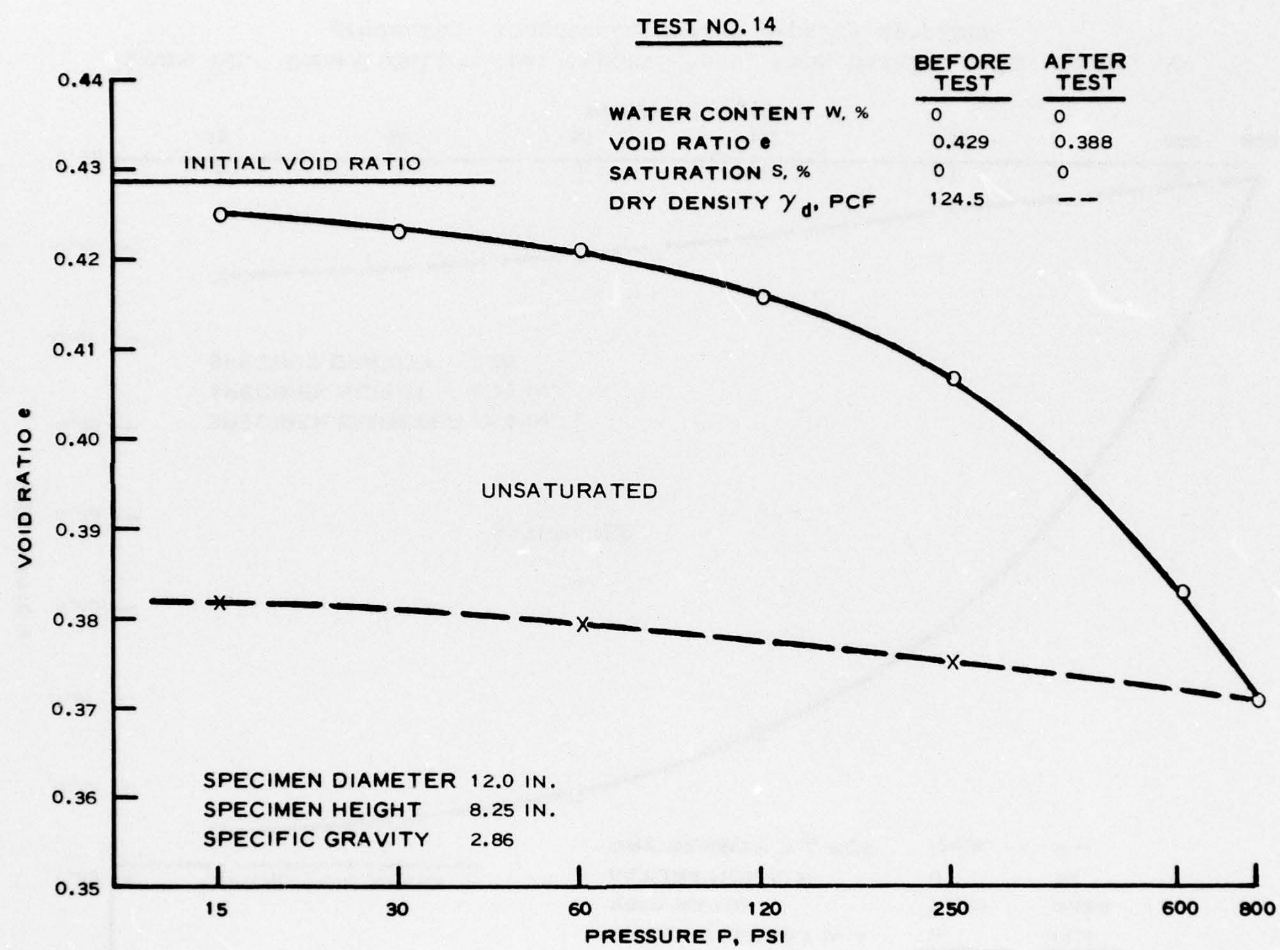

Figure 63. Consolidation test report sheet, Napa basalt, 2 in. to No. 30 gradation, dry, medium density specimen

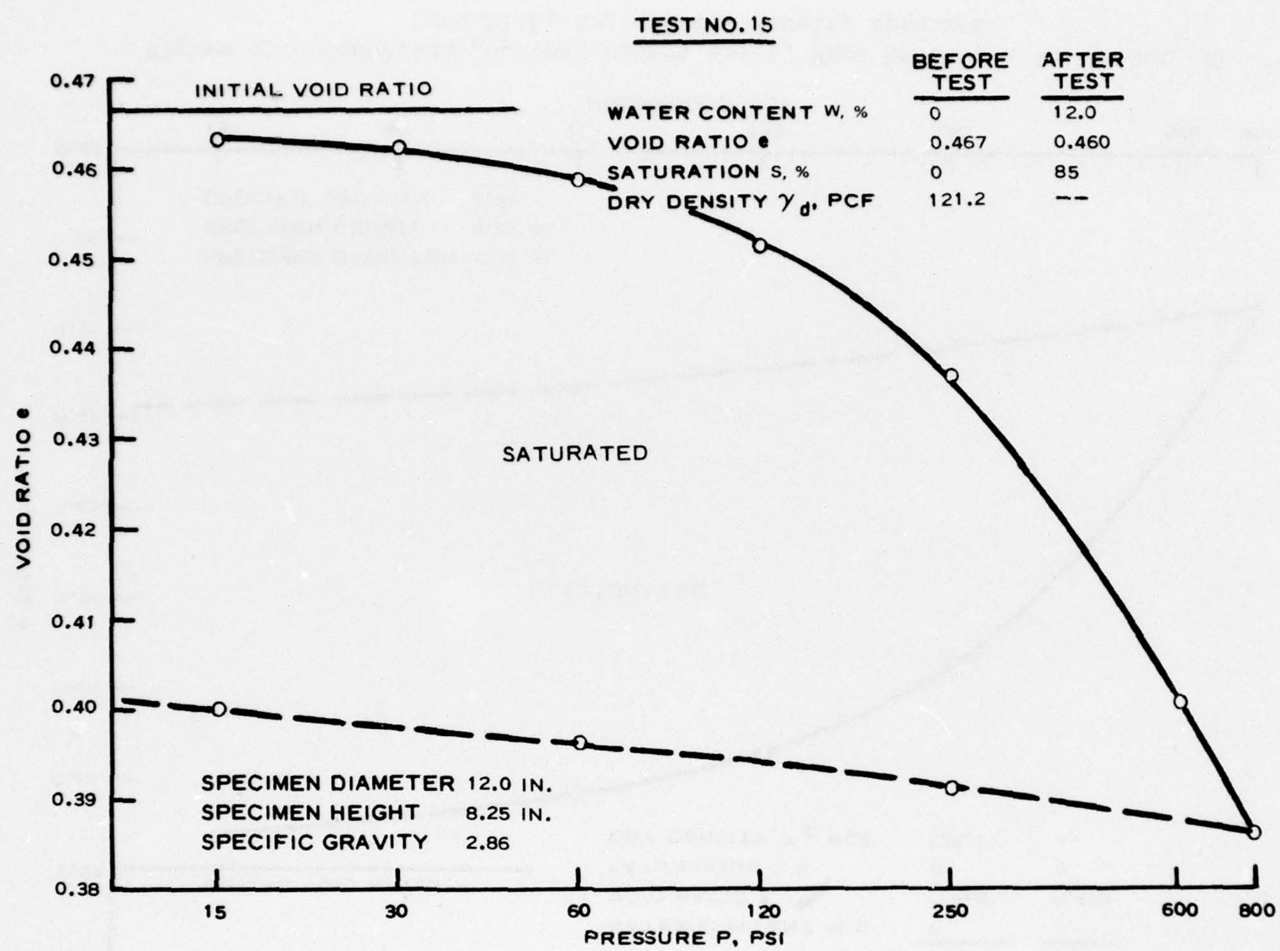

Figure 64. Consolidation test report sheet, Napa basalt, 1 in. to No. 30 gradation, inundated, medium density specimen

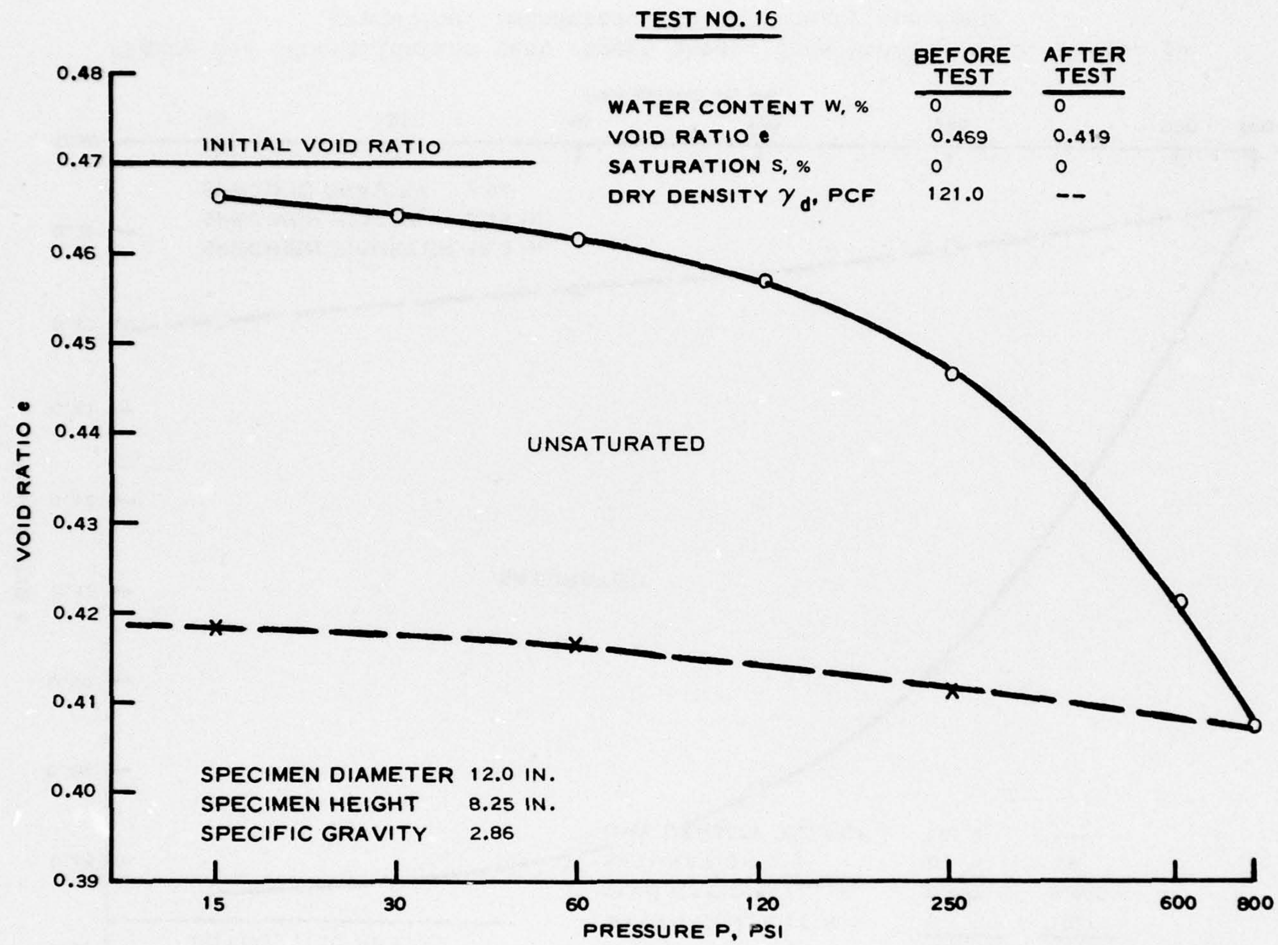

Figure 65. Consolidation test report sheet, Napa basalt, 1 in. to No. 30 gradation, dry, medium density specimen

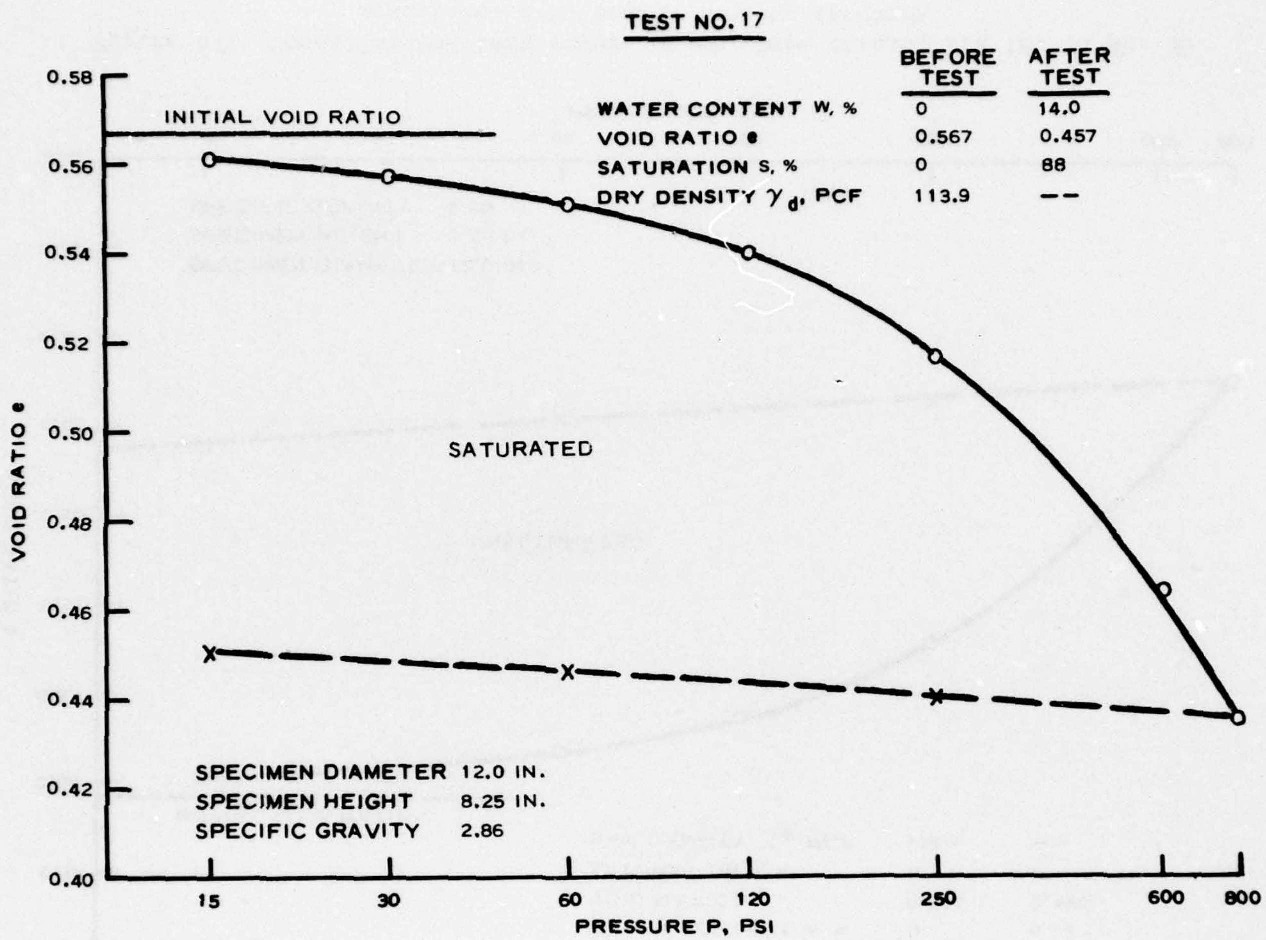

Figure 66. Consolidation test report sheet, Napa basalt, 1/2 in. to No. 30 gradation, inundated, medium density specimen

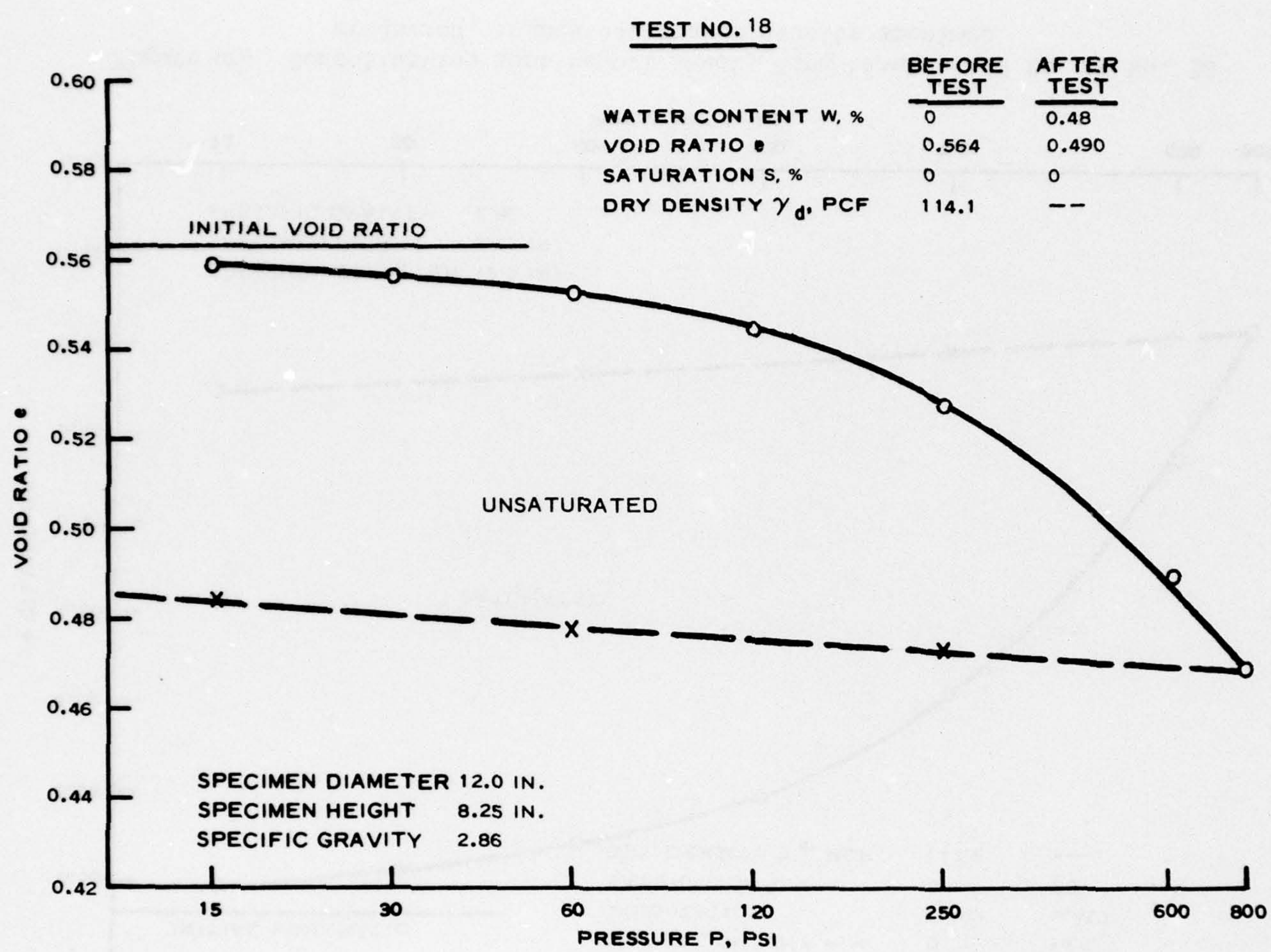

Figure 67. Consolidation test report sheet, Napa basalt, 1/2 in. to No. 30 gradation, dry, medium density specimen

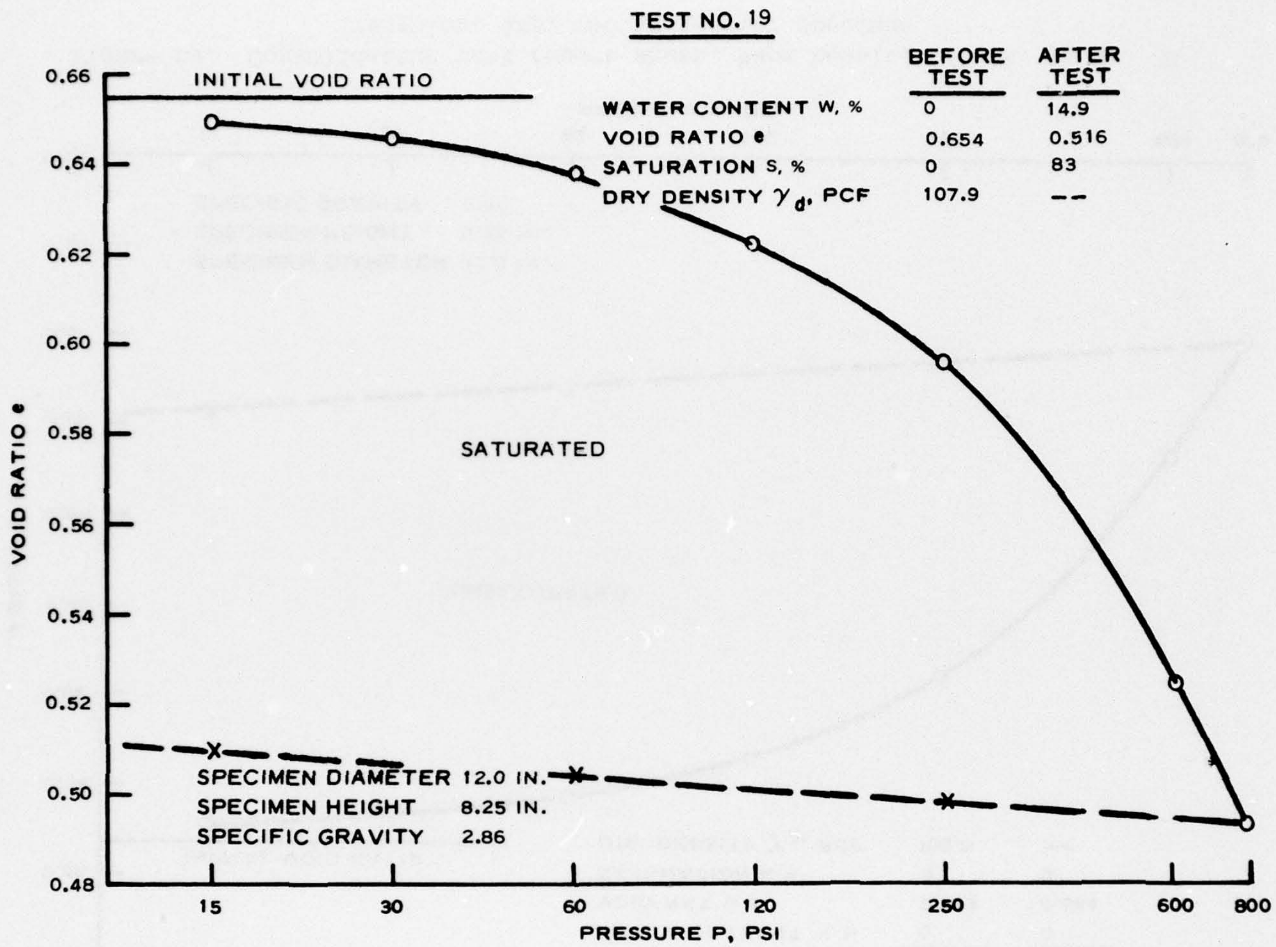

Figure 68. Consolidation test report sheet, Napa basalt, 1/4 in. to No. 30 gradation, inundated, medium density specimen

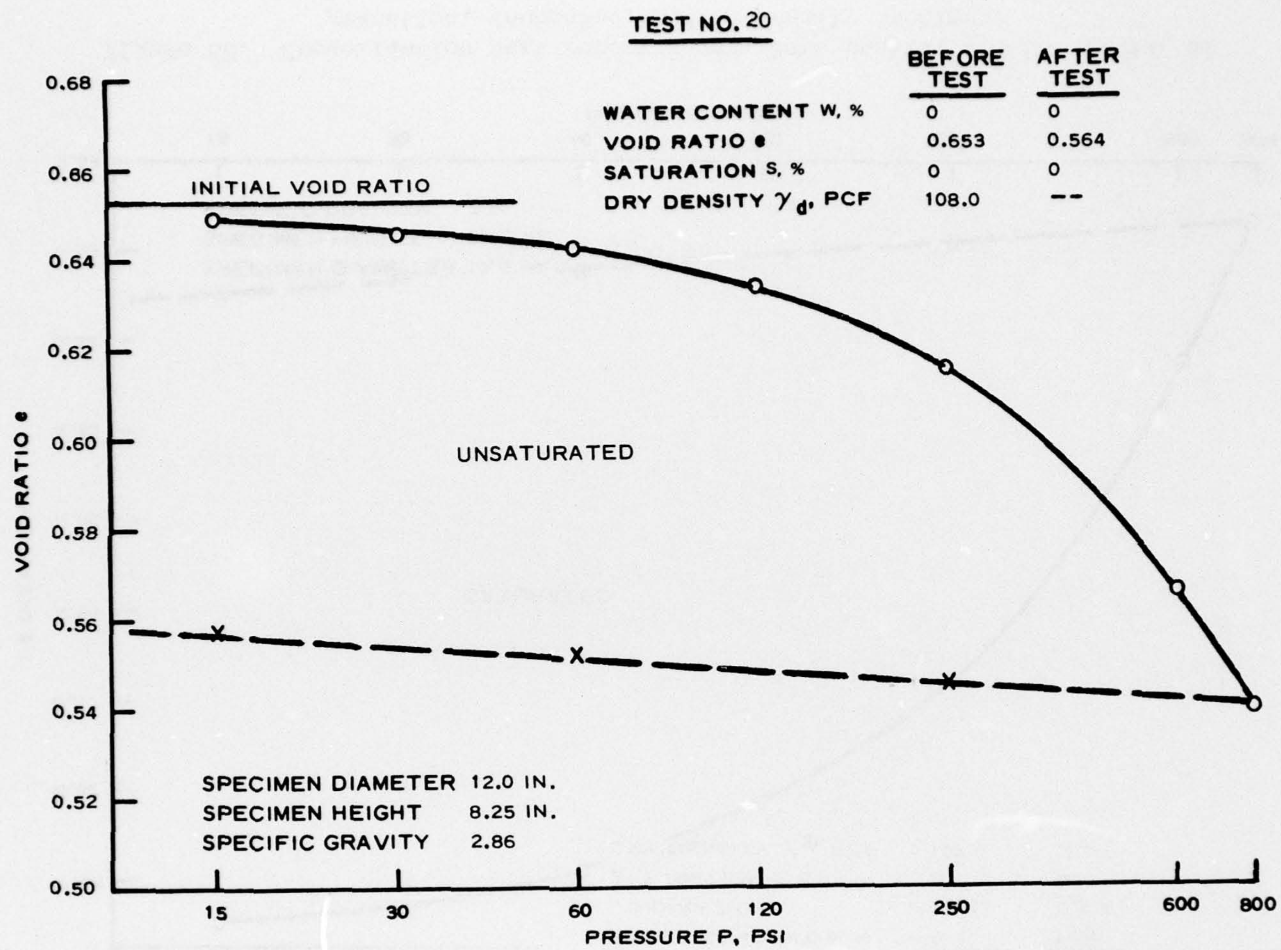

Figure 69. Consolidation test report sheet, Napa basalt, 1/4 in. to No. 30 gradation, dry, medium density specimen

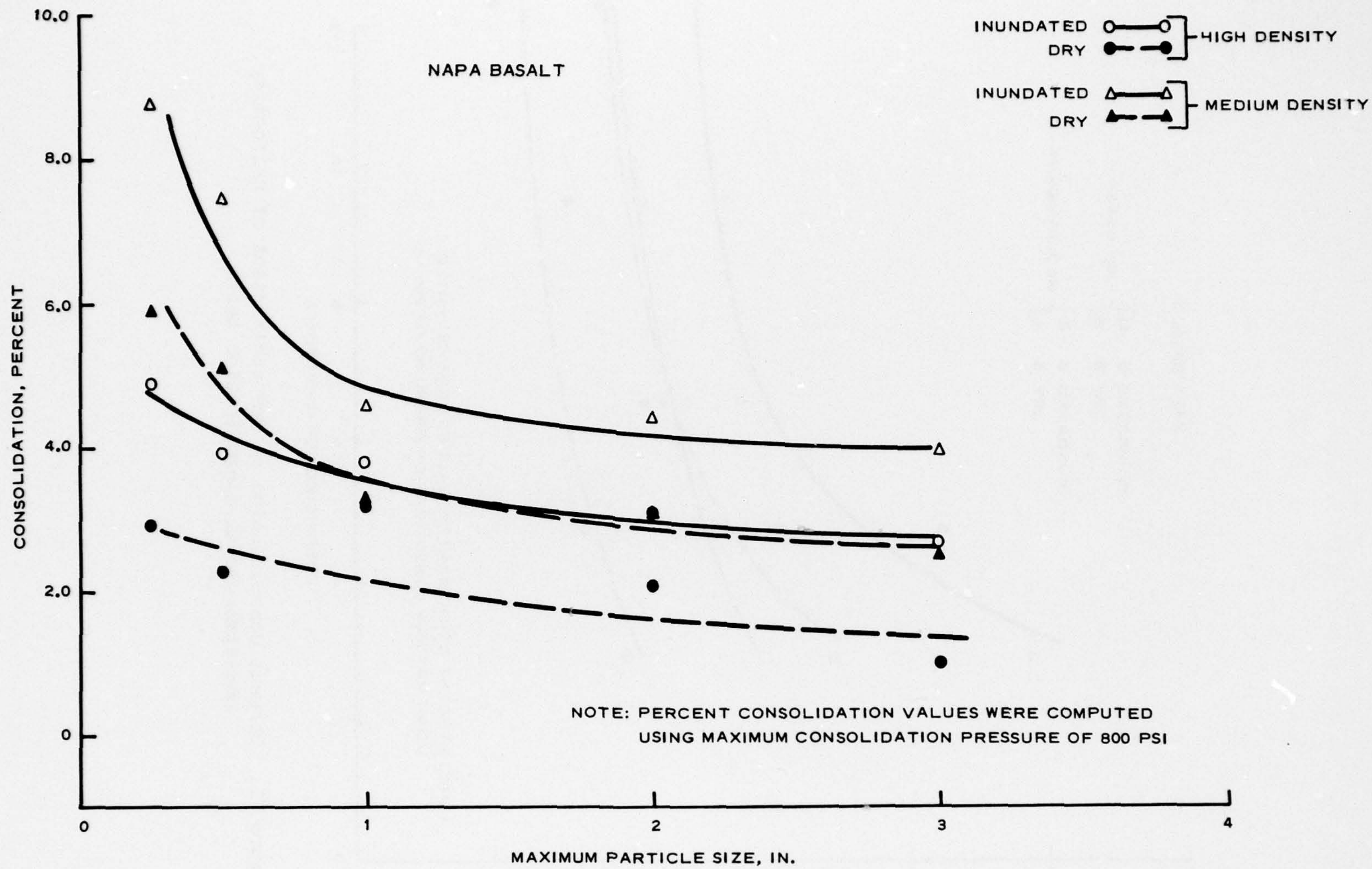

Figure 70. Percent consolidation versus maximum particle size, one-dimensional consolidation tests

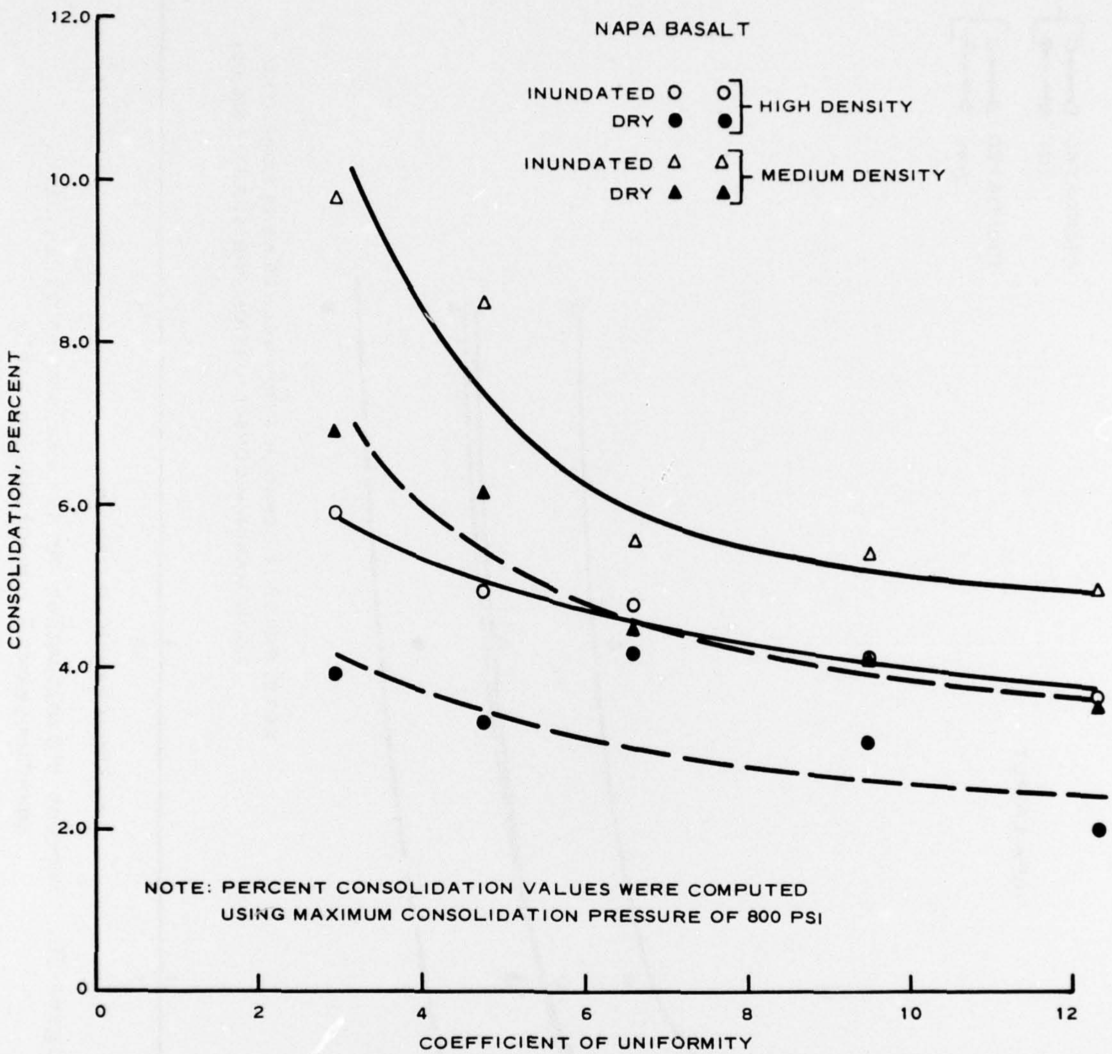

Figure 71. Percent consolidation versus coefficient of uniformity, one-dimensional consolidation tests

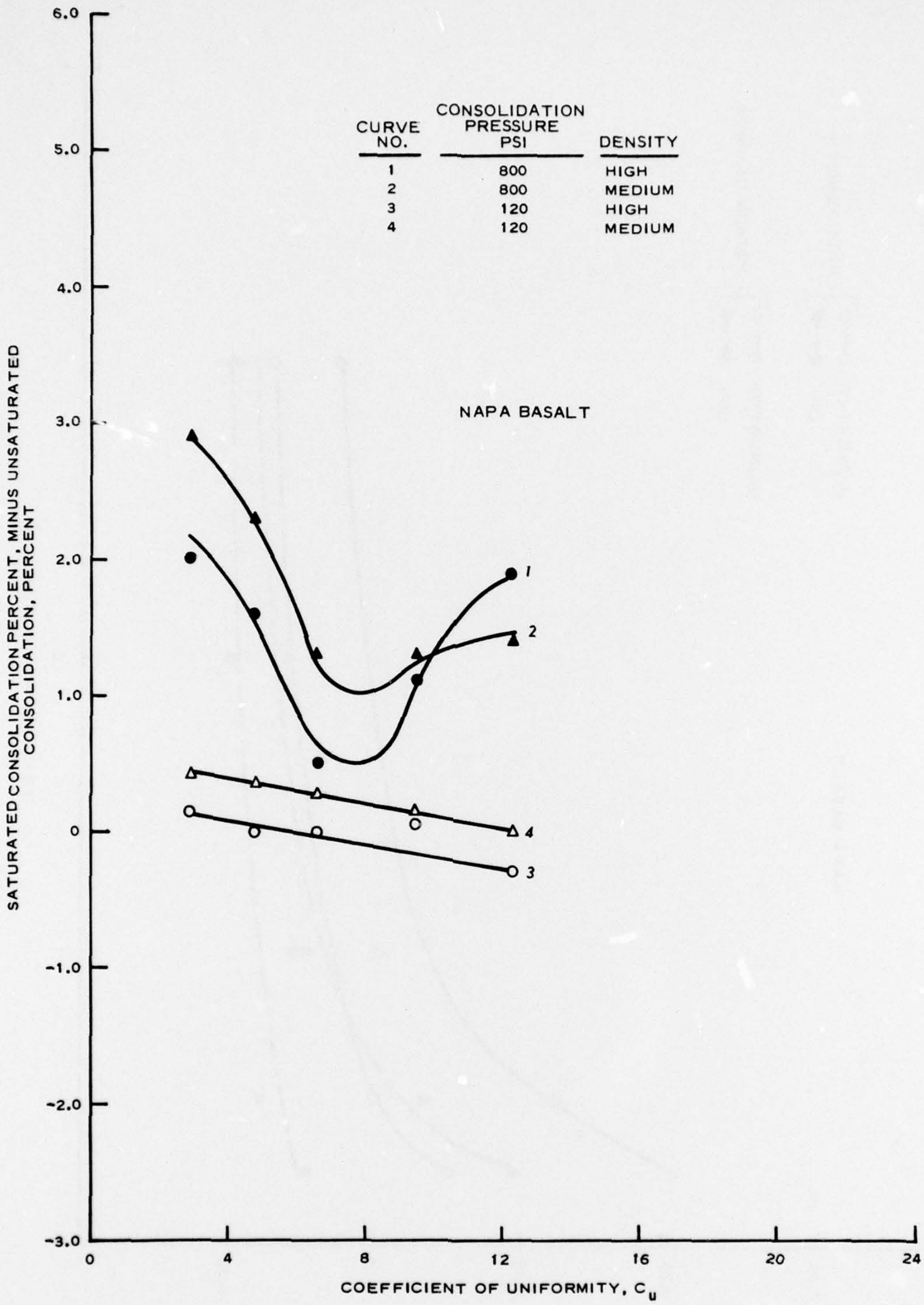

Figure 72. Saturated percent consolidation minus unsaturated percent consolidation versus coefficient of uniformity, one-dimensional consolidation tests

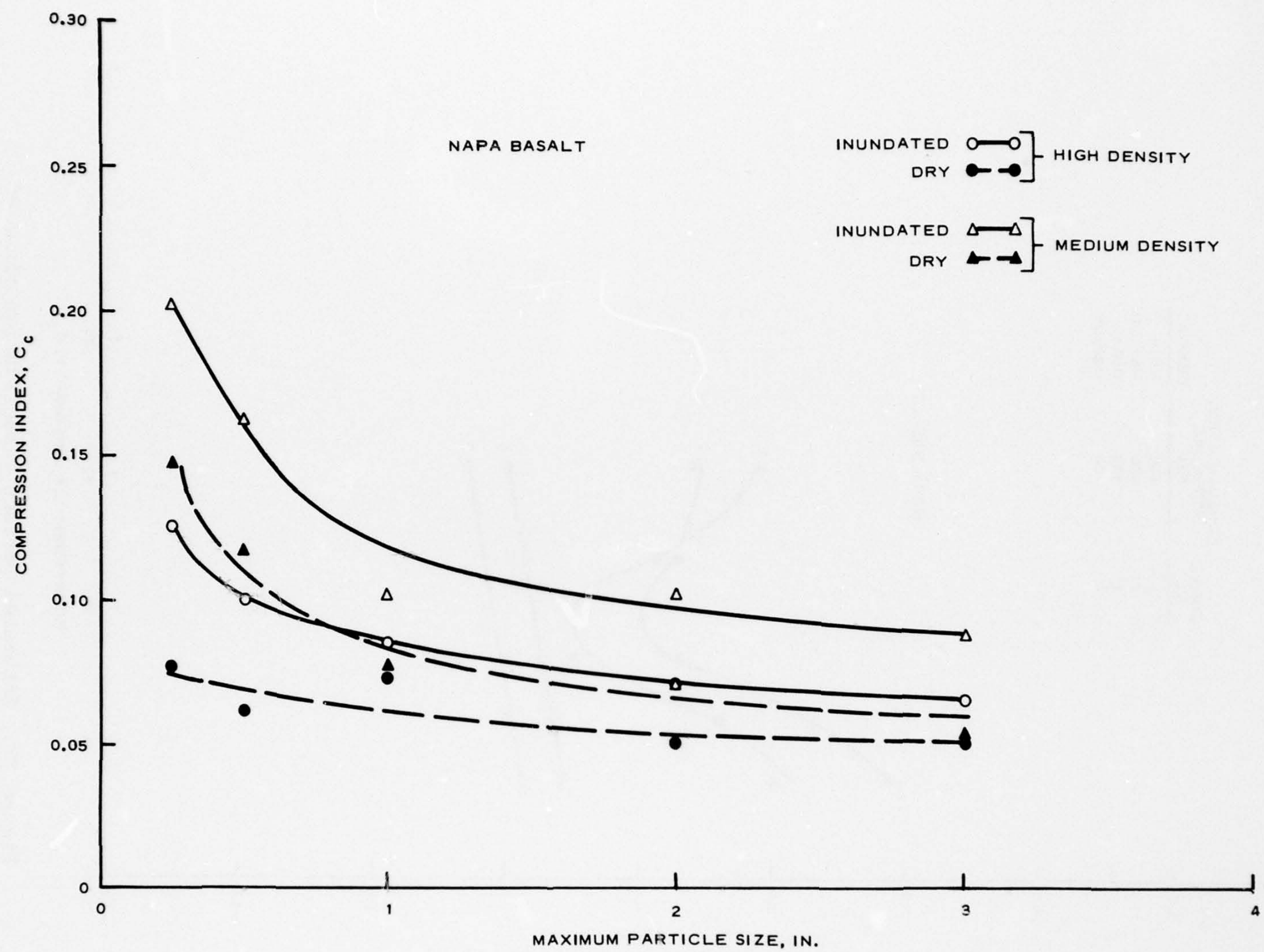

Figure 73. Compression index versus maximum particle size, one-dimensional consolidation tests

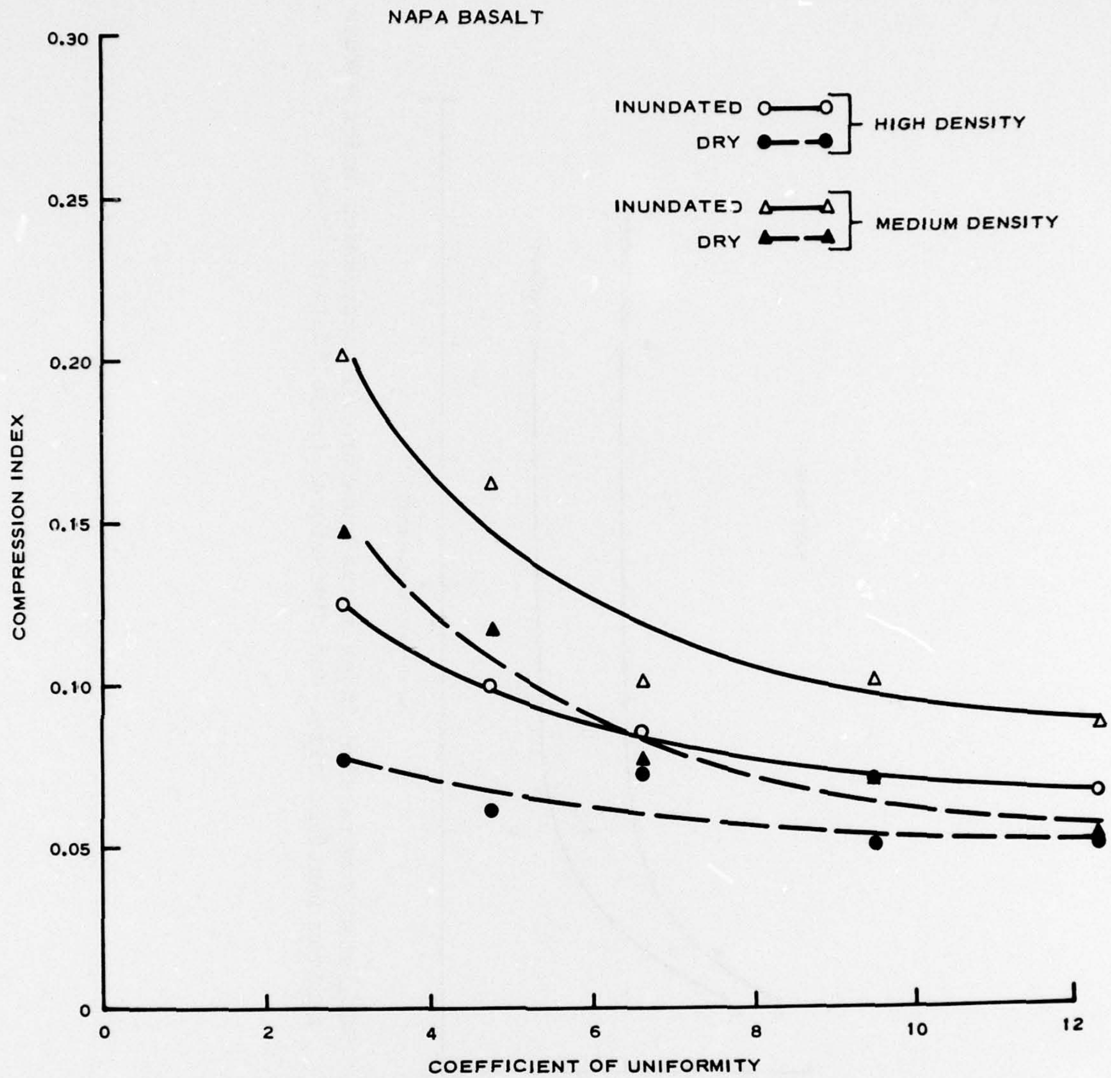

Figure 74. Compression index versus coefficient of uniformity, one-dimensional consolidation tests

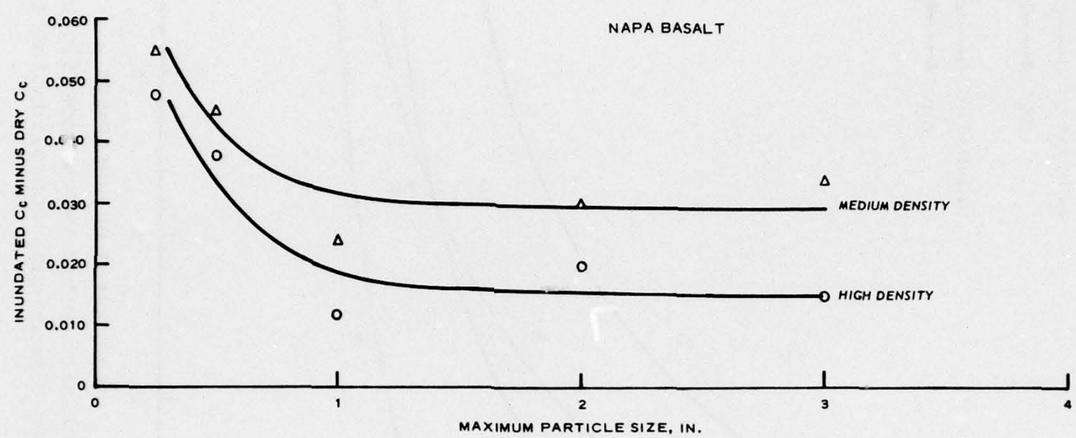

Figure 75. Saturated compression index minus unsaturated compression index versus maximum particle size, one-dimensional consolidation tests

In accordance with letter from DAEN-RDC, DAEN-ASI dated 22 July 1977, Subject: Facsimile Catalog Cards for Laboratory Technical Publications, a facsimile catalog card in Library of Congress MARC format is reproduced below.

Donaghe, Robert T
  Strength and deformation properties of rock fill / by Robert T. Donaghe and Melvin W. Cohen. Vicksburg, Miss. : U. S. Waterways Experiment Station ; Springfield, Va. : available from National Technical Information Service, 1978.
  24, [84] p. : ill. ; 27 cm. (Technical report - U. S. Army Engineer Waterways Experiment Station ; S-78-1)
  Prepared for Office, Chief of Engineers, U. S. Army, Washington, D. C.

1. Aggregates. 2. Consolidation. 3. Deformation. 4. Gravels. 5. Rock fills. I. Cohen, Melvin W., joint author. II. United States. Army. Corps of Engineers. III. Series: United States. Waterways Experiment Station, Vicksburg, Miss. Technical report ; S-78-1.
TA7.W34 no.S-78-1